CHARACTERIZATION OF INTERMOLECULAR INTERACTIONS USING HYPERPOLARIZED NMR

A Dissertation

by

RATNAMALA MANDAL

Submitted to the Graduate and Professional School of
Texas A&M University
in partial fulfillment of the requirements for the degree of

DOCTOR OF PHILOSOPHY

Chair of Committee,	Christian Hilty
Committee Members,	Dong Hee Son
	Matthew Sheldon
	Jae-Hyun Cho
Head of Department,	Simon North

December 2021

Major Subject: Chemistry

ABSTRACT

Nuclear magnetic resonance (NMR) spectroscopy is a widespread analytical technique used to characterize intermolecular interactions. However, due to the inherent insensitivity of NMR, long experimental times and large sample concentrations are required. Hyperpolarization methods are combined with NMR to broaden its application in characterizing intermolecular interactions rapidly. Here, hyperpolarization methods, based on Dissolution Dynamic Nuclear Polarization (D-DNP) and *Para*-Hydrogen Induced Polarization (PHIP) were developed to provide detailed interactions between proteins and small molecules.

D-DNP was used to characterize the interaction between hyperpolarized lipid molecules and an unfolded Outer membrane X (OmpX) under refolding conditions for the protein. Cross-relaxation rates between the different functional groups in the lipid and OmpX were determined in the absence of any denaturant. The fast experimental timescale of D-DNP allowed to access these conditions and may be useful for investigating structural changes in proteins during the refolding process. The PHIP technique requires minimal instrumentation and can be a cost-effective hyperpolarization technique for characterizing biomolecular interactions. Signal Amplification by Reversible Exchange (SABRE), the non-hydrogenative variant of the PHIP, allows renewal of polarization in solution. The pool of biological ligand motifs hyperpolarized by SABRE was broadened by developing a method, which allowed to hyperpolarize *ortho*-substituted N-heterocyclic molecules. Previously, these molecules yielded low polarization due to hindered binding

to the SABRE catalyst. This steric hindrance was solved by adding smaller coligand molecules that allowed the formation of the polarization transfer complex. The incompatibility of the SABRE catalyst in water and proteins in alcohol required to develop a two-step approach involving flow-NMR for characterizing protein-ligand binding. The ligand was hyperpolarized in methanol, and subsequently mixed with protein to characterize binding interactions in a predominantly aqueous medium. Changes in the transverse relaxation rate (R_2) in the presence and absence of protein was monitored to identify binding. Thereafter, the hyperpolarization of a molecule acting as a reporter ligand was used in a competitive binding experiment to find dissociation constants (K_D) that differ in three orders of magnitude for various ligands. Using a single reporter ligand allowed to determine K_D of ligands not hyperpolarizable by SABRE.

DEDICATION

Ma, Baba, Bhai

&

Sajal

ACKNOWLEDGEMENTS

I want to thank Dr. Hilty for all his guidance, patience and help throughout my PhD. I would also like to thank my committee members Dr. Son, Dr. Sheldon and Dr. Cho for their support in my research.

I want to thank all my lab members, past and present, for all their help as I learnt many things from them. Especially I want to thank Pierce for all the discussions and suggestions while working on our projects together.

I want to thank all my friends here in College Station with whom I have spent time and celebrated festivals and birthdays together. They made me miss home less during my stay here. I also want to thank all my friends back home in India who despite the time difference are always there for me.

Finally, I want to thank my parents and younger brother Suman. Their strong support let me survive these years away from home. Also, thanks to Sajal for his unconditional love and friendship for the last 10 years and standing by my side through all the ups and downs.

CONTRIBUTORS AND FUNDING SOURCES

Contributors

This work was supervised by a dissertation committee consisting of Professor Christian Hilty, Professor Dong Hee Son and Professor Matthew Sheldon of the Department of Chemistry and Professor Jae-Hyun Cho of the Department of Biochemistry and Biophysics.

The simulations in Chapter 2 were performed by Dr. Jihyun Kim, a former graduate student in the Department of Chemistry. The precatalyst in Chapters 4 and 5 was prepared by Pierce Pham, a current graduate student in the Chemistry Department. All other work conducted for the dissertation was completed by the student independently.

Funding Sources

Funding for this work was provided in parts by National Science Foundation under Grant Numbers CHE-1362691 and CHE-1900406, the Welch Foundation Grant Number A-1658, and Texas A&M University.

NOMENCLATURE

SPR	Surface Plasmon Resonance
ITC	Isothermal Titration Calorimetry
NMR	Nuclear Magnetic Resonance
CPMG	Carr-Purcell-Meiboom-Gill
CSP	Chemical Shift Perturbation
PRE	Paramagnetic Relaxation Enhancement
NOE	Nuclear Overhauser Effect
STD	Saturation Transfer Difference
INPHARMA	Interligand Noes for PHARmacophore Mapping
D-DNP	Dissolution Dynamic Nuclear Polarization
PHIP	*Para*-hydrogen Induced Polarization
SABRE	Signal Amplification by Reversible Exchange
Ir	Iridium
NHC	N-heterocyclic carbene
IMes	1,3-bis(2,4,6-trimethylphenyl)imidazole-2-ylidene
COD	cyclooctadiene
MRI	Magnetic Resonance Imaging
OmpX	Outer Membrane Protein X
DPC	Dodecyl Phosphocholine
CMC	Critical Micelle Concentration

TEMPOL	4-hydroxy-(2,2,6,6-TetraMethylPiperidin-1-yl)Oxy
ppm	parts per million
EXSY	Exchange Spectroscopy
ESI MS	Electrospray Ionization Mass Spectrometry
UV-VIS	UltraViolet-VISible

TABLE OF CONTENTS

Page

LIST OF FIGURES

Page

LIST OF TABLES

Page

1. INTRODUCTION

1.1. Characterization of Intermolecular Interactions

The interactions of proteins with small molecules or other proteins are an essential part of biological processes. Existence of the intermolecular interactions are important for molecular recognition in biological systems as they are responsible for many vital processes such as gene regulation, immune response, signal processing and others.[1] The identification of these interactions are important to improve medicinal chemistry and other related fields.[2] For example, interactions of proteins with small molecules are crucial in drug-discovery. Protein-protein interactions are critical as they are responsible for transmembrane signal transduction, DNA replication, transcription and translation.[3] Characterizing these interactions will allow for modifying them when they are responsible for diseases like cancer, diabetes and chronic inflammatory response. These interactions can be characterized by various methods such as surface plasmon resonance (SPR), fluorescence spectroscopy, isothermal titration calorimetry (ITC), nuclear magnetic resonance (NMR) and others. SPR is an optical technique that allows to determine the binding constants between two molecules without the use of any radioactive or fluorescent tag. However, it requires one component to be immobilized on a film. Fluorescence spectroscopy can give information about complex intermolecular interactions using single molecule. It has the requirement of one component showing a change in fluorescence intensity upon binding. Molecules may also need to be modified by attaching a label in the absence of an appropriate fluorophore tag. NMR spectroscopy is an important

technique that although requires larger sample concentrations, can give information about intermolecular interactions under physiological conditions without modifying the molecules.

1.2. NMR Methods for Characterizing Intermolecular Interactions

NMR spectroscopy can be used to gain atomic level information about intermolecular interactions, binding affinities and binding induced conformational changes. Various NMR methods exist for the study of interactions between different molecules. Some of these experimental techniques include relaxation changes, chemical shift perturbation (CSP), solvent paramagnetic relaxation enhancement (solvent-PRE), nuclear Overhauser effect (NOE) transfer and others. In the CSP, amino acid residues of the protein that are interacting with a ligand or another protein can be identified in a protein-observed experiment. When there are challenges in expressing a protein or having concentrated samples, ligand-observed experiments can be performed. In such cases, a smaller amount of the protein can be used if physiological conditions are needed, and the size of the macromolecule does not affect the experiment. Some of these ligand-observed experiments are based on NOE and changes in NMR relaxation properties.

A ligand molecule binds to a protein under equilibrium conditions in a dynamic chemical exchange, which gives rise to changes in NMR properties such as spin relaxation, chemical shift and others. The chemical exchange can be classified into three basic regimes depending on the magnitude of the exchange rate (k_{ex}) when compared to the nuclear spin precession frequencies of the bound and free ligands $(\Delta\nu) = |\nu_{f\_} \nu_b|$. The

slow exchange regime is reached when the k_{ex} is smaller than $\Delta\nu$. Tight binding ligands fall in this regime. The intermediate binding regime comprises k_{ex} comparable to $\Delta\nu$. Under fast exchange, k_{ex} is much greater than $\Delta\nu$. Ligand observed methods for identifying binding generally work in the fast exchange regime. When in fast exchange, the chemical shift (δ) is the weighted average of free and bound forms:

$$\delta_{obs} = \delta_f f_f + \delta_b f_b \tag{1.1}$$

Here, f_f and f_b are the fraction of free and bound forms respectively. Also,

$$f_f + f_b = 1 \tag{1.2}$$

The fraction of the bound form is expressed as:

$$f_b = \frac{\delta_{obs} - \delta_f}{\delta_b - \delta_f} \tag{1.3}$$

By solving the above equations, the dissociation constant K_D of a protein-ligand binding complex can then be determined[4] from fitting to the equation 1.4:

$$\Delta\delta_{obs} = \Delta\delta_{max}\left[\frac{[P]_T+[L]_T+K_D}{2[P]_T} - \frac{\sqrt{([P]_T+[L]_T+K_D)^2-4[L]_T[P]_T}}{2[P]_T}\right] \tag{1.4}$$

$\Delta\delta_{obs}$ is the observed shift with respect to the free state, $\Delta\delta_{max}$ is the shift change when solution is saturated and $[P]_T$ and $[L]_T$ are the total protein and ligand concentrations respectively.

Relaxation Time to Identify Binding

When a small molecule binds to a protein, the apparent molecular weight of the ligand molecule increases. The rotational correlation time ($\boldsymbol{\tau_C}$), which is the time taken for

the molecule to rotate one radian, changes. The spectral density function describes the distribution of frequencies arising from molecular tumbling as:

$$J(\omega, \tau_c) = \frac{2\tau_c}{1+(\omega\tau_c)^2} \quad (1.5)$$

When the Larmor frequency matches the frequency components of τ, NMR transitions take place, and relaxation occurs. For a certain value of τ_c, $J(0) = \tau_c$, is the maximum value of *J*. The NMR parameters depending on *J*(0), therefore will exhibit a large change upon binding.

The R_2 relaxation and cross relaxation rates are two such parameters:

$$R_{2,DD} = \frac{1}{20} b^2 (5J(0) + 9J(\omega_0) + 6J(2\omega_0)) \quad (1.6)$$

$$R_{cross} = \frac{1}{10} b^2 ((J(0) - 6J(2\omega_0)) \quad (1.7)$$

In the equations 1.6 and 1.7, $b = \frac{\mu_0 \hbar \gamma_H^2}{4\pi r^3}$ ($\mu_0$is the vacuum permeability, *r* is the distance between the nuclei, γ_H is the gyromagnetic ratio of the proton and $\hbar$ is Planck's constant). For the free ligand, the correlation time is short ($\tau_c\omega << 1$). The R_2 relaxation rate is therefore slow. When interacting with the protein, the correlation time is longer ($\tau_c\omega >> 1$) and the R_2 rate is faster. The difference in the transverse relaxation rate R_2 can be used to identify binding interactions between a macromolecule and ligand. A Carr-Purcell-Meiboom-Gill (CPMG)[5] experiment is used to measure a series of echoes for this purpose. The R_2 rate can be determined from an exponential fit to the signal intensities of the spin echoes. From a difference in the R_2 relaxation rate due to the difference in the tumbling motion of the ligand in free and bound form, the binding to the macromolecule can be identified.

Chemical Shift Perturbations (CSP)

The chemical shift of the NMR active nuclei is sensitive to the electronic environment that is local to them. Perturbations are caused by binding events and can be detected by analyzing the changes in chemical shifts. In a typical CSP experiment, 2D Heteronuclear Single Quantum Coherence (HSQC) spectrum of a protein is measured that is ^{15}N or ^{13}C labeled. The binding partner is titrated into the protein solution at an increasing concentration and a series of HSQC spectra are acquired at the different concentrations. Information such as the location of the binding-site, the binding affinity of the ligand and possibly the structure of the complex can be determined from this experiment.[6]

Intermolecular Nuclear Overhauser Effect (NOE)

The determination of 3D structures of molecules by NMR depends on measuring inter-proton distances from NOE experiments. The NOE can be detected for protons that are spatially close (distance < 6 Å). The NOE strength depends on the intermolecular distance as r^{-6}. Intermolecular NOEs are primarily weaker due to the dynamics and the percentage of the bound form. Experiments are used that purge the intramolecular interactions allowing for the observation of the intermolecular dipolar couplings only. Isotope-edited/isotope-filtered experiments are powerful techniques to achieve this in biomolecular complexes.[7] In the editing step, the magnetization associated with the protons attached to the ^{15}N or ^{13}C are selected. The filtering step consists of eliminating

these magnetizations. As a result, the protons from the labeled proteins are not detected but other protons that are bonded to ^{12}C or ^{14}N from another protein or ligand are observed. Other experiments using the NOE for detecting protein-ligand interactions are based on observation of ligand signals. These include the WaterLOGSY (Water-Ligand Observed with Gradient Spectroscopy), Saturation Transfer Difference (STD), transfer NOE (trNOE) and Interligand NOEs for pharmacophore mapping (INPHARMA). In the STD experiment,[8] the protein signal is saturated on-resonance. This saturation is transferred to the bound ligand, and through exchange into the free ligand. A reference spectrum is measured with saturation that is off-resonance and the difference in the two spectra has peaks only from the saturated ligand that interacts with the protein. The STD technique works well for proteins of large molecular weight as there is efficient transfer of magnetization to the bound ligand.

Water is present at the binding interface of the two molecules. In the WaterLOGSY[9] experiment, magnetization is transferred from water to the bound ligand. The water resonance is saturated during the on-resonance experiment. The off-resonance saturation is applied at chemical shift that is outside the ligand and protein resonances. The subtraction of the two spectra gives a negative NOE signal in case of ligand binding. The WaterLOGSY experiment allows to identify the ligand protons that are protein bound and exposed to water, thereby giving information about the ligand binding orientation.

The NOE signals between protons of small molecules are small and positive, while they are large and negative for macromolecules. When a small ligand is in fast exchange with a protein, it develops a large and negative NOE when bound to the protein. This is

observed in the trNOE and gives important distance information about the ligand in the bound state.

The INPHARMA gives information about ligands binding competitively to a protein.[10] Here, magnetization is transferred through NOE from one ligand to another through the protein, when both are binding to the same pocket in the protein.

Solvent Paramagnetic Relaxation Enhancement (PRE)

In solvent-PRE effects, an NMR active nucleus interacts with an unpaired electron that is located on a paramagnetic molecule. It is used as a solvent accessibility probe. The coupling interaction between the nucleus and this unpaired electron can increase the spin relaxation rates by an amount that is proportional to the local concentration of paramagnetic molecules. For identifying the intermolecular interactions between a ligand molecule and the protein, the relaxation rate is determined by calculating the difference in R_2 rates for the sample with a paramagnetic probe and the diamagnetic reference sample.[11] The PRE can also be used for identifying protein-protein interactions.[12] In such cases, the initially solvent exposed component will have an enhanced R_2 relaxation but this will decrease upon complex formation with the other component as less of the surface is exposed to the paramagnetic component.

Although NMR is a widespread analytical technique for the characterization of molecules, the low detection sensitivity limits its application in characterization of intermolecular interactions. Using higher concentrations for biomolecules in the millimolar range may lead to solubility concerns. Long experimental times of several

hours for multi-dimensional NMR may not be suitable for proteins that are unstable for long durations of time. The long experimental times will also prevent the detection of fast processes like protein folding.

1.3. Hyperpolarization Methods in NMR

To increase the NMR signal intensity, hyperpolarization techniques have been developed. The intensity of the NMR signal depends on the difference in the population of the Zeeman energy levels. When a spin ½ nuclei like the ^{1}H, ^{13}C or ^{19}F, is placed in a magnetic field, two Zeeman energy levels, corresponding to the $|\alpha\rangle$ = +½ and $|\beta\rangle$ = -½ states are produced. The energy difference between the two states is given by

$$\Delta E = \hbar \gamma B_0 \tag{1.8}$$

In this equation, $\hbar$ is the Planck's constant, γ is the gyromagnetic ratio of the nucleus and B_0 is the strength of the magnetic field. The nuclear spin polarization ($\boldsymbol{P}$) can then be calculated from:

$$P = \frac{n_\alpha - n_\beta}{n_\alpha + n_\beta} = \frac{1 - e^{-\Delta E/k_B T}}{1 + e^{-\Delta E/k_B T}} = \tanh\left(\frac{\gamma \hbar B_0}{2 k_B T}\right) \tag{1.9}$$

n_α and n_β are the number of spins in the two states respectively, k_B is Boltzmann's constant and T is the temperature in Kelvin. The spin polarization depends on the type of nucleus as it depends on the gyromagnetic ratio γ, and increases with increasing magnetic field B_0 and with decreasing temperature T. Due to the cancellation of the emissive and absorptive transitions, the net spin polarization (P) is important as the NMR signal intensity is

proportional to this term. The polarization for ^{1}H calculated from equation 1.9 at a temperature of 300 K would be only 0.003%.

Hyperpolarization techniques are therefore combined with NMR to resolve the issues of insensitivity and increase this polarization percentage. In hyperpolarization, a non-Boltzmann population difference is created between the two energy states, α and β. Since the NMR signal intensity depends on the population difference, an increase in intensity of 100 to 1000-fold or more over the equilibrium signal intensity can be achieved depending on the hyperpolarization technique used.

1.3.1.1. Dissolution-Dynamic Nuclear Polarization (D-DNP)

In D-DNP,[13] the high spin polarization of electrons is transferred to nuclear spins via hyperfine coupling to achieve the non-Boltzmann distribution. The difference in the gyromagnetic ratio (γ) makes the electron spin polarization greater than the nuclear spin polarization ($\gamma_e \approx 660\gamma_p$).[14] The hyperpolarization of the sample takes place in the solid state. The molecule to be hyperpolarized is mixed with an organic radical, which is the source of an unpaired electron. This is then dissolved in a glass-forming solvent. Examples of mixtures of solvents that form the glass-matrix are dimethyl sulfoxide/water (1:1, v/v) or ethylene glycol/water (3:2, v/v). This composition of the sample is immersed in a liquid helium bath, that has temperatures reaching ~1 K and this leads to the sample being frozen. The purpose of the glass-matrix is to ensure that the sample is well dispersed after it is frozen. The frozen aliquot is then irradiated with microwave near the electron resonance frequency.

After the sample is hyperpolarized in the solid state, it is rapidly dissolved by a preheated solvent and finally injected into an NMR tube where the acquisition takes place. Once the polarization is established, it starts to decay according to the T_1 time of the sample. Therefore, some ways to preserve the polarization and have the maximum signal enhancement include shortening the transfer time, capturing the radical and using deuterated solvents to prolong the T_1 relaxation time.

Application of D-DNP in Characterizing Intermolecular Interactions

D-DNP has been used to characterize various intermolecular interactions. Solvent-macromolecule interactions that are important for the structure of the macromolecule have been characterized by this technique. Interactions have been studied between hyperpolarized water and folded and unfolded proteins. Exchange-rates between a folded protein and hyperpolarized water were determined at different pH values.[15] In this case, polarization transfer through exchange and NOE between water and protein led to a maximum signal enhancement of 47 and 2.5 for the amide and aliphatic regions of the protein, respectively. Polarization transfer from hyperpolarized water to the amide protons was further propagated to the backbone and side-chain ^{15}N through a one bond Overhauser effect to increase the ^{15}N signal ~500-fold.[16] Fast 2D NMR spectra of proteins under refolding conditions have been measured by dilution of the denaturant urea for a fast-folding protein *RNase Sa* after polarization transfer from hyperpolarized water.[17] Addition of urea in the dissolution solvent allowed to tune the folding-rate of this protein and different 2D HMQC spectra were measured for varying urea concentrations.[18] Harnessing

polarization transfer from hyperpolarized water to nucleic acids allowed to monitor the real-time changes in the structures of the nucleic acid upon substrate binding.[19] Protein-ligand interactions have also been characterized by D-DNP. Hyperpolarizing the ligand and admixing with proteins have allowed to characterize the binding pocket in proteins due to the polarization transfer via the nuclear Overhauser effect.[20] Binding modes of proteins were identified in combination with fast multi-dimensional measurement and docking calculations.[21] Ligands containing ^{19}F have been used to detect binding to proteins in the strong-, weak- and intermediate regimes.[22] Use of ^{19}F allows to eliminate background signals and interference from solvent signals. Competitive binding experiments have been performed, where a single ligand in fast-exchange with the protein is hyperpolarized to screen ligands with a large range of binding affinities.[23] This experiment has the advantage that only one ligand needs to be hyperpolarized, allowing a large number of ligands to be screened. Also, the K_D of tight-binding ligands can be determined using this method. The polarization transfer from hyperpolarized ligand benzamidine led to increase in the protein signal trypsin, that is different from the equilibrium signal pattern, but matches closely to that obtained from a STD NMR experiment.[24]

1.3.1.2. Application of Chemically Induced Dynamic Nuclear Polarization (CIDNP)

CIDNP[25] is a hyperpolarization technique to achieve non-Boltzmann nuclear spin states for products derived from thermal and photochemical reactions. In an experiment involving CIDNP for studying proteins, a laser is used to irradiate a solution of the protein

and a photosensitizer. By using laser-induced photochemical reactions, the solvent accessibility of residues in proteins like tyrosine, tryptophan and histidine can be probed.[26] Flavins, such as lumiflavin and riboflavin are the most used photosensitizer as they are water soluble and can absorb laser light of the desired wavelength.[27] The interaction between the photosensitizer and the aromatic residues in the proteins are investigated by this technique. Amino acid residues in the proteins such as tryptophan, tyrosine and histidine are polarizable with the CIDNP technique as they interact with the photosensitizer dye via electron transfer or hydrogen atom transfer mechanisms.[28] CIDNP is used to probe the surface of proteins. It has been used to monitor the real-time refolding of a protein.[29] Components of DNA and RNA like the nucleotide bases have also been hyperpolarized by CIDNP.[30]

1.3.1.3. Applications of Overhauser Dynamic Nuclear Polarization

In the Overhauser DNP, the electron spin ensemble is saturated with continuous microwave irradiation. The spin polarization of the electron is transferred to nuclear spin polarization via cross-relaxation in the liquid state. The Overhauser effect depends on the magnetic field and the dynamics between the interacting two spins. Overhauser DNP has been used to probe the dynamics of hydration water at sites on the surface of an unfolded protein.[31] It allows to separate the signals of local water surrounding a protein from those of the bulk water.[32,33] This is done by selectively labeling the surface of the protein with radicals. The translational diffusion of water molecules affects the dipolar interaction between the radicals and the nuclear spins, thereby allowing to detect picosecond to

nanosecond timescales. In Overhauser DNP, the signal of the water molecule directly interacting with the spin-labeled site can be amplified while suppressing signals from the bulk water. This signal from specific sites has been used to characterize the interaction between water and a membrane-inserting peptide and the water accessibility determined at the labeled locations.[34]

1.3.1.4. Applications of Hyperpolarized Xenon

Hyperpolarized noble gases are a source to increase the sensitivity of NMR signals. To establish the hyperpolarization, optical pumping is used,[35] where the noble gas is mixed with an alkali metal vapor in a cell. Circularly polarized light from lasers at a particular wavelength are passed through the mixture. The angular momentum of this polarized light is absorbed by the electrons in the alkali metal vapor, and they become polarized. When the alkali metal vapor and the noble gas comes into contact, the polarization can be transferred from the vapor to the noble gas through spin exchange. The noble gas xenon (Xe) has a large chemical shift range of 300 ppm related to its large electron polarizable cloud and is highly sensitive to the chemical environment.[36] This property has allowed it to be used to probe biological systems. The hyperpolarized Xe can be used to increase the NMR signals of other solute molecules through spin polarization-induced nuclear Overhauser effect (SPINOE) when it is dissolved in solution.[37] The binding interaction of hyperpolarized Xe with the surface of several proteins have been investigated.[38] The conformational change in a maltose binding protein was studied by ^{129}Xe NMR spectroscopy.[39]

1.3.1.5. *Para*-Hydrogen Induced Polarization (PHIP)

The D-DNP, CIDNP, Overhauser DNP and hyperpolarized Xe have all found applications in characterizing interactions involving biomolecules. Another common hyperpolarization technique is the *para*-hydrogen induced polarization (PHIP). It requires minimal instrumentation and is cost-effective. Its application in biological systems has however been more limited. The PHIP requires catalysts which are insoluble in water. Therefore, it has found more applications in organic medium where the catalyst and hydrogen have greater solubility.

The ortho- and para-hydrogen are the two spin isomers of molecular hydrogen that differ in their nuclear spin configuration. As the hydrogen is a particle with spin ½, from quantum mechanics it is required that the overall wave function (Ψ) of hydrogen should be anti-symmetric. The wave function is composed of several terms including translational rotational, vibronic, electronic and nuclear:

$$\Psi = \Psi_{(electronic)}\Psi_{(vibronic)}\Psi_{(rotational)}\Psi_{(translational)}\Psi_{(nuclear)}$$

Out of these terms the electronic, vibronic and translational wavefunctions are always symmetric. Therefore, to fulfil the condition of the overall wavefunction being anti-symmetric, the nuclear and rotational terms should be different in symmetry. For the *ortho*-hydrogen, to fulfil this condition, the rotational states should be antisymmetric (J=1, 3, 5…). For the *para*-hydrogen, which has the anti-symmetric nuclear spin configuration the rotational states should be symmetric (J=0, 2, 4..). The J=0 is the lowest rotational state and therefore the *para*-isomer of molecular hydrogen is the intrinsically more stable

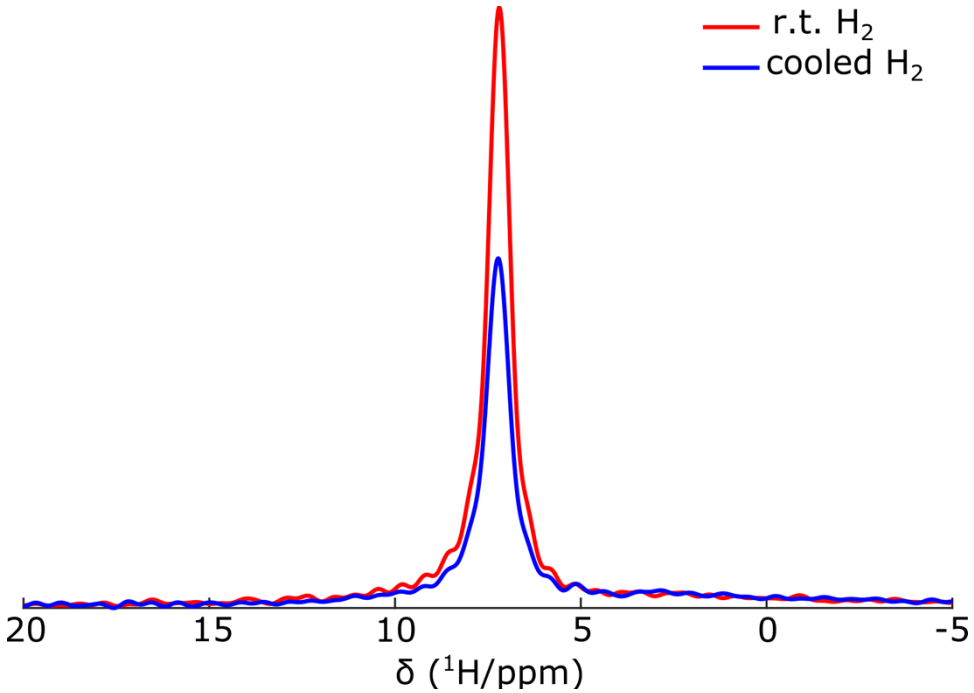

Figure 1.1: Spectra of room temperature (r.t.) hydrogen (–) and hydrogen cooled (–) to temperature of 77 K using liquid nitrogen and passed over spin flip catalyst iron (III) oxide.

isomer. This implies that lowering the temperature would enrich this *para* state of molecular hydrogen. At room temperature, all the four isomers are populated evenly, with the *ortho*-hydrogen comprising 75% and the *para*-hydrogen 25%. *Para*-hydrogen is produced by cooling room temperature hydrogen gas in the presence of a suitable spin-flip catalyst. The relative populations of the two isomers can be estimated from the Boltzmann's distribution of the rotational energy levels where θ_R is the rotational temperature:

$$\frac{N_{para}}{N_{ortho}} = \frac{\sum_{even\ J}(2J+1)\ exp\left(\frac{-J(J+1)\theta_R}{T}\right)}{3\sum_{odd\ J}(2J+1)\ exp\left(\frac{-J(J+1)\theta_R}{T}\right)} \qquad (1.10)$$

In the above equation, the para-hydrogen has the even rotational quantum number *J* due to the symmetric rotational wave function. The *ortho*-hydrogen has an odd rotational quantum number because of the antisymmetric rotational wave function. At lower temperatures of 77 K the *para*-hydrogen percentage is 50%. It increases to 99.8% when the temperature is lowered to 20 K. Figure 1.1 shows the *para*-enrichment at 77 K. The interconversion between the *ortho*- and *para*- isomers are forbidden. Therefore, if a specific isomer is produced, it will be stable for a long duration of time when stored in an appropriate vessel. In an aluminum container, the para-isomer was found to be stable on the order of weeks once produced.[40] From the spectra in Figure 1.1, the fraction of *para*-enrichment can be calculated from the equation:

$$1 - \frac{3S_{cooled\ H_2}}{4S_{room\ temperature\ H_2}} \tag{1.11}$$

Here the $S_{cooled\ H_2}$ and $S_{room\ temperature\ H_2}$ represent the integrals of the signal of the cooled hydrogen gas and the hydrogen gas at room temperature respectively.

As *para*-hydrogen has no net spin angular momentum, it itself is NMR silent. It is visible when its symmetry is broken when it is involved in a reaction. The reaction products exhibit enhanced NMR signals. The concept of the *Para*-hydrogen Induced Polarization (PHIP) was introduced theoretically by Bowers and Weitekemp in 1986.[41] Subsequently, the same authors demonstrated a hydrogenation reaction using acrylonitrile and Wilkinson's catalyst to generate the hyperpolarized hydrogenated product propionitrile.[42]

Depending on where the *para*-hydrogen is incorporated in the reaction, there can be two types of PHIP. When the incorporation takes place in the high field, it is known as *Para*-hydrogen and Synthesis Allow Dramatically Enhanced Nuclear Alignment (PASADENA). When the incorporation of the hydrogen takes place in the absence of a strong magnetic field, the process is known as Adiabatic Longitudinal Transport After Dissociation Engenders Net Alignment (ALTADENA). Under PASADENA conditions, the PHIP has found applications in characterizing organometallic complexes.[43,44] It has been used to hyperpolarize molecules such as ^{13}C succinate[45] and phospholactate[46] that are used as contrast agents for magnetic resonance imaging (MRI). The hydrogenated product of acetylenedicarboxylic acid dimethyl ester under ALTADENA conditions has been used to obtain the angiogram of an animal.[47]

The limitation of the hydrogenative PHIP is that it requires unsaturated substrates across which the hydrogen molecule can add. Several studies have modified substrates by adding a conjugated arm that is unsaturated[48,49] to hyperpolarize substrates using PHIP. The discovery of the non-hydrogenative variant of the PHIP, signal amplification by reversible exchange (SABRE) further allowed to solve this problem as in this technique the need to modify the chemical structure of the substrate is removed.

1.3.1.6. Signal Amplification by Reversible Exchange (SABRE)

In 2009, the non-hydrogenative version of the PHIP technique, SABRE was developed.[50] It allowed to hyperpolarize substrates that were not unsaturated. N-heterocyclic molecules, amines and nitriles are some common substrates that are

hyperpolarized by SABRE. The SABRE is a catalytic process. It requires a metal-catalyst, that binds the *para*-hydrogen as hydride, along with the substrate to be hyperpolarized, forming a polarization transfer complex. The spin-order of the hydride derived from *para*-hydrogen is then transferred to the substrates through *J*-coupling at a low field. The polarization transfer occurs where the level anti-crossings (LACs) theory is satisfied. The suitable magnetic field (B) is determined from the equation[51]

$$B = \frac{2\pi J_{H1H2}}{\gamma_p(\delta_{H1} - \delta_L)} \qquad (1.12)$$

In this equation, J_{H1H2} is the coupling between the hydrides, γ_p is the gyromagnetic ratio of the proton and $(\delta_{H1} - \delta_L)$ is the chemical shift difference between the hydrides and the substrate protons (~30 ppm). For the polarization of ^{1}H, the field is suitable at 6.5 mT calculated from equation 1.12. Fields in the μT regions are required when hyperpolarizing lower frequency such as ^{15}N or ^{13}C.[52] This process is known as SABRE-SHEATH (Signal Amplification by Reversible Exchange in SHield Enables Alignment Transfer to Heteronuclei).[52] SABRE has also been demonstrated at high fields where a radio-frequency field is used (RF-SABRE) with a chosen frequency and amplitude to model the low field condition.[53] High-field SABRE in the absence of radio-frequency field is also reported, where the mechanism of transferred polarization is attributed to SPINOE-type cross-relaxation and polarization transfer to the substrate.[54] The high field SABRE however gives lower enhancement compared to the case where polarization is established in the low field followed by acquisition at high field.

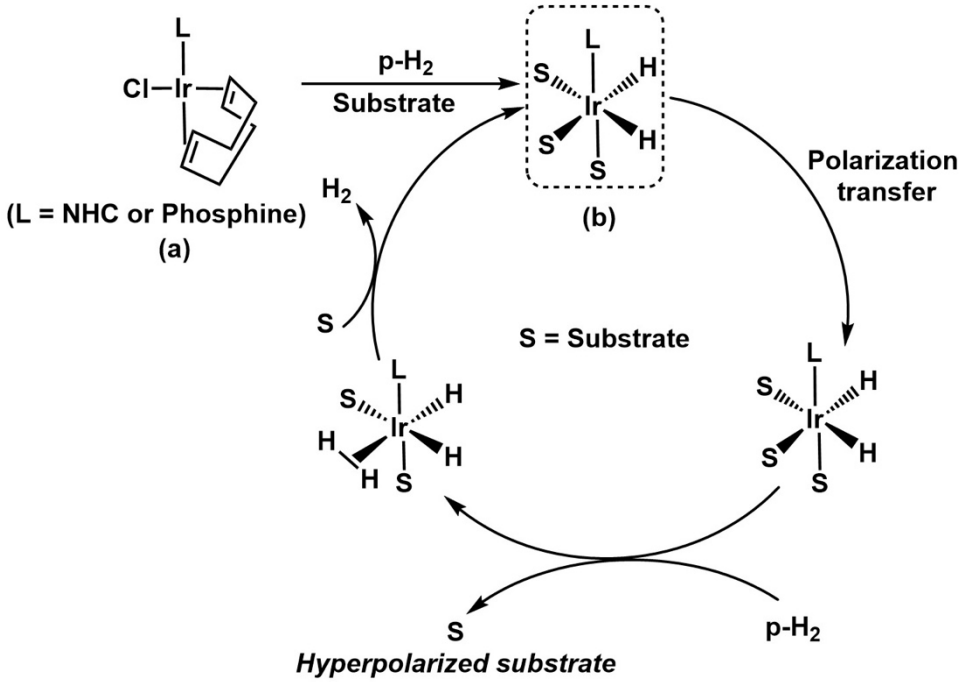

Figure 1.2: SABRE catalytic cycle. The L is the phosphine or the N heterocyclic carbene (NHC). S represents the substrate to be hyperpolarized.

In SABRE, the binding of the substrate and the hydride to the metal center is a reversible process. The polarization builds up on the substrate, which is finally detected in an experiment. As the substrate remains chemically unchanged, hyperpolarization can be renewed in solution by bubbling fresh *para*-hydrogen into the reaction mixture. The catalyst used for SABRE is an iridium (Ir) metal-based structure. Initially, the precatalyst had the structure with the electron-donating phosphine group, $[Ir(PCy_3)(py)(COD)]BF_4$ (Cy=cyclohexyl, py=pyridine and COD=1,5-cyclooctadiene) (Figure 1.2a). The precatalyst is activated by introducing *para*-hydrogen into the reaction mixture. The COD is hydrogenated and removed as cyclooctane. The coordination sites left free by the COD are then occupied by three substrate molecules and the *para*-hydrogen as hydrides in an octahedral complex, which is also referred to as the activated complex or the polarization

transfer complex (Figure 1.2b). The use of a more electron donating ligand compared to the phosphine, the N-heterocyclic carbene (NHC)[55], allowed to increase the achievable polarization greatly, from 2.5% to 8.1%.

[Ir(IMes)(COD)]Cl (IMes=1,3-bis(2,4,6-trimethylphenyl)imidazole-2-ylidine) was the first introduced precatalyst with an N-heterocyclic carbene ligand instead of the phosphine ligand to increase the signal enhancement values of pyridine. The difference in the performance of the two catalysts was mainly attributed to the difference in the substrate exchange rates caused by the two catalysts. The ligands in the catalysts have been developed to expand the pool of molecules that can be hyperpolarized by this technique. Asymmetric catalysts[56] are used to hyperpolarize bulky substrates which give low polarization with the standard symmetric catalyst. Bidendate catalysts have been developed to hyperpolarize substrates[57,58] that are *ortho*-substituted and have hindered binding to the polarization transfer catalyst. The halide ligands of the catalysts are tuned to further accommodate weakly-binding substrates for hyperpolarization, such as *ortho*-substituted lutidines and picolines.[59] Recently, catalysts that utilize metals different from iridium, such as cobalt (Co) have been developed for SABRE.[60] These catalysts allowed to hyperpolarize olefins using SABRE. The hyperpolarization was not possible with the Ir metal as it causes hydrogenation of the double bond in the olefins, changing the structure. The appropriate catalyst is important to establish large signal enhancements, but its removal after the hyperpolarization has been established allows to further increase the signal gain. This is because coordination to the catalyst is known to promote spin-lattice (T_1) relaxation[61] and therefore cause loss of polarization. Several methods have been

developed to remove the polarization transfer catalyst. These methods involves using chelating agents,[62] scavenger molecules,[63] or biphasic solvents,[64] among others. To increase the signal enhancement values of the desired substrates in SABRE, further tuning of the reaction mixture is necessary. For instance, deuterated molecules as coligands are introduced to facilitate polarization transfer to the substrate protons.[65]

Several reaction monitoring studies have been conducted with SABRE in organic solvents perhaps due to the high solubility of hydrogen in organic solvents.[66] SABRE was employed to hyperpolarize ^{29}Si and the resulting signals were used to monitor a reaction between tris(tert-butoxy)silanol and triflic anhydride and for detecting reaction intermediates.[67] The rate of reaction for the decarboxylation of sodium pyruvate was determined after hyperpolarizing ^{13}C pyruvate by SABRE-SHEATH and subsequently reacting with peroxide.[68] Esterification of glycine was further monitored by SABRE.[69] Monitoring of fast reactions is facilitiated due to the absence of a need of signal averaging, which shortens the experimental time. Apart from reaction-monitoring, SABRE has been used in organic solvents to hyperpolarize biological drug molecules on both ^{1}H and ^{15}N. The SABRE-Relay[70] method allowed to hyperpolarize molecules via proton exchange process for substrates that are unable to bind to the polarization transfer catalyst directly. Such molecules include glucose, carbonates,[71] sterically hindered secondary and tertiary amines[72] and alcohols.[73] Although SABRE has been used widely in organic solvents, its application in aqueous medium is limited, in part due to the lower solubility of hydrogen in water and catalyst insolubility.[66] Several techniques have been adopted to establish hyperpolarization in aqueous medium, such as reconstitution in water after catalyst

activation[74] and methanol evaporation followed by water addition.[75] The above-described limitations may have precluded the application of SABRE to probe biological samples including proteins which have been studied by other hyperpolarization techniques. However, as the SABRE is a cost-effective technique with relatively simple instrumentation needs, developing methods by which biomolecules can be characterized by it will be an important direction.

2. CHARACTERIZATION OF MEMBRANE PROTEIN-LIPID INTERACTIONS IN UNFOLDED OMPX WITH ENHANCED TIME RESOLUTION BY HYPERPOLARIZED NMR*

2.1. Introduction

Intermolecular interactions with water, specific ligands or other molecules play an important role in protein structure and function. Membrane proteins in particular are naturally present in a complex environment, which includes lipid molecules and other components of the biological membrane. Interactions of lipids with membrane proteins are based on specific structural features, such as hydrophobic surface area. In some cases, specific lipid binding modulates the function of a membrane protein.[76] Lipid-membrane-protein complexes can be detected by NMR spectroscopy,[77] mass spectrometry,[78] and X-ray crystallography,[79] among other methods. A feature of NMR spectroscopy is the possibility to identify specific contacts, even when corresponding molecular structures are not unique or ordered.

NMR-based methods to investigate the insertion of membrane proteins into lipid structures have been explored extensively for the outer membrane protein X (OmpX) from *Escherichia coli.* This β-barrel protein is involved in cell adhesion through a feature protruding from the cell membrane. Its structure has been determined by X-ray crystallography[79] and solution NMR.[80] A solid-state NMR structural study revealed the

---

*Reprinted with permission from "Characterization of Membrane Protein-Lipid Interactions in Unfolded OmpX with Enhanced Time Resolution by Hyperpolarized NMR" by Kim, J.;[+] Mandal, R.;[+] Hilty, C.[[+]Equal author contribution] *ChemBioChem*, **2020**, 2861-2867. Copyright John Wiley and Sons.

orientation of the protein in oriented bilayers.[81] The interactions of OmpX with dihexanoyl phosphocholine (DHPC) micelles in solution were identified by observing intermolecular nuclear Overhauser effect (NOE) cross peaks in three-dimensional NOESY spectra.[82] Contacts with methyl groups in the tail of lipids cover the hydrophobic surface area of the protein normally inserted in the outer membrane of *E. coli.* Additional NOEs were identified to head groups of DHPC, near a belt of aromatic residues that is sometimes referred to as an aromatic girdle in this class of membrane proteins. In small bicelles formed from dimyristoyl phosphocholine (DMPC) capped with DHPC, which exhibit a hydrophobic cross-section more closely matching that of the natural bilayer, essentially the same surface area was found to be covered by lipids.[83]

As an alternative to the observation of NOEs, molecular contacts can be determined by paramagnetic relaxation induced by molecular probes that contain a spin label. Probe molecules can be chosen with specific physicochemical properties. For OmpX in DHPC micelles, a water-soluble spin label induced enhanced amide proton relaxation in the normally extracellular and periplasmic structural regions of the protein, whereas hydrophobic spin labels affected a complementary region normally inserted into the membrane.[84] The use of appropriate molecular probes in combination with spin labels therefore can result in a similar selectivity as the NOE-based methods.

NMR methods can also be used for determining interactions in denatured, and therefore unstructured proteins. Urea denatured OmpX interacts with DHPC micelles in two regions of the extended polypeptide.[85] The two regions contain two hydrophobic clusters that exist even in the absence of micelles.[86] These clusters were hypothesized to

be involved in the initiation of folding of the protein. The actual process of folding, however, occurs on a timescale that is not directly accessible to these NMR spectroscopic methods.

Recently developed methods of hyperpolarization can dramatically enhance NMR signals, and thereby also the polarization that is transferred in intermolecular interactions due to the NOE. Dissolution dynamic nuclear polarization (D-DNP)[13] provides nuclear spin polarization that is enhanced by 3–4 orders of magnitude compared to high-field NMR. Signals from hyperpolarized spins are detectable in a single scan. Therefore, this method lends itself to real-time NMR spectroscopy with a sub-second time resolution.[87] On this timescale, non-equilibrium chemical and physical processes, among others protein folding, can directly be followed.[88]

Even under chemical equilibrium, hyperpolarization enabled real-time NMR spectroscopy can reveal information on molecular interactions and dynamics through the dependence of signals on polarization transfer dynamics. Polarization transfer to a protein can be observed from specifically binding ligands,[24,89] as well as due to non-specific interactions with water acting as a solvent.[15] This polarization transfer can occur through NOE or proton exchange.

Here, we use polarization transfer from hyperpolarized dodecyl phosphocholine (DPC) lipids to the membrane protein OmpX as a means for characterizing protein-lipid interactions under refolding conditions. We demonstrate that significant hyperpolarization can be achieved for lipid molecules below the critical micelle concentration (CMC), and that this polarization can transfer to the denatured protein already dissolved in micelles.

Polarization originating from head or tail groups of the lipids is distinguished using selective radio-frequency pulses in combination with simulations of spin polarization transfer. Finally, we discuss the applicability of this method for enhancing the time resolution in the characterization of membrane protein-lipid complexes.

2.2. Results and Discussion

Signals of hyperpolarized DPC at the final concentration of 0.6 mM are shown in Figure 2.1a. The signal enhancements due to hyperpolarization were calculated for each functional group, and are indicated in the figure. The functional groups of interest are the hydrophobic tail groups 1 and 2, and the choline head group 7. In a series of 6 measurements at a concentration below 0.8 mM, these functional groups show signal enhancements of 1610 ± 550, 550 ± 220 and 1210 ± 400, respectively (Figure 2.1a). The signal enhancements correlate with the spin- lattice relaxation rates of DPC monomers measured at high field, shown in the Figure 1b. The relaxation rates of the groups 1, 2 and 7 are 0.57, 1.00 and 0.93 s^{-1}, respectively. The fact that groups possessing slower relaxation rates yield a higher signal enhancement suggests that relaxation losses during sample injection rather than solid-state polarization efficiency dominate the achievable hyperpolarization.

Apart from the different signal enhancements obtained for different functional groups, there is a strong concentration dependence of the enhancement (Figure 2.1b). For example, the tail methyl protons on DPC (group 1) show a 2.5-fold decrease in signal enhancement when the final concentration is increased from 0.5 to 1.0 mM.

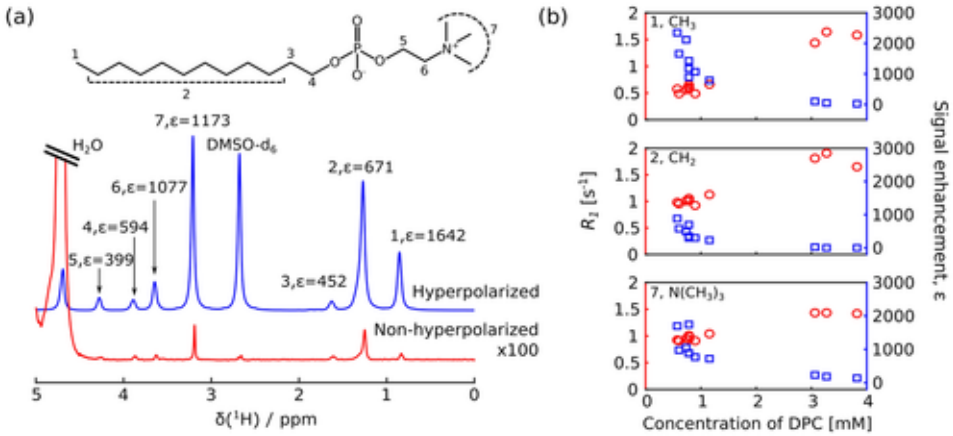

Figure 2.1: a) Comparison between a hyperpolarized (blue, top) and a non-hyperpolarized (red, bottom) ^{1}H NMR spectrum of the same sample of 0.6 mM DPC. The molecular structure of DPC with proton resonance assignments is shown. Signal enhancement factors ε are the ratios of the peak integrals from the hyperpolarized and non-hyperpolarized spectra. The peak near 2.6 ppm is from residual protons in the DMSO-d_6 used as a glassing solvent. (b) Spin-lattice relaxation rate R_1 (red circles) and signal enhancement ε (blue squares) of groups 1, 2 and 7 plotted as a function of the final concentration of DPC after dissolution and sample injection.

Although the spin-lattice relaxation rate measured at high field increases only slightly between 0.5 and 1.0 mM, the reduction in signal enhancement can be explained by the presence of micelles during the dissolution process, which increase spin relaxation. The critical micelle concentration (CMC) of DPC under the conditions used is 1.49 mM as shown in Figure 2.2.[90] As the final concentration is increased above the CMC, up to 4 mM, there is a further reduction of the signal. The observed signal enhancements are almost two orders of magnitude lower, reaching values of 26 and 5 for groups 1 and 2 in the tail group and to 131 for group 7. This decrease in signal enhancements is associated with a marked increase in the measured spin-lattice relaxation rates attributed to the presence of micelles.

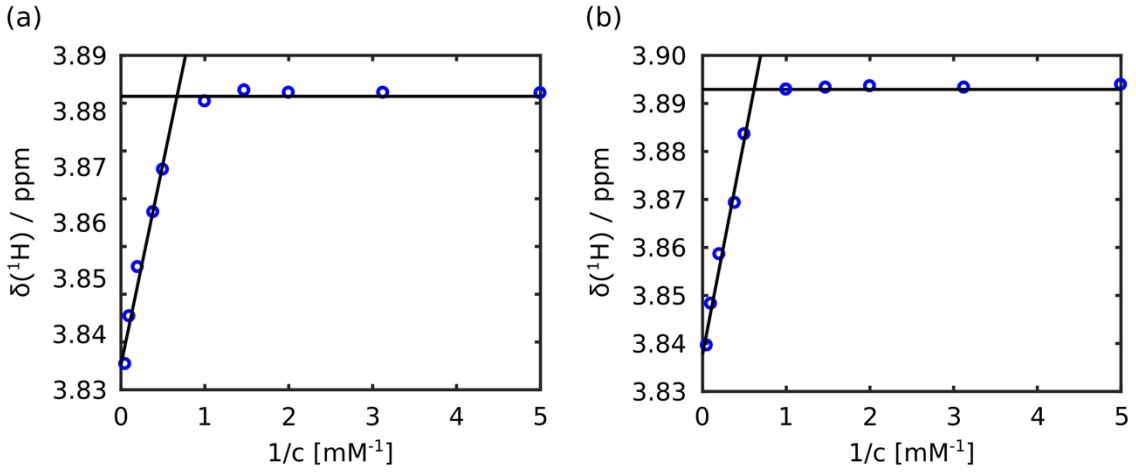

Figure 2.2: Plot of chemical shift of the DPC peak near 3.89 ppm as function of the total DPC concentration reciprocal in (a) 50 mM sodium phosphate buffer at pH 6.5 and (b) 50 mM sodium phosphate buffer at pH 6.5 with 0.8 M urea. For both cases, the intersection of the two solid lines obtained from the least square data fitting, indicates the CMC. The fitted values are CMC = 1.49 mM for (a) and 1.62 mM for (b).

In order to transfer spin polarization to the protein, hyperpolarized DPC was added to a solution of unfolded OmpX pre-mixed with DPC micelles. As a result, the signals of the protein were enhanced several times compared to protein signals with lipids after the polarization had decayed (Figure 2.3). In the ^{1}H NMR spectrum, the signals of the amide region of the spectrum (7.5 – 9.5ppm) are enhanced close to uniformly, showing a similar pattern of protein signals when compared to the reference spectrum. The region of the spectrum that contains signals of side-chain NH and aromatic protons shows a large enhancement near 7.2 ppm. The peaks in the range between 7.0 – 7.3 ppm, belong to the aromatic protons of phenylalanine, tyrosine, or tryptophan, and also to the side chain NH protons of arginine. A large enhancement in the region of aromatic resonances compared to amide resonances, is consistent with the expectation that hydrophobic residues are

strongly interacting with the lipids. This observation is also in-line with the result of ref. [45], where the chemical shifts of amino acids in two hydrophobic clusters in OmpX were predominantly affected by the addition of DHPC micelles.

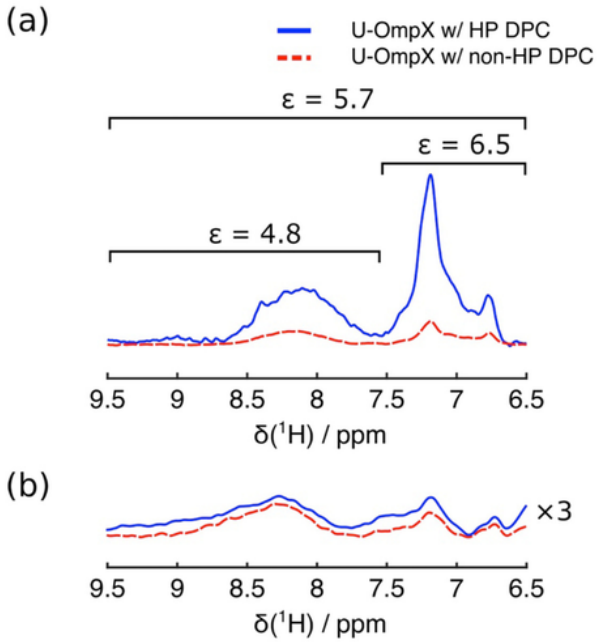

Figure 2.3: (a) ^{1}H NMR spectrum measured after addition of hyperpolarized DPC monomers to unfolded OmpX with DPC micelles (blue solid line). A spectrum measured after hyperpolarization has decayed is shown for comparison (red dashed line). The signal enhancement factors ε in the spectral regions indicated are calculated from the ratio of signal integrals. (b) Spectrum measured after addition of hyperpolarized DPC monomers to unfolded OmpX, where no DPC was pre-mixed (blue solid line), and spectrum measured after decay of hyperpolarization (red dashed line). The final concentration of DPC is 0.3 mM, which is below the CMC.

Enhanced protein signals were only observed when the hyperpolarized lipid was injected into a sample, where non- hyperpolarized DPC was pre-mixed with the protein. For the spectra in Figure 2.3a, DPC was included to reach a final concentration of lipid above the CMC even after the sample mixing. Spectra measured under the same conditions, but without pre-existing DPC micelles are shown in Figure 2.3b. In this case,

no signal enhancement of the protein was detected. The injected lipid resulted in a concentration below the CMC. It can be concluded that micelles are required for efficient polarization transfer to the protein. The existence of micelles bound to the protein effectively increases the local lipid concentration. At the same time, it increases the rotational correlation time, which can increase the cross-relaxation rate. In OmpX, these micelles presumably are associated with the protein at the location of the two hydrophobic clusters.

Although it would be possible to achieve a final concentration of DPC above the CMC using the hyperpolarized lipid only, a lower polarization transfer would be expected due to the lower spin polarization that can be achieved in lipids above the CMC, as discussed above. Instead, non-hyperpolarized DPC at a concentration of 100 – 150 mM was pre-mixed with the protein, allowing the formation of micelles prior to the injection of the hyperpolarized lipid. As the injection results in a dilution of 10 – 15-fold, the lipid concentration remained above the CMC during the experiment.

After injection, the hyperpolarized lipid molecules can either be inserted into micelles or remain dissolved in bulk solution. Based on typical exchange rates of ~ 10^4 s^{-1} [91] between lipids in bulk and in micelles, it is expected that insertion into pre-existing micelles is sufficiently rapid for polarization to be preserved. The injected lipids carry a spin polarization that is enhanced ~ 1000–fold (Figure 2.1a). These hyperpolarized lipids after injection constitute about 4–8% of the total lipid in the sample. The resulting overall lipid signal enhancement is therefore expected to be ~40- to 80-fold. The lipid peaks 1, 2 and 7 were experimentally found to be on average 30 times larger than those in a spectrum

measured after the polarization had decayed. The slightly lower enhancement of the lipid compared to the expected value likely indicates some relaxation loss while exchanging into the micelles. When the polarization from the lipids is transferred to protein, an overall signal enhancement of the protein of 5–6 was observed for the amide and side-chain protons visible in Figure 2.3.

This enhancement may be compared to a protein signal enhancement of up to 50-fold that was previously observed for polarization transfer from hyperpolarized water. In that case, a different protein, trypsin in its native form, was studied, and the water signal was enhanced ~500-fold.[15] The ratio of the signal enhancement of initially hyperpolarized agent to the final enhancement of the protein is about 5 for the NOE transfer from lipids, and about 10 for the predominantly exchange-based polarization transfer from water. Although the experimental conditions, concentrations and the transfer mechanism are different, it may still be interesting to note that the overall efficiency of the NOE transfer of hyperpolarization from the lipids in the present experiment was higher.

Along with the dilution of non-hyperpolarized lipid pre-mixed with the protein, the denaturant, urea at an initial concentration of 8 M, is also diluted by a factor of 10 or more. This dilution may cause re-folding of the protein during the experimental time. However, both the DNP and non-hyperpolarized reference spectra show the pattern of protein signals corresponding to unfolded protein. This observation is consistent with the folding rate of 0.0027 s^{-1} for OmpX into DPC micelles, determined in ref.[52] by real-time tryptophan fluorescence spectroscopy[92], although the buffer compositions are not identical in the two cases. Based on the difference in the folding rate and the experimental

timescale, it is therefore assumed that the structure of OmpX remains in the unfolded form for the duration of the experiment.

To determine the origin of transferred polarization, the protein signals were measured with and without a selective inversion pulse at a specific chemical shift of the hyperpolarized lipid molecules. Since the chemical shift of each functional group of lipid is well resolved, this pulse can effectively invert a target resonance without perturbing neighboring resonances. Among the functional groups, the tail and head groups of the lipid were chosen to be inverted (Figure 2.4). The inversion of the tail group caused a readily identifiable signal reduction of the protein, indicating that a significant portion of the transferred polarization originates from this group. The observed difference in signal intensity was further quantified using a calculation of the polarization transfer in terms of apparent cross-relaxation rates (see Data Analysis in the Experimental Section).

The calculated signal evolution for the protein at a final lipid concentration of 15 mM is shown in Figure 2.5. In all cases, the calculated protein signal immediately builds up after mixing with hyperpolarized lipids, and subsequently decays toward equilibrium. Without inversion pulse (Figure 2.5a), the signal of the protein decays more slowly than with inversion (Figure 2.5b), resulting in the difference of the observed protein signals at time point of t=1.3 s. For the inversion of the tail group of the lipid (Figure 2.4b), the decrease in the intensity of the protein signal is clearly discerned, while a minor effect is seen for the inversion of the head group. From the calculation, the apparent cross-relaxation rates were determined as $\sigma_{tail} = -2.8\times10^{-2}$ s^{-1} and $\sigma_{head} = -3.5\times10^{-3}$ s^{-1} for the tail

and head groups respectively. The larger magnitude of σ_{tail} compared to σ_{head} indicates a larger contribution to the transferred polarization.

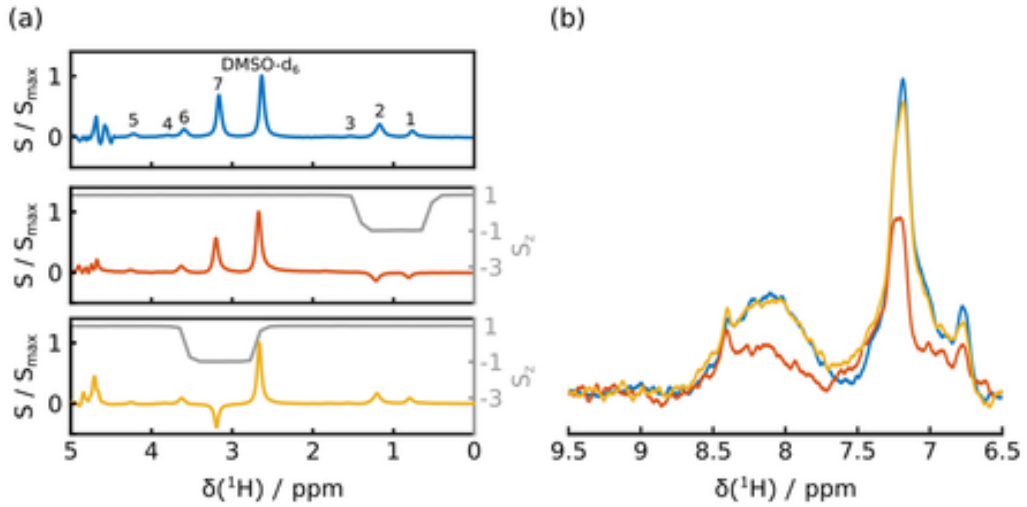

Figure 2.4: a) ^{1}H NMR spectrum of hyperpolarized DPC acquired using 1° hard pulse in the first scan of the experiment without inversion pulse (blue), spectrum with selective inversion of the hydrophobic tail groups 1 and 2 (orange), and spectrum with selective inversion of methyls in the choline head group 7 (yellow). In each case, the lipid signal is normalized by the maximum signal intensity in the spectrum, S_{max}. The experimental profile of the 15 ms selective spin-inversion pulse is superimposed in gray (right axis). b) ^{1}H spectra of unfolded OmpX after mixing with hyperpolarized lipid from the experiment with no selective inversion (blue), with inversion of head group methyls (yellow), and inversion of tail group (orange). The protein spectra were normalized by the protein concentration and initial spin polarization, this allowing a direct comparison of protein signal enhancements between experiments.

The same experiments were performed while varying the concentration of the pre-mixed DPC, resulting in a final concentration of DPC from 7 mM to 15 mM. Because the apparent cross-relaxation rate is dependent on the concentrations of the respective species, the resulting values are different for each of these data sets, summarized in Table 2.1. The concentration independent cross-relaxation rates were calculated from three experiments,

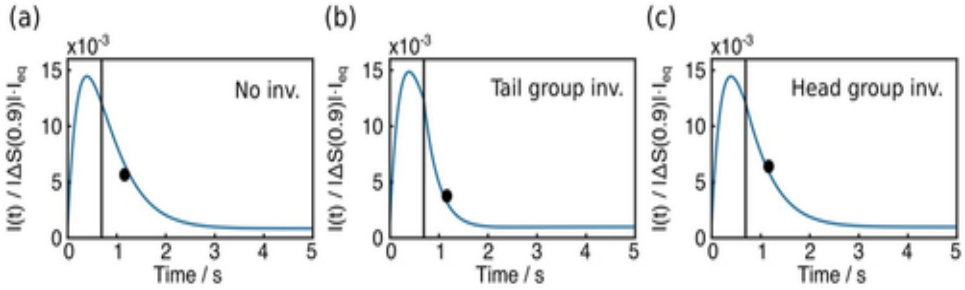

Figure 2.5: Calculated signal evolutions of the protein in the case of (a) no inversion, (b) inversion of the tail group, and (c) inversion of the head methyl group of lipid molecules. The black circles indicate the experimentally measured protein signal intensities. The vertical black lines show the time, $t = 0.7$ s, when the selective inversion pulse was applied. The apparent cross-relaxation rates fitted for the data set shown are $\sigma_{tail} = -2.8\times10^{-2}$ s^{-1} and $\sigma_{head} = -3.5\times10^{-3}$ s^{-1}. The final sample contained 0.2 mM unfolded OmpX with 15 mM DPC, resulting in normalized cross-relaxation rates of $\sigma_{N,tail} = -1.8$ s^{-1}M^{-1} and $\sigma_{N,head} = -0.2$ s^{-1}M^{-1}. For plotting, the protein signals are normalized by the deviation of lipid signals of tail and head groups from the equilibrium measured at $t = 0.9$ *s* ($|\Delta S(0.9)|$) and the protein signals measured after decay of hyperpolarization (I_{eq}), resulting in $I(t)/(|\Delta S(0.9)|I_{eq})$. This normalization compensates for differences in the initial spin polarization of the lipids and in the concentration of the protein in different experiments.

resulting in $\sigma_{N,tail} = -1.8 \pm 0.1$ s^{-1}M^{-1} and $\sigma_{N,head} = -0.5 \pm 0.3$ s^{-1}M^{-1}. It can be seen that the magnitude of $\sigma_{N,tail}$ is larger than that of $\sigma_{N,head}$, suggesting that the hydrophobic tail group of lipid is the major source of polarization transfer to the protein compared to the apparent cross-relaxation rate is dependent on the concentrations of the respective species, the resulting values are different for each of these data sets, summarized in Table 2.1. The concentration independent cross-relaxation rates were calculated from three experiments, resulting in $\sigma_{N,tail} = -1.8 \pm 0.1$ s^{-1}M^{-1} and $\sigma_{N,head} = -0.5 \pm 0.3$ s^{-1}M^{-1}. It can be seen that the magnitude of $\sigma_{N,tail}$ is larger than that of $\sigma_{N,head}$, suggesting that the hydrophobic tail group of lipid is the major source of polarization transfer to the protein compared to the hydrophilic head group of DPC. The lower precision in the $\sigma_{N,head}$ is due to the smaller

difference in signal intensities between the experiments without inversion and with head inversion.

Cross-relaxation rates were also measured using a conventional 2D NOESY experiment with the sample containing 0.2 mM OmpX with 15 mM DPC, which are conditions similar to those for the data set shown in Figure 2.5, excepting the final urea concentration. This measurement yielded values of $\sigma_{N,tail}$ = -3.8 $s^{-1}M^{-1}$ and $\sigma_{N,head}$ = -0.8 $s^{-1}M^{-1}$ for the normalized cross-relaxation rates. These rates are approximately the double of the rates observed in the DNP experiments. The difference may be expected due to the different properties of the samples for the DNP and the non-hyperpolarized NOESY experiments. The latter contains 8 M urea, whereas the final concentration of the denaturant in the former sample is 0.8 M after dilution by the dissolution solvent. This causes a significant difference if only in viscosity[93], which would affect the observed relaxation rates.

The presence of a high concentration of urea needed to stabilize unfolded proteins, such as for equilibrium NMR measurements, can disrupt the CMC of the detergents[94] or change the micelle size,[95] which may alter the structure or dynamics of the protein under investigation. The dilution of urea following the dissolution process in the DNP experiment allows to measure cross-relaxation rates while avoiding these effects. No significant influence of 0.8 M urea was observed on the CMC of DPC (Figure 2.2). The interaction of the unfolded membrane protein with the lipid micelles can be measured with D-DNP at this low urea concentration because this measurement completes within a time of seconds. The fast experimental timescale circumvents the potential problem of protein

precipitation under the present experimental conditions. The low urea concentration in the sample is also closer to the native environment of proteins.

Table 2.1: Experimental parameters and fitted apparent and normalized cross-relaxation rates (σ and σ_N) from the DNP measurements.

Set		C_{DPC} [mM]	r_{tail} [s^{-1}]	r_{head} [s^{-1}]	σ_{tail} [s^{-1}]	σ_{head} [s^{-1}]	σ_{tail} [$s^{-1}M^{-1}$]	σ_{head} [$s^{-1}M^{-1}$]
1	No inv.	14.8	2.3	2.0	$-2.8\cdot10^{-2}$	$-3.5\cdot10^{-3}$	-1.8	-0.2
	Tail inv.	17.1	2.1	2.0				
	Head inv.	13.8	2.3	2.0				
2	No inv.	7.5	2.1	2.0	$-1.5\cdot10^{-2}$	$-5.2\cdot10^{-3}$	-1.8	-0.6
	Tail inv.	9.3	2.0	2.0				
	Head Inv.	9.2	2.0	2.0				
3	No inv.	6.9	2.0	2.0	$-1.2\cdot10^{-2}$	$-5.1\cdot10^{-3}$	-1.7	-0.7
	Tail inv.	7.3	2.1	2.0				
	Head inv.	7.2	2.1	2.0				
Average and Standard Deviation							-1.8±0.1	-0.5±0.3

Although lipid-protein NOEs can be observed by conventional NMR methods in static samples, their measurement requires multiple scans typically on a time-scale of minutes. Fast events occurring on the time-scale of seconds, such as membrane protein folding, cannot be monitored. The DNP experiment, which works in a single scan, may be used for the characterization of such dynamic processes. The relevant timescales in the

DNP experiment are a polarization transfer time on the order of a second, as well as an acquisition time below 100 milliseconds. Combining additional chemical shift resolution with the above method by utilizing selective pulses for isotope selection in 1D NMR[20] or fast 2D NMR[96] techniques may further provide residue-specific information.

2.3. Conclusion

In summary, dodecyl phosphocholine molecules were hyperpolarized by D-DNP and exchanged into pre-formed micelles. Contact with the hyperpolarized lipids resulted in polarization transfer to an unfolded membrane protein, OmpX, which was associated with the micelles. The DNP experiment was performed in the absence of a large denaturant concentration, under refolding conditions. A signal enhancement of up to 6-fold was directly observable for the amide and aromatic side-chain protons of the protein in a single NMR scan. The origin of this transferred polarization was determined using NMR with selective inversion pulses, indicating that the hydrophobic tail group of lipids is the major source of the polarization transfer. Although protein signals were measured at a single time point, the cross-relaxation rates involving different functional groups in the lipid could be quantified. In the future, polarization transfer from lipids to proteins may give more insight into the nature of such interactions that occur in unfolded, folded or refolding membrane proteins.

2.4. Experimental Section

2.4.1. Sample Preparation

The unfolded OmpX (U-OmpX) protein was expressed and purified as reported.[86] For hyperpolarizing lipids, solutions of 50 – 100 mM dodecylphosphocholine (DPC) were prepared in a mixture of D_2O/DMSO-d_6 (v/v 1:1) with 15 mM 4-hydroxy-2,2,6,6-tetramethylpiperidine 1-oxyl radical (TEMPOL; Sigma-Aldrich, St. Louis, MO). Samples of denatured OmpX/DPC were prepared at a concentration of 1.7 mM OmpX, in a buffer of 50 mM sodium phosphate, pH 6.5, 8 M urea, and 100 – 150 mM DPC. 4,4-dimethyl-4-silapentane1-sulfonic acid (DSS) was included in the sample at a final concentration of 1 mM as a reference. The concentrations of OmpX solutions were determined by UV/vis spectrophotometry, using an extinction coefficient of 34,840 M^{-1} cm^{-1}.[97]

2.4.2. Hyperpolarized NMR Experiments

Volumes of 25 – 100 µl of lipid sample were inserted into a HyperSense DNP polarizer (Oxford Instruments, Abingdon, U.K.). Hyperpolarization was generated by irradiating with microwaves (100 mW power, 94.005 GHz frequency) at a temperature of 1.4 K. After 20 min, the hyperpolarized sample was dissolved by 4 mL of preheated buffer (50 mM sodium phosphate, pH 6.5) and automatically transferred to a 5 mm NMR tube that was preinstalled in a 9.4 T NMR magnet (Bruker Biospin, Billerica, MA). In all experiments, a triple-resonance inverse detection probe (TXI; Bruker Biospin), at a temperature of 304 K was used. This temperature corresponded to the sample temperature arriving in the NMR tube after dissolution, as determined with a thermocouple in test

injections. The sample transfer occurred through a sample injector described elsewhere.[98] The injection was accomplished with a forward pressure of 1772 kPa applied against a back pressure of 1034 kPa. The injection time was 385 ms, followed by stabilization for 500 ms.

To measure the signal enhancement and spin–lattice relaxation rates as a function of the lipid concentration, hyperpolarized lipid samples were injected into an empty NMR tube. A series of NMR spectra were measured with the pulse sequence [{water suppression}$_{x3}$-pα-acquisition]$_{x64}$. For the water suppression, the water resonance was selectively excited by repeated EBURP2 shaped 90° pulses of 20 ms duration, and dephased by randomized pulsed-field gradients G_x, G_y or G_z. The pα is a hard pulse of 1 μs duration, corresponding to a flip angle of approximately 10°, which was determined separately for each experiment. In each scan, 4096 data points were acquired during an acquisition time of 0.32 s, with an interval of 0.4 s between scans. The signal enhancement was calculated by comparing the signal integrals between hyperpolarized and non-hyperpolarized spectra of the same sample, in the first scan. The spin–lattice relaxation rate was determined by fitting the decay of the hyperpolarized signal with $S(t) = S(0)e^{-(r_1+\lambda)t}$ where S represents the signal intensity, r_1 indicates the spin–lattice relaxation rate, and $\lambda = -\ln[\cos(\alpha)]/\Delta t$is an additional parameter to account for the depletion of polarization by the detection pulses with flip angle, α, and the time interval between NMR acquisitions, Δt.[99]

To identify the interactions between protein and lipid molecules, 50 μL of denatured OmpX/DPC solution was preloaded into the NMR tube and mixed with the

hyperpolarized lipid during sample injection. The final concentrations of protein and lipid were 0.2 mM and 6 – 15 mM, respectively. NMR spectra were acquired using the pulse sequence (optional shaped p180)–{water suppression}$_{x3}$–pα–acquire–{water suppression}–(shaped p90)–acquisition. The water suppression block was as described above. The first scan was acquired after a hard pulse pα with a flip angle of α = 1°, to determine the polarization of lipid molecules. In the second scan, the protein signals were selectively excited by a shaped p90 pulse (EBURP2 shape, 90° flip angle, 2.48 ms duration) centered at 9 ppm and covering a bandwidth ± 2.5 ppm. In the case of the selective inversion experiments, an optional shaped p180 pulse (IBURP-2 shape, 180° flip angle, 15 ms duration) was preceding the experiment. This pulse was centered at 1 ppm or 3.2 ppm, to invert the signal of either the hydrophobic tail group or head group of the lipids, respectively. In both scans, a total of 3196 data points were collected over an acquisition time of 250 ms. The time t = 0 for the NMR experiment was defined as the midpoint between the start and end of the sample injection and mixing. The optional inversion pulse was applied at time t = 0.7 s, or was substituted with an equivalent delay in the experiments without inversion. The signal acquisitions for the first and second scans started at t = 0.9 s and t = 1.3 s, respectively. Lipid concentrations were measured using ^{1}H NMR spectroscopy before and after the DNP experiment.

2.4.3. Data Analysis

All the data were analyzed using Matlab (MathWorks, Natick, MA). An exponential window function with 10 Hz line broadening was applied to each individual

transient of the DNP measurements, and the resulting data was Fourier transformed. Spectra were individually phase corrected and baseline corrected in Matlab. The time evolution of protein and lipid signal intensities including the inversion pulse effect on the lipid signal as well as polarization transfer to protein via NOE were analyzed using the Solomon equations for lipid (*S*) and protein (*I*) signals.[100]

$$\frac{d\Delta S_{tail}(t)}{dt} = -r_{tail} \cdot \Delta S_{tail} \quad (2.1)$$

$$\frac{d\Delta S_{head}(t)}{dt} = -r_{head} \cdot \Delta S_{head} \quad (2.2)$$

$$\frac{d\Delta I(t)}{dt} = -\sigma_{tail} \cdot \Delta S_{tail}(t) - \sigma_{head} \cdot \Delta S_{head}(t) - r_p \cdot \Delta I(t) \quad (2.3)$$

In these equations, $\Delta S(t)$ and $\Delta I(t)$ are $S(t) - S_{eq}$ and $I(t) - I_{eq}$ and S_{eq} and I_{eq} are the signal intensities at thermal equilibrium. The signals from the CH_n groups of the hydrophobic tail of the lipids (chemical shifts of 0.8 and 1.2 ppm) were grouped together to be considered as S_{tail}, and the signal of the head groups (3.2 ppm) was designated S_{head}. In this model, it is assumed that hyperpolarized lipid shows a one-way polarization transfer to the protein. This assumption is reasonable when the concentration and initial polarization of lipid are much higher than that of protein. Then, the time evolution of the lipid signals was calculated from the exponential function solving equations. 1 and 2, based on signals measured in the first scan of the DNP experiment, at $t = 0.9$ s. In the case of the inversion experiments, the lipid signals before the inversion pulse were calculated by dividing the observed signals with the inversion pulse effect, f_{inv}, for describing the imperfection of this pulse. This factor was determined experimentally as a ratio of the integral of non-hyperpolarized signals without and with the inversion pulse. The spin-lattice relaxation

rates of the respective lipid groups, r_{tail} and r_{head}, were experimentally determined by an inversion recovery experiment from the same sample after the D-DNP experiment.

OmpX signals detected in the second scan of the DNP experiment were integrated over the chemical shift range of 6.5 to 9.5 ppm, and considered as spin *I*. The spin-lattice relaxation rate of the protein was independently measured using an inversion recovery experiment, resulting in $r_p = 2.8\ s^{-1}$. The time evolution of protein signal intensities was calculated by numerically solving the differential equation (eq. 3) using the ode45 solver in Matlab, and fitted to the measured protein signal intensities at $t = 1.3$ s. The three datasets with and without inversion of lipid signals were simultaneously fitted to obtain the cross-relaxation rates σ_{tail} and σ_{head}. Concentration independent cross-relaxation rates were calculated by dividing the apparent cross-relaxation rates by the concentration of lipid, $\sigma_N = \sigma / c_{DPC}$.

2.4.4. Reference NMR Experiments

To validate the cross-relaxation rates from hyperpolarized NMR experiments, a ^{1}H-^{1}H NOESY spectrum without hyperpolarization was acquired on a 500 MHz NMR spectrometer with a TCI cryoprobe (Bruker Biospin). A solution of 0.2 mM unfolded OmpX and 15 mM DPC was prepared in buffer under the same conditions as the DNP experiments except the urea concentration of 8 M. The spectrum was measured with 4096 × 512 data points, with averaging over 32 scans per increment. The maximum acquisition times were $t_{1,max}$ = 39 ms and $t_{2,max}$ = 315 ms, and the recycle delay was 1 s. The NOE mixing times were 50 and 100 ms. The temperature was set to the same value as in the

DNP experiment, 304 K. The cross-relaxation rates were determined using the volume ratios of the cross-peaks divided by the diagonal peaks in the spectral region of protein signals and each functional group of the lipids. The total experimental time was 28 h.

The sample for determining the profile of the selective inversion pulse was D_2O with residual water content. A series of 121 ^1H spectra were measured with 50 Hz offset where the selective IBURP-2 pulse was followed by a hard $\pi/2$ read pulse. The spectra were not individually phase corrected and the maximum intensities were plotted to obtain the profile of the inversion pulse.[101]

3. NUCLEAR SPIN HYPERPOLARIZATION OF NH_2 AND CH_3-SUBSTITUTED PYRIDINE AND PYRIMIDINE MOEITIES BY SABRE*

3.1. Introduction

Nuclear spin hyperpolarization dramatically enhances the sensitivity of NMR, enabling new applications in chemistry and biochemistry. Among hyperpolarization methods, *para*-hydrogen induced polarization (PHIP)[41,42] is distinguished as cost-effective and applicable with a relatively modest need for additional equipment. Molecular hydrogen gas can be enriched in the *para*-spin state at low temperature. The anti-parallel *para* spin state is subsequently converted into hyperpolarization of a target molecule either in a hydrogenation reaction, or through signal amplification by reversible exchange (SABRE)[50] upon binding to a catalyst. Both methods allow for a substantial signal gain for proton NMR, on the order of $>10^4$ for direct hydrogenation, and at least $>10^2$ for SABRE. Other nuclei can also be hyperpolarized by these methods, either through polarization transfer from the hyperpolarized protons in the same molecule,[48] or in the case of SABRE by direct polarization at a low magnetic field.[52] The reversible nature of the SABRE process in addition supports an in principle indefinite number of repetitions, which can be used for signal averaging or multi-dimensional spectroscopy. A challenge in the application of both these techniques for the hyperpolarization of a broader range of

*Reprinted with permission from "Nuclear Spin Hyperpolarization of NH_2 and CH_3 Substituted Pyridine and Pyrimidine Moieties by SABRE" by Mandal, R.; Pham, P.; Hilty, C. *ChemPhysChem*, **2020**, 2166–2172. Copyright John Wiley and Sons.

compounds are the requirement for a suitable molecular catalyst that interacts both with molecular hydrogen and the compound of interest. For SABRE, Ir[(COD)(IMes)]Cl (COD = cyclooctadiene, IMes =1,3-bis(2,4,6-trimethylphenyl)imidazol-2-ylidene) has become the most widely used catalyst.[55] This catalyst is capable of binding other N-heterocyclic ligands, such as pyridine in a planar configuration with molecular hydrogen as hydrides, allowing for the transfer of spin-order through *J*-coupling. The efficiency of the polarization transfer is governed by factors including binding affinity and chemical exchange rates, steric accessibility of the binding site, magnetic field, and solubility constraints. Considerable efforts have been devoted to the design of catalysts with the ability to hyperpolarize specific compounds. A series of structurally related iridium catalysts were developed containing different substituents in the aryl group of the NHC ligand and functional groups in the imidazole backbone to improve the SABRE performance.[102] Asymmetric catalysts, where the aryl group on one side of the NHC ligand is replaced with a smaller group, were found to enhance polarization of sterically hindered substrates such as 3,4- and 3,5-lutidine.[56] Recently, the development of an asymmetric, bidendate catalyst with Phox group (Phox = 2- (2-(diphenylphosphanyl)phenyl)-4,5-dihydrooxazole) has enabled the polarization of *ortho*-substituted molecules such as 2-methylpyridine and 2-fluoropyridine.[57] Interestingly, the enhancement of pyridine, which in previous work was often used as a reference ligand for SABRE, was found to decrease considerably, although the reason not elucidated. Other molecules that cannot bind to the SABRE catalyst directly may be hyperpolarized by a relayed polarization transfer process, which can occur through proton exchange from SABRE polarized amines in aprotic

organic solvents,[72] or through a second polarization transfer step when binding to a second metal complex.[70]

The addition of a coligand to the SABRE reaction mixture can further enhance the polarization by stabilizing the polarization transfer complex, breaking its symmetry, assisting in the catalyst activation, or by other mechanisms. The addition of acetonitrile as a coligand was shown to achieve catalyst activation for fused ring N-heterocyclic structures.[103] Acetonitrile and pyridine as coligands were found to increase the polarization of weakly binding compounds such as diazirines,[104] and imidazole and indazole.[105] Dimethyl sulfoxide (DMSO) as a coligand enables the hyperpolarization of pyruvate, thereby expanding the range of SABRE active substrates to a molecule with an oxygen instead of a nitrogen donor for binding to the catalyst.[106] Acetonitrile also increases the attainable spin polarization of aromatic amines such as aniline,[72] which do not activate the SABRE catalyst by themselves. At low ligand concentrations, the SABRE enhancement is observed to decrease. The coligand 1,2,3-triazole stabilizes the polarization transfer complex in such cases.[107] The addition of d_7-benzylamine as coligand allowed the natural abundance detection of ^{15}N polarization for a range of compounds.[108] Deuterated ligands have been proposed to direct the polarization to fewer protonated substrate molecules, thereby increasing the net spin polarization. Acetonitrile has been used as an additive for the detection of low concentration species having important role in the SABRE process.[109]

In this chapter, hyperpolarization of biological compounds containing NH_2 and CH_3 *ortho*-substituted pyrimidines and pyridines with an Ir-IMes SABRE catalyst is

demonstrated. Molecules with *ortho*-substitutions have previously been reported to yield no SABRE signal, which may be attributed to steric hindrance.[110] It is found that large SABRE hyperpolarization can be achieved through the use of coligands with the Ir(COD)(^{Me}IMes)Cl ((COD = trimethylphenyl)imidazol-2-ylidene)), for NH_2 but not for CH_3 substituted substrates. This difference is discussed in terms of the electronic properties of the substituents. The NH_2 substituted molecules form the core structures of metabolites in the folate pathway. The effect of these coligand additions dependent on the type of substituent at the *ortho*-position is identified, and the hyperpolarization of trimethoprim is demonstrated, an inhibitor of dihydrofolate reductase (DHFR) that has found widespread application as an antibacterial agent.

3.2. Results and Discussion

3.2.1. Hyperpolarization of NH_2 and CH_3 substituted molecules

Spectra of a selection of NH_2 and CH_3 substituted pyridine and pyrimidine molecules hyperpolarized by SABRE are shown in Figure 3.1. In each panel, the top two traces represent NMR and SABRE NMR spectra of a sample without coligand. The middle two traces show the corresponding spectra of separate samples with acetonitrile, and the bottom two traces show the spectra of a separate sample with allylamine. The substrate 2,4-diaminopyrimidine (S1) is a prototype for an NH_2 substituted pyrimidine. In the SABRE experiment, only weak signals with enhancements of -7 for H_6 and -4 for H_5 were obtained for this ligand, despite multiple possible N-binding sites in the molecule. The substrate S1 can be hyperpolarized with the addition of acetonitrile, which has previously

been used as a coligand with other substrates. With the addition of acetonitrile to S1, the enhancement dramatically increased to give values of -160 ± 10 for H_6 and -100 ± 10 for H_5 at 318 K. In addition, the acetonitrile is itself enhanced -70 ± 20-fold. For a sample with allylamine, the SABRE signal enhancements increased further to -210 ± 20 for H_6 and -170 ± 30 for H_5 at 326. Table 3.1 contains signals under conditions achieving highest signal enhancement, which is most relevant for practical application of the method. These signal enhancements compare favorably to those of pyridine, which is perhaps the most widely reported SABRE substrate. The enhancements for pyridine obtained under similar conditions but without coligand were -220 ± 30 for H_1, -210 ± 30 for H_3 and -170 ± 20 for H_2 at 298 K. The addition of acetonitrile was observed to have no significant effect on the pyridine enhancements giving a value of -170 ± 20 for H_1 at 298 K. However, the addition of allylamine lead to almost a 2-fold increase in the signal enhancement, albeit at a higher temperature of 310 K.

Subsequent comparisons of polarization efficiency were performed with coligands. The substrate 4-aminopyrimidine (S2), without NH_2 group in the ortho position of one of the N-atoms in the heterocycle, gave large SABRE signals even without a coligand. The proton *ortho*- to the binding site generally gains more polarization, as the 4-bond *J*-coupling is stronger than the 5- or 6- bond couplings. Based on the observed signal enhancements, the binding site for S2 is likely the N without any *ortho*-substitution. The substrate 2-aminopyridine (S3) contains a NH_2 substitution in the ortho-position of a single heterocyclic N. For this substrate, a maximum enhancement of -10 could be achieved for H_6 without a coligand. The addition of acetonitrile gave an enhancement of -

120 ± 30 for H_6 at 318 K and allylamine resulted in an increase in the enhancement to a value of -200 ± 30 for H_6 and 326 K, comparable to the enhancement of pyridine without coligand addition. These observations support the idea that an *ortho*-substitution hinders binding, and that the addition of coligands remove this restriction. Comparing S2 with S1 and S3 further indicates that the presence of at least one N-atom in the heterocycle without an adjacent substituent can result in large polarization values of the substrate without the coligand.

To compare the enhancements from substrates with a different functional group, a pyridine with a methyl instead of NH_2 substitution in the *ortho*-position was tested. The substrate 2-methylpyridine (S4) previously did not yield any ^{15}N signal enhancement in a SABRE-SHEATH (shield enables alignment transfer to heteronuclei) measurement with the Ir-IMes catalyst.[111] Here, no signal enhancement was observed with the Ir-^{Me}IMes catalyst without coligand addition. After the addition of acetonitrile, SABRE signals of this substrate were obtained, although the maximum enhancement value of -25 ± 7 obtained for H_6 is much smaller than those for the NH_2 substituted substrates, S1 and S3. An enhancement of -5 fold was also observed for the aliphatic CH_3 group. With the addition of allylamine, no signal enhancements were observed for S4. These observations show that the polarization for the CH_3 substituted molecules is less compared to the NH_2 substituted molecules for both coligands.

Table 3.1: Summary of the signal enhancements ε (calculated as a ratio of signal integrals from the SABRE spectrum to that of a spectrum at thermal equilibrium) of pyridine and pyrimidine substrates hyperpolarized in methanol-d_4 with 5 mM of Ir-catalyst and 50 mM of substrate and coligand. The temperatures indicated are where the highest enhancements were obtained for each of the substrates without and with coligand, amongst the temperatures scanned.

Substrate	Without coligand		With allylamine coligand		With acetonitrile coligand	
	ε	T/ K	ε	T/ K	ε	T/ K
S1	-7 ± 1 (H_6) -4 ± 1 (H_5)	298	-210 ± 20 (H_6) -170 ± 30 (H_5)	326	-160 ± 20 (H_6) -100 ± 10 (H_5)	318
S2	-150 ± 20 (H_2) -150 ± 30 (H_6) -90 ± 10 (H_5)	298	-230 ± 30 (H_2) -220 ± 20 (H_6) -160 ± 20 (H_5)	310	-110 ± 20 (H_2) -100 ± 20 (H_6) -70 ± 10 (H_5)	298
S3	-7 ± 3 (H_6) -6 ± 1 (H_4) -6 ± 1 (H_3 H_5)	298	-200 ± 30 (H_6) -160 ± 20 (H_4) -150 ± 10 (H_3 H_5)	326	-120 ± 30 (H_6) -100 ± 20 (H_4) -70 ± 10 (H_3 H_5)	318
S4	Not detected		0 > ε > -1 (H_6) 0 > ε > -1 (H_3) 0 > ε > -1 (H_5)	293	-25 ± 7 (H_6) -23 ± 7 (H_4) -13 ± 5 (H_3) -10 ± 7 (H_5)	288
pyridine	-220 ± 30 (H_1) -210 ± 30 (H_3) -170 ± 20 (H_2)	298	-410 ± 40 (H_1) -400 ± 40 (H_3) -320 ± 70 (H_2)	310	-170 ± 20 (H_1) -160 ± 10 (H_3) -120 ± 30 (H_2)	298

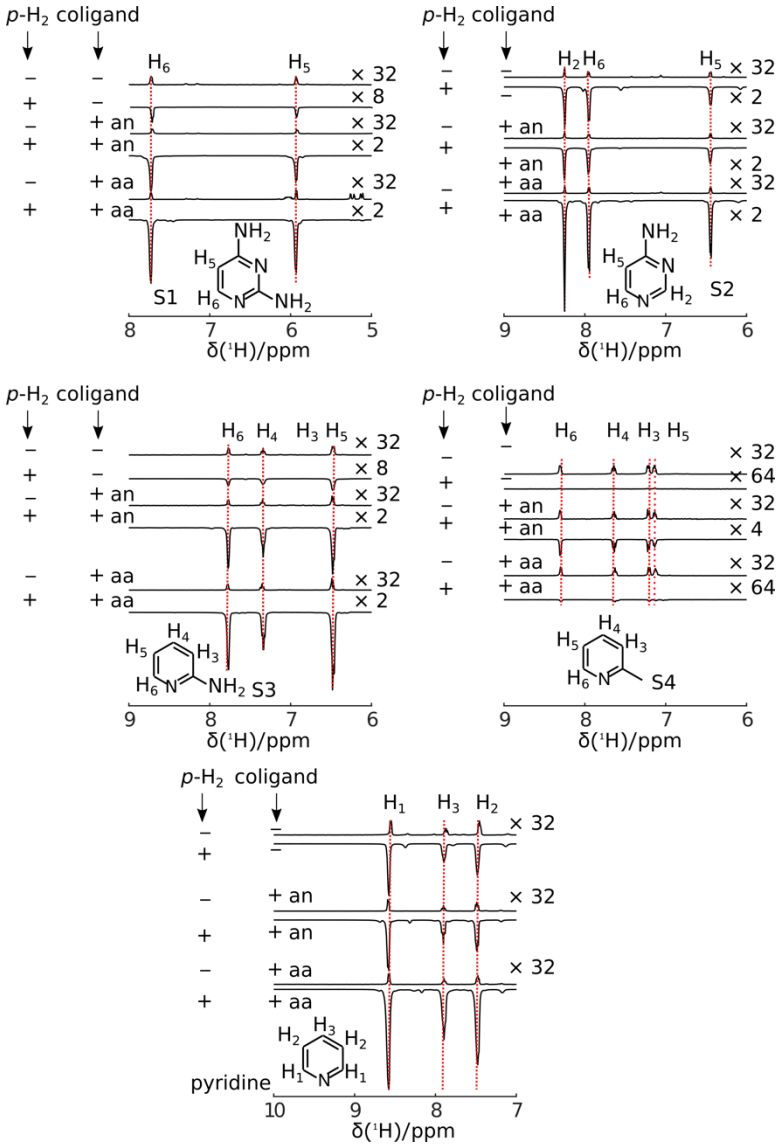

Figure 3.1: SABRE hyperpolarization of pyridine and pyrimidine substrates with and without addition of coligands. In each panel, the '+' and '−' signs in the first column indicate whether *para*-H_2 was introduced. The signs in the second column indicate the presence of the coligand acetonitrile (an) or allylamine (aa), or their absence. The solvent is methanol-d_4. *para*-H_2 was bubbled into the sample at 6.5 mT field for 30 s, and the spectra were acquired after manual transfer of the sample to 9.4 T in a time of 5 s. The temperature for *para*-H_2 bubbling in each sample is reported in Table 3.1.

Hence, it is observed that firstly, the addition of the coligands restores the polarization for substrates with NH_2 substitutions adjacent to the catalyst binding site to yield almost the same enhancements as for substrates without *ortho* substitutions. Secondly, the addition of coligands does not restore the enhancement for the CH_3 substituted ligand, *i.e.* the polarization efficiency depends strongly on the nature of the substituent and the substrate-coligand pair.

The large difference in signal enhancements of the substrates with NH_2 and CH_3 substituents after coligand addition is not explained by the steric bulk of the substrates. The steric bulk of the two compounds in transition metal complexes is expected to be similar, with similar calculated cone angle values of 110.7 degrees and 112.8 degrees, reported for cobaloximes.[112] Instead, an enhanced electron density at the N-atom of molecules with NH_2 substitutions may lead to more favorable binding to the Ir-center compared to the CH_3 substituted molecules, resulting in larger polarization values for the NH_2 substituted molecules. To exclude the possibility of spin-lattice (T_1) relaxation causing the low polarization of the CH_3 substituted substrate, the T_1 relaxation time of the substrates S3 and S4 was measured in the presence of acetonitrile and catalyst, under H_2-pressure (Figure 3.2). The T_1 values for the H_6 protons of S3 with NH_2 substitution (7.76 ppm) and S4 with CH_3 substitution (8.32 ppm) were calculated to be 10 s and 19 s respectively from an inversion recovery experiment. The difference in polarization for the two substrates with the different substituents is therefore not governed by the relaxation times.

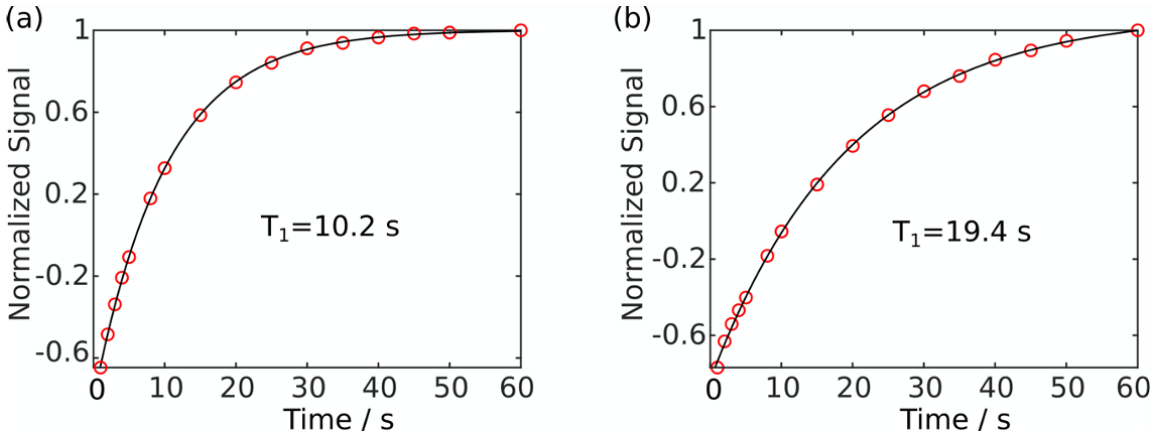

Figure 3.2: Inversion-recovery data for T_1 relaxation measurement of (a) free *ortho*-resonance of S3 (2-aminopyridine) and (b) free *ortho* resonance of S4 (2-methylpyridine).

3.2.2. Catalyst Activation

The hydride signals that arise due to the binding of *para*-H_2 to the metal center during the SABRE were analyzed to correlate with the enhancements observed without and with the coligands for the different substrates (Figure 3.3). Signals measured with pyridine as substrate are shown in Figure 3.3a. A transient intermediate species 1 can be observed after introducing *para*-H_2. After the activation is complete, this species disappears, and only the activated complex, the final tris substituted product 2, $[Ir(^{Me}IMes)(H)_2(pyridine)_3]Cl$, remains at -23.0 ppm. In the presence of the coligands, the peak corresponding to the activated complex changes, with the peak at -23.0 ppm being replaced by two distinct peaks. For acetonitrile, this is the species 2' with peaks at -21.2 ppm and -22.5 ppm and for allylamine species 2" with peaks at -22.5 ppm and -22.8 ppm, indicating that the coligands bind to the catalyst along with the substrate. For the substrate S2, the peak for the activated complex is also detected both in the absence and presence

of coligands. The observation of signals for the activated catalyst complex is in line with the large enhancement values obtained for these substrates both without and with the coligands.

Examining the spectra with the substrate S3 indicates smaller intermediate hydride signal 1, which disappear after bubbling *para*-H_2 for 10 seconds (Figure 3.3b). A signal that would be due to the activated complex [Ir(^{Me}IMes)$(H)_2(S3)_3$]Cl was not detected, likely because such a complex is sterically prevented from forming. When the coligands are separately included in the reaction mixture, metal hydride resonances representing the activated SABRE complex at -21.8 ppm and -22.6 ppm (2') with acetonitrile and at -22.8 ppm and -23.6 ppm (2") with allylamine are observed. In these spectra, the activated SABRE complex with S3 can only be detected in the presence of coligands. This observation correlates with the fact that a large SABRE polarization for S3 is obtained only with the addition of the coligand. Similar peaks for the activated complex with coligands are observed for the substrate S1 with NH_2 substitutions. For the substrate S4 with the CH_3 substitution, the signals corresponding to an activated complex were absent prior to the addition of coligand (Figure 3.3c). After the addition of coligands, these signals appear. However, the intensity is weaker compared to the S3 that contains an NH_2 substitution, suggesting that the concentration of the activated complex in solution is less for the CH_3 substituted molecules compared to the NH_2 substituted molecules.

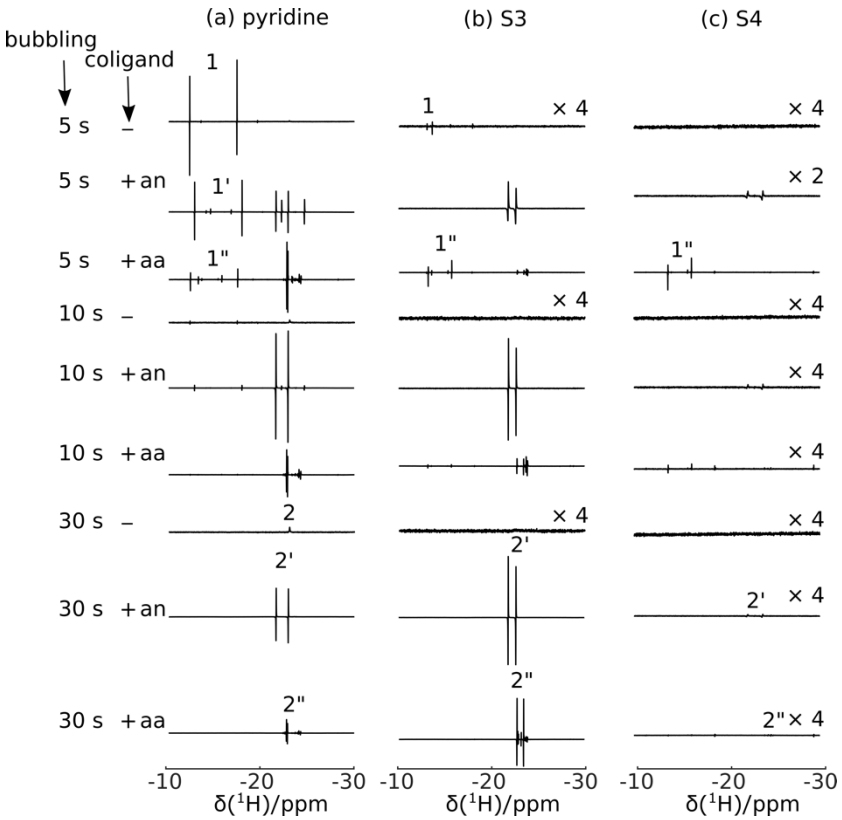

Figure 3.3: Hydride region of ^{1}H NMR spectra of the catalytic complex acquired with a hard π/4 pulse after bubbling *para*-H_2 into catalyst and substrate mixtures at 9.4 T. The substrates are pyridine, S3 and S4. Spectra are shown for a sample without ("–") and with ("+") addition of the coligand. The spectra were measured at time points of 5 s, 10 s and 30 s after initiation of bubbling of *para*-H_2. The species 1 corresponds to the reaction intermediate, and species 2 is the activated Ir-hydride species. The prime sign (') designates the corresponding species containing bound acetonitrile (an) and (") designates bound allylamine (aa).

In an electrospray ionization mass spectrum (ESI-MS) of a sample of activated Ir-catalyst with substrate S1 and acetonitrile, the major peak appears at m/z = 747.3222 (Figure 3.4) and with allylamine at m/z = 747.3240 (Figure 3.5). This mass corresponds to Ir(^{Me}IMes)(S1)$_2$(H)$_2$, indicating the presence of an activated complex with two substrate molecules. The presence of the two anti-phase metal hydride signals in 2' or 2" in Figure 3.3 indicates an asymmetric complex, where the two hyride positions are inequivalent.

This inequivalence may be caused by two different molecules, the substrate and the coligand, binding to positions trans to the hydrides. In the case of the NH_2 containig substrate S3, it could further be caused by the binding of an NH_2 group to one of the coordination sites. Although the NH_2 group may coordinate to the catalyst, the presence of the two antiphase hydride signals for S4 (-21.8 ppm and -23.5 ppm), which contains a CH_3 instead of an NH_2 group, would not be explained. Since the SABRE experiment results in hyperpolarization of the coligands in addition to the substrate molecules, it is likely that in both cases, the SABRE active complex comprises a substrate and a coligand molecule bound trans tot he hydrides.

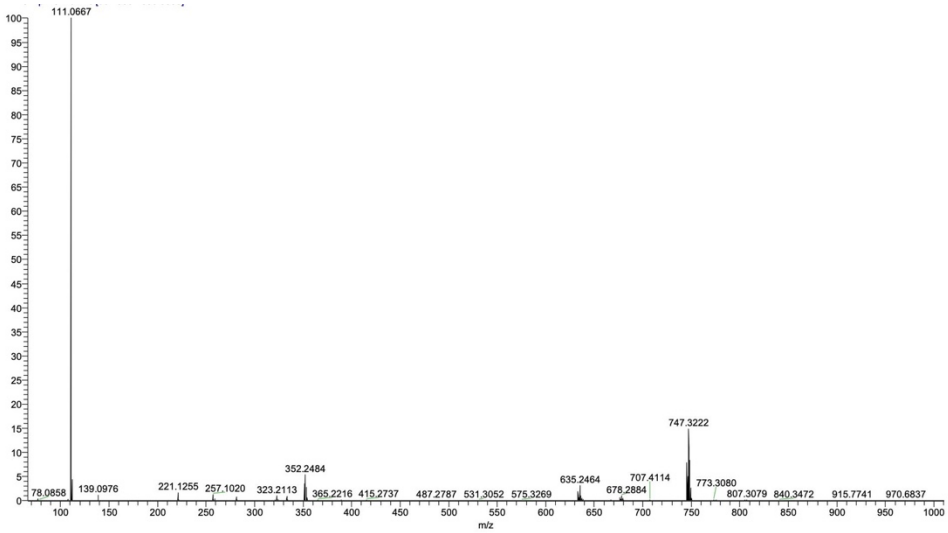

Figure 3.4: Positive ESI mass spectrum of the activated Ir-^{Me}IMes complex with 2,4-diaminopyrimidine (S1) as substrate and acetonitrile as coligand. The spectrum was measured of a sample after the SABRE was carried out.

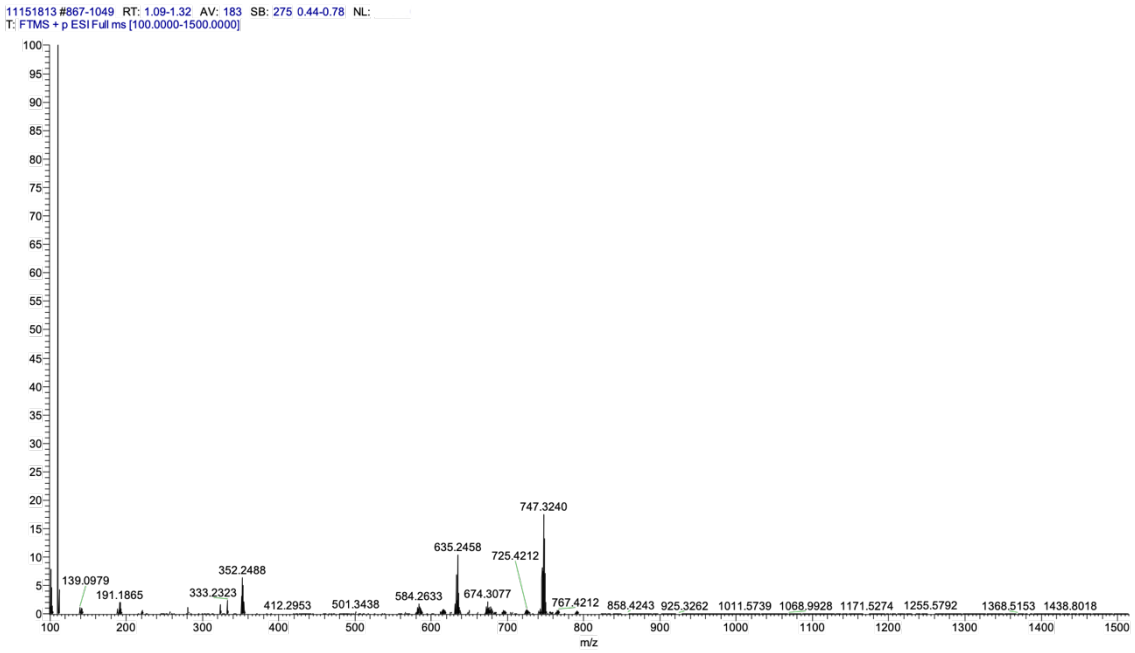

Figure 3.5: Positive ESI mass spectrum of the activated Ir-^{Me}IMes complex with 2,4-diaminopyrimidine (S1) as substrate and allylamine as coligand. The spectrum was measured of a sample after the SABRE was carried out.

3.2.3. Temperature Dependence of Polarization

The temperature affects the polarization values by changing the exchange rate for binding to the SABRE catalyst.[72] The temperature dependence of SABRE polarization for S1, S3 and S4 in the presence of coligands was measured (Figure 3.6). The substrates S1 and S3 with the NH_2 substitutions show a maximum signal with the coligands at a temperature near 320 K. In contrast, the substrate S4 with CH_3 substitution gives the highest polarization at the temperature of 288 K. Likewise, the substrate S2, as well as the model compound pyridine, without substitutions in the *ortho*-positions, require lower temperature compared to the NH_2 substituted molecules to show the maximum enhancements.

The higher temperature required for the NH_2 substituted molecules with the coligands indicates that the binding to the catalyst is stronger compared to the CH_3 substituted or unsubstituted molecules. This tight binding may be attributed to the strong electron donating property of the NH_2 group, which increases the basicity of the N-center in these molecules.

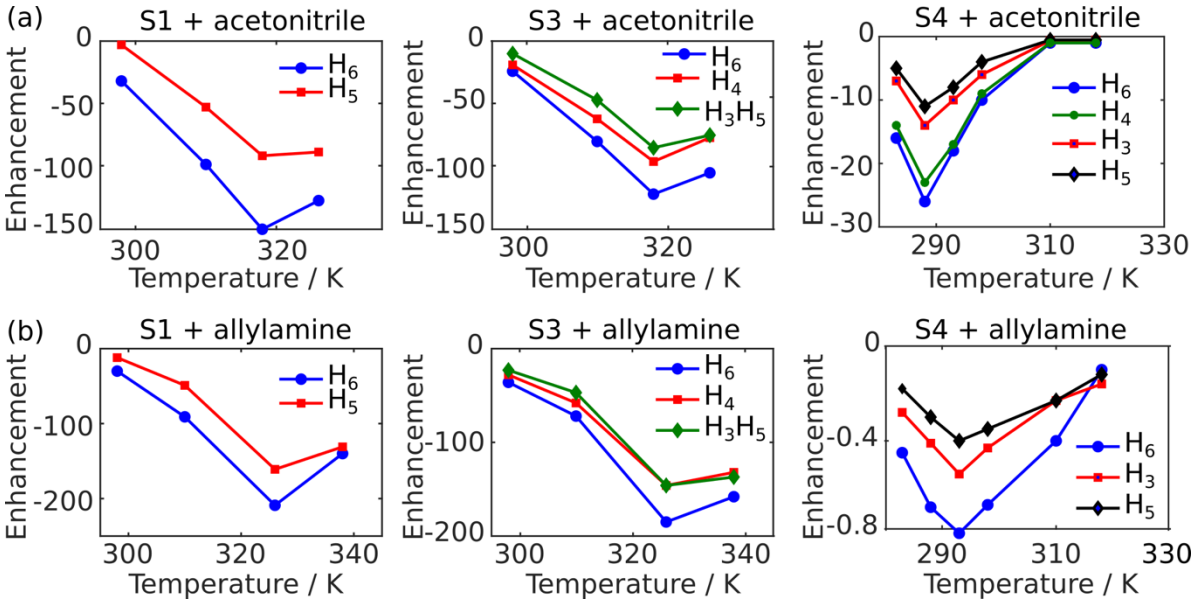

Figure 3.6: Dependence of signal enhancement of substrates as a function of temperature for a single run. Samples were prepared in methanol-d_4, polarized at a field of 6.5 mT, and measured after manual transfer to 9.4 T. The largest signal corresponds to the most negative enhancement. The panels correspond to (a) substrates with acetonitrile and (b) substrates with allylamine. The symbols representing the individual protons are indicated in the panels.

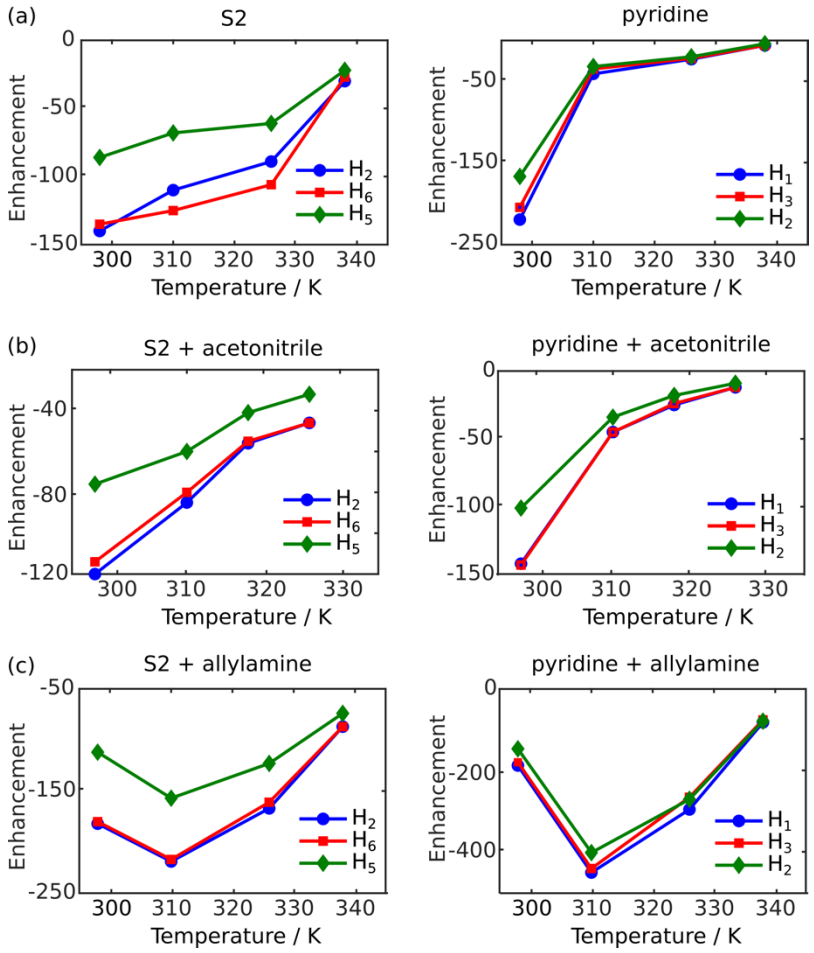

Figure 3.7: Dependence of signal enhancement of substrates S2 and pyridine on the temperature used for *para*-H_2 bubbling. Samples were prepared in methanol-d_4, polarized at a field of 6.5 mT, and measured after manual transfer to 9.4 T. The largest signal corresponds to the most negative enhancement. The panels correspond to (a) substrate (b) substrate + acetonitrile and (c) substrate + allylamine. The symbols representing the individual protons are indicated in the panels.

In order to compare trends in obtained signal enhancements with ligand exchange rates, exchange rates were measured at two different temperatures for S3 with acetonitrile (Figure 3.8). To determine the exchange rates, the *ortho* protons of bound 2-aminopyridine (S3) were selectively excited and after a variable waiting period, a spectrum was acquired.

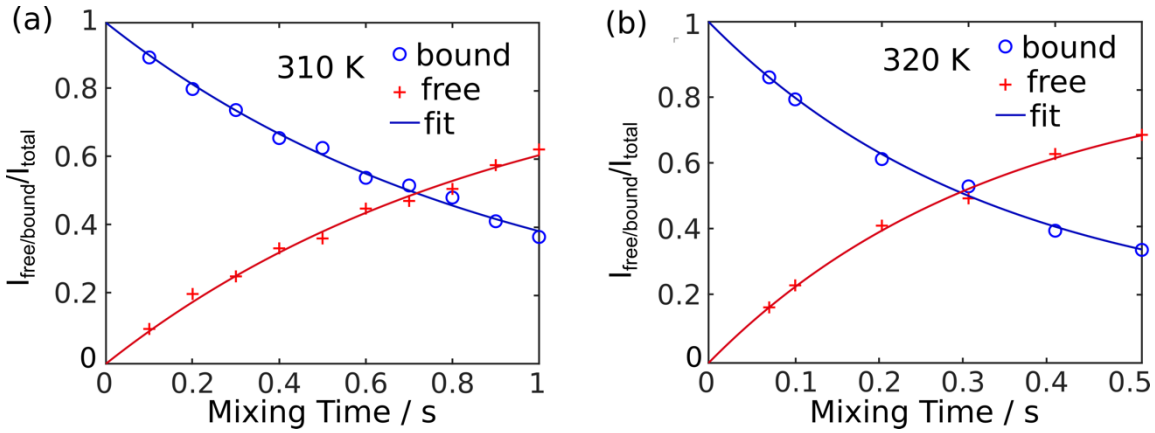

Figure 3.8: Plot of ratio of the signal integrals of free or bound form to the total signal integral ($I_{free/bound}/I_{total}$) as a function of the mixing time for sample with 5 mM catalyst with 50 mM S2 (2-aminopyridine) and 50 mM acetonitrile at (a) 310 K (b) 320 K The 'O' represents the bound form, the '+' represents the free form and the solid line represents the fit. The exchange rates k_1 are (a) 1.0 s^{-1} and (b) 2.8 s^{-1} respectively.

The signals for bound and free ligand were integrated and expressed as a fraction of the total signal. Exchange rates k_1 and k_2 were obtained by fitting the data according to a two-site exchange model where A is the bound resonance and B is the free resonance,

$$A \leftrightarrow B$$

$$\frac{dA}{dt} = -k_1 A + k_2 B \qquad (2.1)$$

$$\frac{dB}{dt} = k_1 A - k_2 B \qquad (2.2)$$

The higher temperature of 320 K, around where the highest SABRE enhancement was obtained for this substrate with the coligands, resulted in a ligand dissociation rate of 2.8 s^{-1}. At the lower temperature of 310 K, the dissociaiton rate was 1.0 s^{-1}. This value can be compared to a value of 1.04 s^{-1} reported for pyridine or 2.37 s^{-1} for metroindazole in

complexes of the type [Ir(IMes)(substrate)$_2$(coligand)]Cl at 298 K to show maximum enhancement for ^{1}H.[108]

3.2.4. Hyperpolarization of Trimethoprim

The NH_2 *ortho*-substituted pyridines and pyrimidines, which give high enhancement values with the addition of coligands to the Ir-^{Me}IMes catalyst, form the core structures for several biologically active enzyme inhibitors or substrates. The ability to hyperpolarize these molecules may assist in the characterization of enzyme mechanisms and metabolic pathways. Figure 3.9 illustrates the level of hyperpolarization that can be obtained for trimethoprim, an inhibitor of dihydro folate reductase (DHFR) that is used as an antibiotic drug. In the absence of any coligand, a maximum enhancement of -1 was achieved for this molecule, indicating that there is no benefit from the hyperpolarization. In the presence of the amine the enhancement increases to a value of -70 for the hydrogen atom (H_6) in the N-containing ring, and to -40 with acetonitrile addition. Further, the hydrogen atoms in the adjacent ring ($H_{2'}H_{6'}$) is hyperpolarized to an enhancement of -6. As the H_5 does not give observable SABRE signal, the polarization transfer may be due to dipolar interaction instead of through the *J*-coupling.

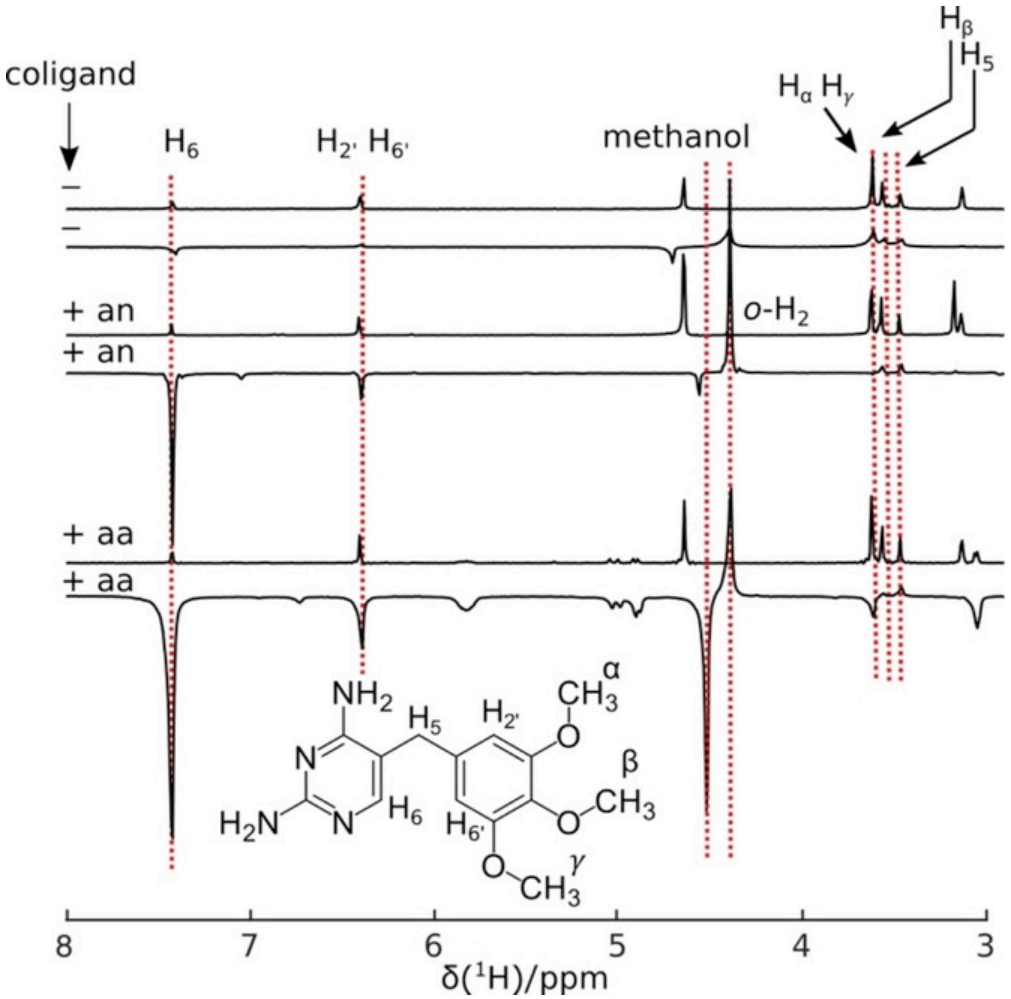

Figure 3.9: Non-hyperpolarized and hyperpolarized spectra of 35 mM trimethoprim without and with coligands in methanol-d_4 at 298 K. The maximum signal enhancement with the acetonitrile (an) was at 318 K and with the allylamine (aa) at 326 K. *Para*-H_2 was bubbled for 30 s at 6.5 mT followed by NMR measurement at 9.4 T

3.3. Discussion

Here, the NH_2 substituted pyridine and pyrimidine moieties are hyperpolarized with a catalyst containing the widely used IMes motif. The addition of a coligand, either allylamine or acetonitrile, most likely by resolving steric hindrance, allowed to achieve enhancement levels comparable to the model compound pyridine. Further, the signal

enhancement of pyridine was not attenuated by coligand addition. By contrast, CH_3 substituted molecules were polarized to a significantly smaller extent. Based on the temperature dependence of the NMR signals, this difference is attributed to a stronger binding of the ligand with an electron donating NH_2 substitution, which causes the optimal ligand exchange rate for SABRE hyperpolarization to occur at a higher temperature.

These results may be compared with an asymmetric, bidendate catalyst containing a Phox group (Phox = 2- (2-(diphenylphosphanyl)phenyl)-4,5-dihydrooxazole), which was recently developed for SABRE. The hyperpolarization of substituted pyridines including 2-methylpyridine and 2-fluoropyridine was reported for the Phox based catalyst. Hyperpolarization was achieved without using a coligand, which was attributed to the reduced steric bulk of the ligand sphere. Interestingly, this catalyst resulted in a low polarization value for pyridine, which is otherwise often used as a model compound for SABRE polarization.

SABRE catalysts with phosphine ligands were previously found to exhibit lower substrate exchange rates than catalysts with NHC ligands. A corresponding difference in the property of the two catalysts in modulating the exchange rates may have allowed the Phox catalyst to stabilize the SABRE complex for 2-methylpyridine but decreasing the polarization for pyridine. The increase of polarization by coligand addition for the NH_2 substituted molecules with the ^{Me}IMes ligand here suggests that the exchange rate for SABRE with this catalyst might be more favorable for this molecule, compared to the weakly binding CH_3 substituted molecule.

3.4. Conclusion

Pyridine and pyrimidine moieties with NH_2 substitutions in the *ortho*-position are ubiquitous in biological molecules and play an important role in drug-motifs. This class of molecule was shown to be hyperpolarizable with a commonly used SABRE catalyst upon coligand addition. The larger enhancement of the NH_2 substituted molecules compared to the CH_3 substituted ones was attributed to the difference in binding affinity of the two molecules due to the difference in electron density, as the steric bulk and the T_1 relaxation times under the experimental conditions do not account for these differences. The SABRE provides a fast and renewable way to generate hyperpolarized molecules in solution. Broadening the pool of compounds that can be hyperpolarized by this process may open future applications such as the characterization of protein-ligand binding and drug-discovery.

3.5. Experimental Section

3.5.1. Sample Preparation

Samples for NMR consisted of 5.0 mM of SABRE pre-catalyst mixed with 50 mM of the pyridine and pyrimidine substrates (S1 - S4 (Sigma-Aldrich, St. Louis, MO)) in 500 µl methanol-d_4 (Cambridge Isotope Libraries, Andover, MA) prepared in the glovebox under argon atmosphere. The precatalyst was Ir(COD)(Cl)(^{Me}IMes) with ^{Me}IMes =4,5-dimethyl-1,3-bis(2,4,6-trimethylphenyl)imidazol-2-ylidene (Strem Chemicals, Newburyport, MA). For the experiments with coligands, 50 mM allylamine (Alfa Aesar, Tewksbury, MA) or acetonitrile (Sigma Aldrich) was included in addition. For

hyperpolarization of trimethoprim (Alfa Aesar), 35 mM of the substrate was polarized with 35 mM coligand.

3.5.2. *Para*-hydrogen Polarization

Para-hydrogen (*p*-H_2) enriched gas (~50% *para*-spin state prepared by passing H_2 gas over iron(III)oxide (Sigma-Aldrich) in a heat exchanger immersed in liquid nitrogen) was bubbled through the sample solutions at a flow rate of ~8 (standard mL)·s^{-1} and a pressure of $8.3 \cdot 10^5$ Pa. The Ir-^{Me}IMes precatalyst was activated in the NMR spectrometer (Bruker Biospin, Billerica, MA) at 9.4 T and at 303 K, by bubbling *p*-H_2 into the samples. The activation was monitored by observing the ^{1}H chemical shifts of the metal hydride species between -10 and -25 ppm in spectra acquired following a hard pulse with flip angle of π/4. The SABRE experiments were carried out by bubbling *p*-H_2 into the samples located in a magnetic field of 6.5 mT, for 30 s (Figure 3.10 and 3.11). The field was generated by a solenoid (diameter 22 cm and length 28 cm). To identify the range in which maximum enhancement occurs, four temperatures were scanned at an interval of nominally 10 K. The sample temperature during bubbling was adjusted using a stream of air at a regulated temperature (FTS Systems Kinetic Air Jet Temperature Controller TC-84). The actual temperature in the coil close to the sample was measured with a thermocouple. After the *p*-H_2 bubbling was stopped, the sample was manually transferred within 5 s into the 9.4 T magnet. SABRE NMR spectra were acquired following a π/2 hard pulse.

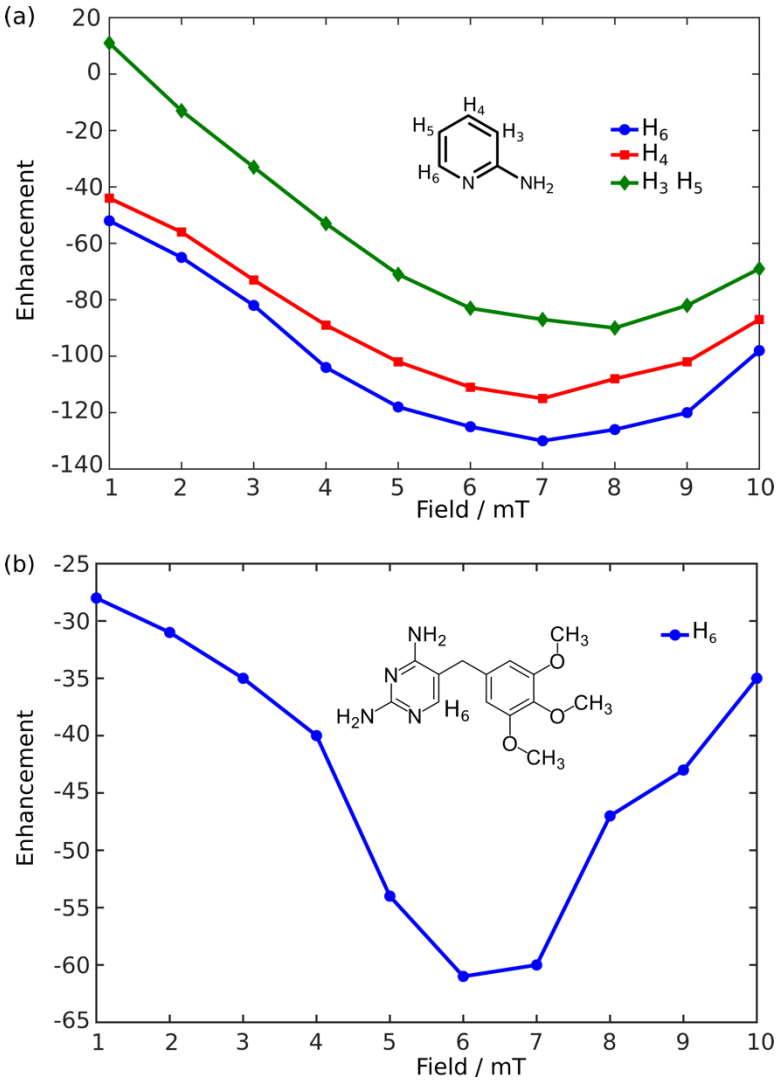

Figure 3.10: The field dependence of enhancement for (a) 5 mM Ir-^{Me}IMes catalyst and 50 mM S3 with 50 mM acetonitrile coligand at 318 K and (b) 3.5 mM Ir-^{Me}IMes catalyst and 35 mM trimethoprim with allylamine coligand at 323 K. Signals were measured after manual transfer to 9.4 T.

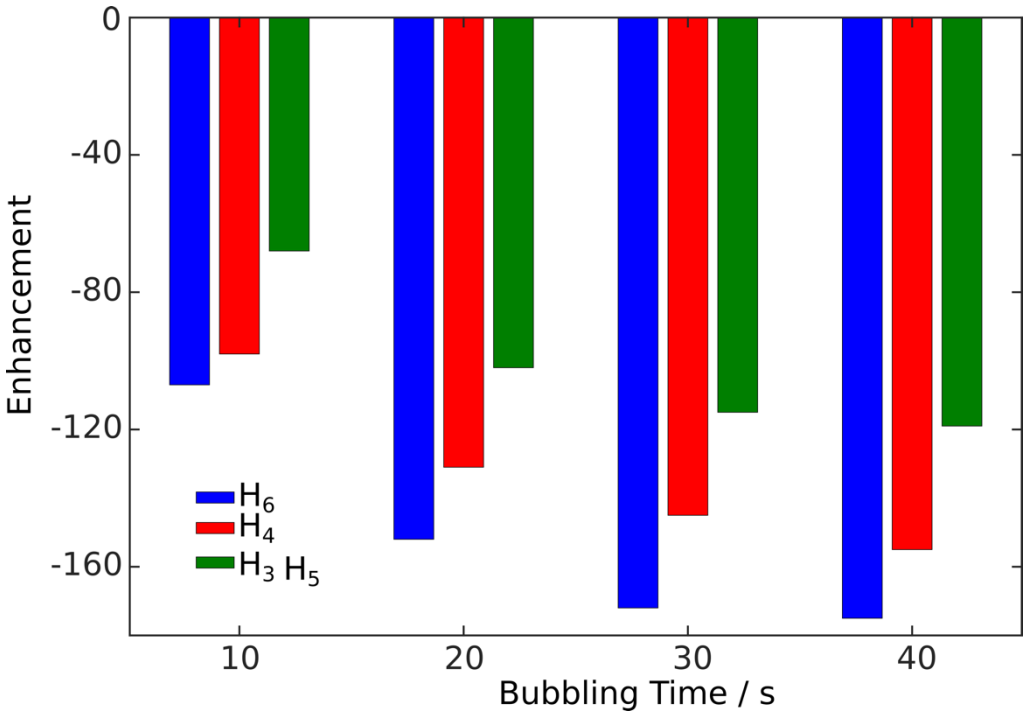

Figure 3.11: The dependence of signal enhancement on the *para*-H_2 bubbling time for 5 mM Ir-^{Me}IMes catalyst and 50 mM S3 with 50 mM acetonitrile coligand. The magnetic field during bubbling was 6.5 mT. Signals were measured after manual transfer of the sample into a 9.4 T NMR spectrometer.

4. CHARACTERIZATION OF PROTEIN-LIGAND INTERACTIONS BY SABRE*

4.1. Introduction

Nuclear spin hyperpolarization has the potential to extend on biological applications of NMR by enhancing signals of molecules including ligands, enzyme substrates, proteins and others. Using hyperpolarized molecules, spectroscopy under conditions close to physiological concentration becomes possible. NMR detection is thus brought closer to the realm of widespread but less structurally specific detection methods for biological interactions, such as fluorescence spectroscopy.

Hyperpolarization techniques are readily applicable for the detection of the binding of small molecules to proteins. Non-hyperpolarized NMR alone is a recognized technique for the screening of these interactions in drug discovery. The utility of hyperpolarization by dissolution dynamic nuclear polarization (D-DNP)[13] has previously been demonstrated for ligand binding experiments. A reduction in the required target protein concentration can potentially enable NMR based ligand binding experiments with a broader range of proteins that are difficult to purify or that are unstable. D-DNP is capable of hyperpolarizing ^{13}C, ^{1}H, ^{19}F and other nuclei in small molecules. One way of identifying binding of drug candidates is by observing the unique signals from ^{19}F. Different methods of detection are applicable in the strong-, weak- and intermediate- binding regimes, reaching up to dissociation constants in the hundreds of micromolar.[22] These include the

*Reprinted with permission from "Characterization of protein-ligand interactions by SABRE" by Mandal, R.; Pham, P.; Hilty, C. *Chemical Science*, **2021**, Copyright Royal Society of Chemistry

direct detection of broadened signals from bound ligands, as well as of changes in or other relaxation rates in the presence of fast exchange between free and bound forms. Broadening the range of possible applications, molecules containing ^{19}F can be used as reporter ligands for the screening of non-fluorinated ligands in binding competition experiments.[23]

Spin hyperpolarization, such as of ^{1}H, can transfer from a ligand to the macromolecule,[20] transfer within two sites in a ligand,[113] or transfer between two competitively binding ligands.[114] Each of these cases offers a pathway to detecting the binding of the ligand. The polarization transfer provides added information on the proximity of the spins involved, which is useful to determine the structure of the binding epitope.[115] Fast multi-dimensional and pseudo multi-dimensional NMR spectroscopy of the hyperpolarized ligand and macromolecule provide the necessary spin correlations.[21] The structures are then determined with the assistance of simulations of the signals arising from a network of dipolar coupled spins in combination with computational optimization or scoring procedures.

The effectiveness of spin relaxation or polarization transfer parameters in identifying a small fraction of bound ligand increases with increasing molecular weight. For this reason, methods of hyperpolarized NMR for the detection of ligand binding are applicable to immobilized proteins, which can further reduce protein consumption in screening experiments.[113] In addition to ligands, D-DNP can be used to directly hyperpolarize polypeptides, such as in the denatured form.[116] The protein folding process and protein-protein interactions can be characterized in real-time on a time scale of several

seconds. Similar information is available if proteins or nucleic acids receive polarization transfer from previously hyperpolarized water.[17,117] Water protons exchange with labile protons on amide or hydroxy groups in macromolecules. Enhanced signals observed for the corresponding positions provide sequence specific information on solvent exposure and molecular dynamics.[118]

The above-described modalities of applying hyperpolarization present significant advantages for specific, selective, and highly sensitive NMR spectroscopy of biological molecules. A barrier to entry into the use of these techniques is the added complexity in the instrumentation that is required to generate the hyperpolarized spin states. For example, a D-DNP instrument that is co-sited with an NMR spectrometer comprises an additional superconducting magnet with variable-temperature insert, a microwave source to saturate an electron spin transition, and a dissolution system.

Here, we demonstrate the application of an alternative hyperpolarization technique, signal amplification by reversible exchange (SABRE),[50] to the detection of protein-ligand interactions. SABRE, based on *para*-hydrogen,[41,42] is among the most inexpensive hyperpolarization methods. Molecular hydrogen spontaneously transfers to the anti-parallel *para*-spin state at cryogenic temperatures in the presence of a paramagnetic spin flip catalyst. The ordered spin state of *para*-hydrogen gas is then converted into hyperpolarization of nuclear spins on a target molecule. This conversion occurs either by catalytic hydrogenation in *para*-hydrogen induced polarization (PHIP), or by binding to a polarization transfer catalyst facilitating SABRE. Signal enhancements

of at least thousands-fold for PHIP and hundreds-fold for SABRE are routinely obtained, whereby SABRE does not require a substrate undergoing a chemical change.

SABRE polarization transfer catalysts are organometallic complexes that bind an electron donating group in the target molecule, often an N-heterocycle, together with H_2 in a co-planar arrangement. Ligands of the catalyst, like the N-heterocyclic carbenes, are chosen for an appropriate substrate exchange rate and to provide solubility. SABRE was successfully applied to hyperpolarize biological and bioactive molecules. Several drug molecules with nitrogen containing heterocycles that enable catalyst binding were hyperpolarized for ^{1}H[119,120] and ^{15}N.[113,114] The structure of the target molecules, especially when containing substituents near the catalyst binding site necessitates the design of matching catalysts with requisite binding affinities that allow appropriate exchange rates for efficient polarization.[57,58]

Several methods have been developed for achieving SABRE in biocompatible solvents. These include developing water soluble catalysts,[123,124] hyperpolarizing in D_2O and ethanol mixtures,[125] water addition to activated catalyst samples and subsequent methanol evaporation to achieve a methanol component as low as 10%[75] and aqueous reconstitution of the activated SABRE catalyst in pure D_2O.[74] Molecular probes for magnetic resonance imaging have been hyperpolarized using SABRE.[104,121,126] These probes are designed to contain nuclei with long relaxation times, such as ^{15}N, to retain polarization in biomedical imaging experiments.

A challenge in applications of several hyperpolarization techniques is the potential for interference of polarizing agents with the goal of the experiment. In D-DNP

experiments, free radicals are needed to provide spin polarization. Radicals have been removed by chemical reaction, physical separation, or quenching in some *in vitro*, as well as *in vivo* applications. In SABRE, the analogous agent is the polarization transfer catalyst. This catalyst needs to be removed for *in vivo* experiments as the catalyst is identified as the main reason for toxicity of the SABRE approach.[125] Catalyst removal by using chelating ligands[62] and phase separation[64] combined with metal scavengers has been developed to produce biocompatible hyperpolarized samples that are metal-free. Other experiments may have less strict requirements, however, when employing SABRE for monitoring of chemical reactions, the polarization transfer catalyst was reported to modulate the rates of organic reactions.[68] Chelating agents, such as 1,10-phenanthroline and 2,2'-bipyridine, were introduced into the reaction mixture after completion of polarization transfer from *para*-hydrogen, to prevent or reduce effects from binding of other molecules to the catalyst.[62]

In this chapter, we use SABRE to identify binding of a ligand to the trypsin protease. A ligand containing a well-known binding motif for trypsin, as well as a binding site for the polarization transfer catalyst in a different location, is hyperpolarized. The incompatibility of SABRE catalysts with proteins, as well as low polarization efficiency in water, is overcome by a two-step approach. The ligand is first hyperpolarized separately and subsequently injected with the protein for detection. The resulting changes in relaxation rates due to binding of the ligand are analyzed and applications are discussed.

4.2. Results and Discussion

Serine proteases including trypsin are inhibited by amidine containing ligands including benzamidine, forming a salt bridge with an aspartate residue in the active site of the protein.[127] Although the amidine group contains nitrogen atoms, its presence in the cationic form would prevent efficient catalyst binding. SABRE hyperpolarization of benzamidine was not observed using a typical catalyst [Ir(^{Me}IMes)(COD)]Cl (COD=cyclooctadiene, ^{Me}IMes=4,5-dimethyl-1,3-bis(2,4,6 trimethylphenyl)imidazol-2-ylidene). The putative ligand chosen for hyperpolarization was 4-amidinopyridine (Figure 4.1). For the resulting molecule 4-amidinopyridine, SABRE hyperpolarization was observed using [Ir(^{Me}IMes)(COD)]Cl, however, higher signal enhancements were obtained with the asymmetric catalyst [Ir(IMeMes)(COD)]Cl (IMeMes=1-(2,4,6-trimethylphenyl)-3-methylimidazol-2-ylidene.[56] The active form of this catalyst is in the following referred to as Ir(IMeMes). Signal enhancements ranging from -87 and -34 for 1.5 mM 4-amidinopyridine to -230 and -110 for 10 mM 4-amidinopyridine, for the H atoms in the ortho and meta positions with respect to the N was obtained. The nuclear spin polarization increases from 0.003% for ^{1}H at a magnetic field of 9.4 T at 298 K to 0.26% and 0.69% for the H_a enhancement values of -87 and -230, respectively. The spectrum for the 1.5 mM condition is shown in Figure 4.1. This condition was used for the protein ligand interaction data at lower concentration (see below; Figure 4.10). SABRE NMR spectra for the other ligand concentrations are included in Figure 4.2. This confirms that the heterocyclic ring promotes binding to the polarization transfer catalyst. The difference

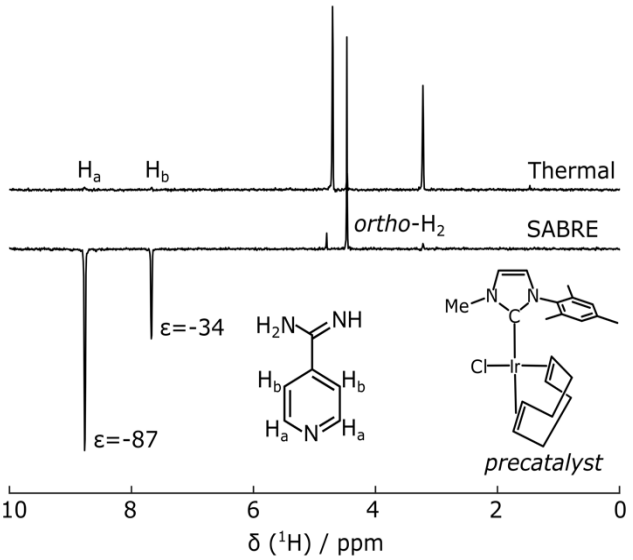

Figure 4.1: 400 MHz NMR spectra of 1.5 mM 4-amidinopyridine with 0.3 mM Ir(IMeMes) polarization transfer catalyst in d_4-methanol (a) non-hyperpolarized ("thermal") and (b) SABRE after bubbling for 30 s in a 6.5 mT magnetic field at 294 K, followed by acquisition at 9.4 T. The structures of the 4-amidinopyridine, and of the precatalyst before activation, are inset.

in polarization efficiency between the two catalysts is likely due to the reduced steric hindrance in the asymmetric catalyst, as the *para*-substituted substrates can also exhibit steric effects.[128]

Despite the ability to hyperpolarize 4-amidinopyridine, the methanol solvent used in Figure 1 would not be conducive to biological applications such as the characterization of ligand binding. For this reason, SABRE polarization was attempted in a mixture of 50% v/v of methanol-d_4 and D_2O buffer. Under these conditions, the enhancement decreased from -93 to -3 for H_a and -46 to -1 for H_b, which would be insufficient for the experiment. The signals were further reduced if the protein was included in the mixture.

Given that the Ir(IMeMes) polarization transfer catalyst is incompatible with a one-pot reaction mixture that includes the protein, a two-step process was designed for

characterizing the protein-ligand interactions using SABRE hyperpolarization. The molecule to be hyperpolarized separately underwent polarization transfer from *para*-hydrogen in methanol-d_4, and was subsequently mixed with a protein solution. This two-step procedure is congruous with previous experiments employing D-DNP for the determination of ligand binding.[129]

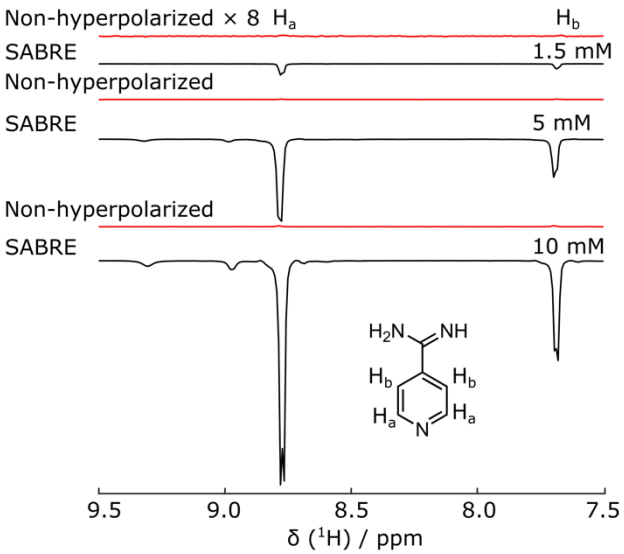

Figure 4.2: Non-hyperpolarized (red -) and hyperpolarized (black -) spectra of 4-amidinopyridine at different ligand concentrations of 1.5 mM, 5 mM and 10 mM. The enhancements obtained were -87 and -34 for H_a and H_b at 1.5 mM concentration, -140 and -60 for H_a and H_b at 5 mM concentration and -230 and -110 for H_a and H_b at 10 mM concentration.

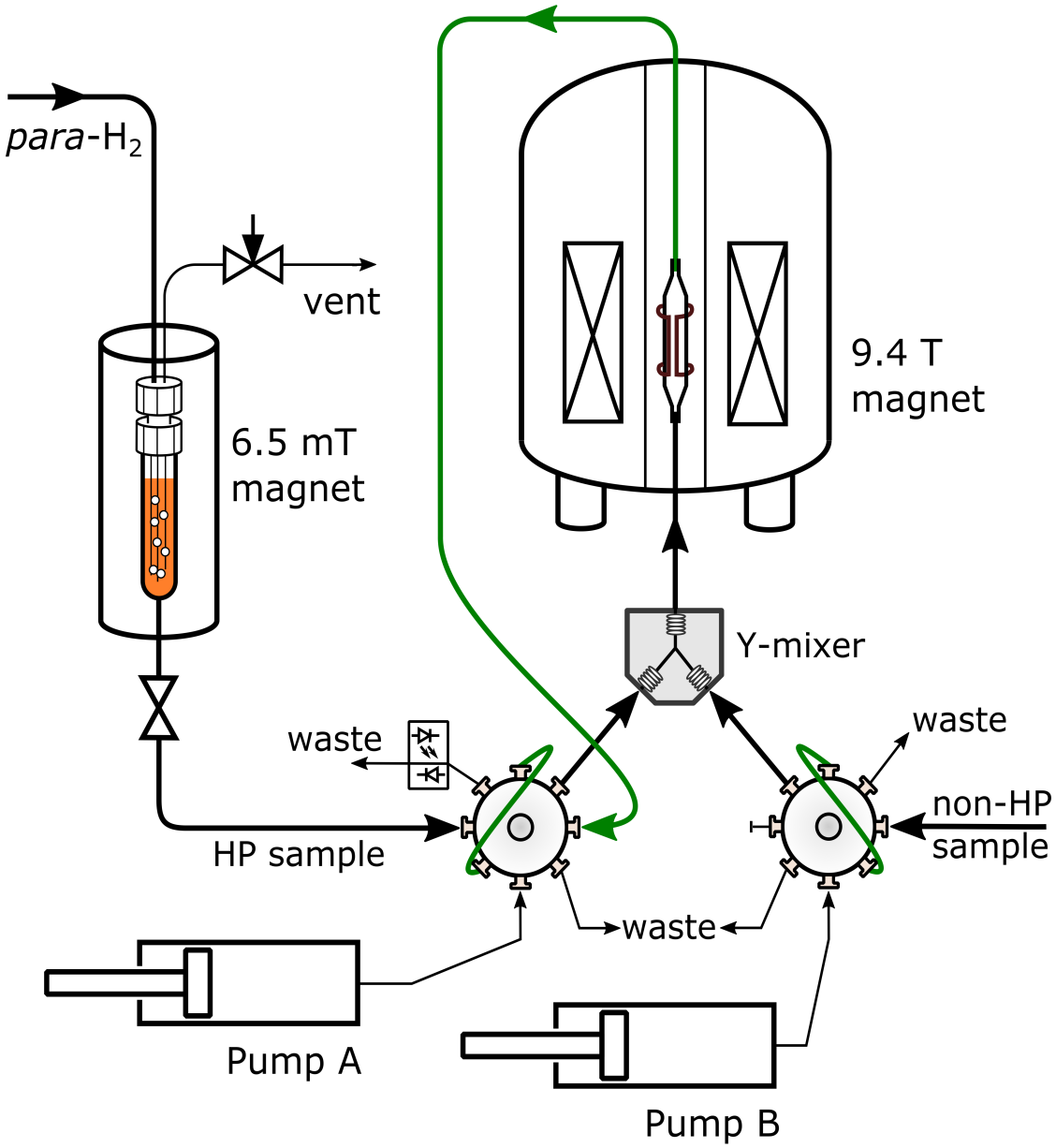

Figure 4.3: Instrument for SABRE NMR measurements of ligand binding. The putative ligand interacts with *para*-hydrogen and polarization transfer catalyst at 6.5 mT. It is subsequently delivered to a sample loop. The ligand and protein samples are pushed by high-pressure syringe pumps through the Y-mixer, to a flow-cell in the NMR magnet, where the measurement takes place.

For SABRE polarization, the solution of the putative ligand with polarization transfer catalyst in methanol-d_4 underwent bubbling with *para*-hydrogen gas (Figure 4.3). These conditions are optimal for polarization transfer. The sample was located in an electromagnet producing the required field of 6.5 mT (see also Experimental Section). Following this polarization step, a discharge valve was opened. Under the pressure of the hydrogen gas, the solution was delivered to an injection valve with sample loop. Injection into a flow-cell installed in the 9.4 T NMR magnet was driven by water from high-pressure syringe pumps, simultaneously for the putative ligand and the protein sample. The two samples mixed in a Y-mixer prior to entering the NMR magnet. A stationary mixture in the flow-cell was obtained by switching the injection valve prior to NMR data acquisition. Single-scan Carr-Purcell-Meiboom-Gill (CPMG) NMR experiments were acquired to measure the transverse relaxation rate (R_2) of the ^{1}H spins of the putative ligand molecule. Spectra obtained from Fourier transforms of selected individual spin echoes are shown in Figure 4.5. Figure 4.5a contains signals from the ligand alone, where hyperpolarized ligand solution in methanol-d_4 was mixed at a ratio of 3:7 (v/v) with a D_2O buffer that did not contain any protein. The hyperpolarized signal from the putative ligand near 8 ppm is strong in the first echo, and decays during the experimental time. The water signal near 4.7 ppm was suppressed using selective pulses and pulsed field gradients. A residual water signal is visible in the spectra, as the syringe pumps used to drive the samples were filled with H_2O. The spectral resolution is limited by the echo time in the CPMG experiment, which is 1.7 ms. The two peaks from the hyperpolarized 4-amidinopyridine molecule seen

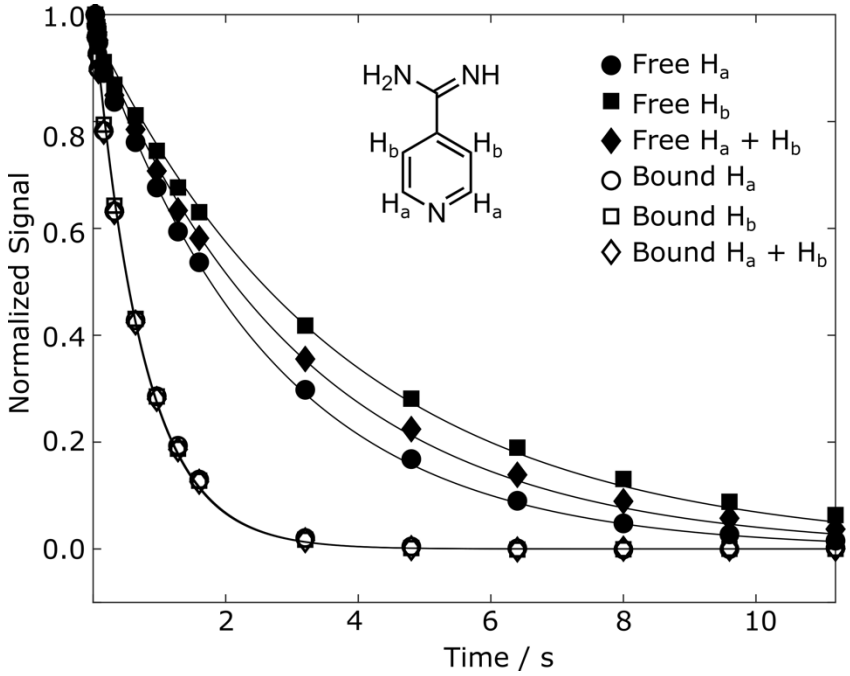

Figure 4.4: R_2 rate determination of 8 mM 4-amidinopyridine without hyperpolarization in 50 mM aqueous sodium phosphate buffer. The filled symbols are for the free ligand and the open symbols for the ligand with trypsin. The rates of the free form are 0.38 s^{-1} for H_a (●), 0.26 s^{-1} for H_b (■), and 0.32 s^{-1} for both protons integrated together (♦). The rates of the bound forms are 1.35 s^{-1} for H_a (O), 1.36 s^{-1} for H_b (□), and 1.35 s^{-1} for both protons integrated together (◊).

in Figure 4.1 merge into one observed signal. Still, this signal of interest is well separated from the residual water signal, and can be analyzed to result in an averaged relaxation rate for the putative ligand. After integration of the signals from each echo, an exponential decay is observed (Figure 4.5b). The R_2 relaxation is obtained by fitting a single exponential curve, here resulting in a value of 2.40 s^{-1} for the 4-amidinopyridine without the presence of protein. This relaxation rate is much larger than R_2 = 0.32 s^{-1} that was determined from a non-hyperpolarized NMR experiment for the same molecule shown in Figure 4.4. The difference in these relaxation rates was found to be due to the presence of the polarization transfer catalyst, as a direct consequence of binding of the molecule to the

Ir center of the catalyst. Similar relaxation changes due to catalyst binding have previously been observed.[62,68] After including a chelating ligand, 2,2'-bipyridine,[33] with the buffer solution to trap the catalyst, the relaxation rate of the hyperpolarized signal was found to be slower, with R_2 = 0.71 s^{-1} (Figures 4.5c and 4.5d). Finally, upon the addition of the trypsin protein, the relaxation rate increased to R_2 = 2.28 s^{-1} (Figures 4.5e and 4.5f).

A summary of the measurements under the different experimental conditions, including several repetitions, is included in Table 4.1. The changes in the observed relaxation rates are represented in Figure 4.6. The comparison of the non-hyperpolarized experiment with R_2-relaxation rate 0.39 ± 0.06 s^{-1} (green bar) with the "ligand + catalyst" (first gray bar) indicates a significant relaxation effect due to the interaction of the hyperpolarized molecule with the polarization transfer catalyst with the R_2 rate 2.30 ± 0.44 s^{-1}. This effect is largely reversed by the addition of the 2,2'-bipyridine (second gray bar). The chelating agent therefore significantly improves the ability to measure the relaxation properties of the free ligand with values 0.86 ± 0.15 s^{-1}. A smaller difference in the rates between the "ligand" (green bar) and the "ligand + catalyst + chelating ligand" (second gray bar), which narrowly exceeds the error limit, is likely due to a residual fraction of catalyst not trapped by the 2,2'-bipyridine chelating ligand. Finally, the inclusion of the protein leads to a significant increase in the relaxation rate with R_2 values 2.16 ± 0.10 s^{-1} (third gray bar). This increase is due to the slower tumbling of the protein-ligand complex in solution hence proving the binding of the ligand to the protein. Importantly, it can be seen that, firstly, the change in the relaxation rate that demonstrates the binding and therefore represents the result of the experiment is highly significant. Secondly, the change

is only observable after removing the relaxation contribution that is introduced by the polarization transfer catalyst.

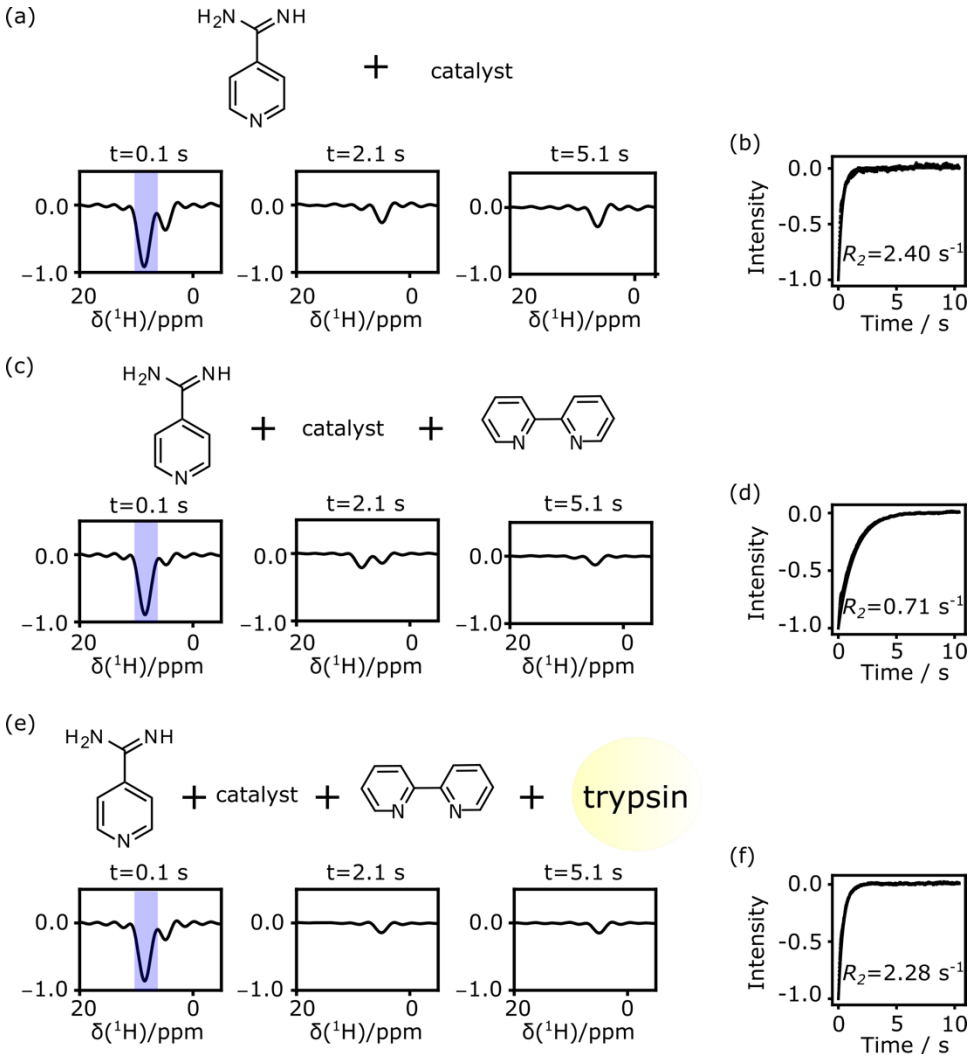

Figure 4.5: Hyperpolarized signals measured using a CPMG experiment. a) Selected spectra from individual spin-echoes of 7.2 mM 4-amidinopyridine with polarization transfer catalyst in 36% methanol in final sample. b) Signal decay and exponential fit of integrals are from (a). c) Spectra from 6.8 mM 4-amidinopyridine, catalyst, and 3.9 mM chelating ligand 2,2'-bipyridine in 34% methanol in the final sample. d) Signal decay and exponential fit of integrals are from (c). e) Spectra from 5.9 mM 4-amidinopyridine, catalyst, 3.0 mM 2,2'-bipyridine and 0.33 mM trypsin in 30% methanol in final sample. f) Signal decay and exponential fit of integrals are from (e).

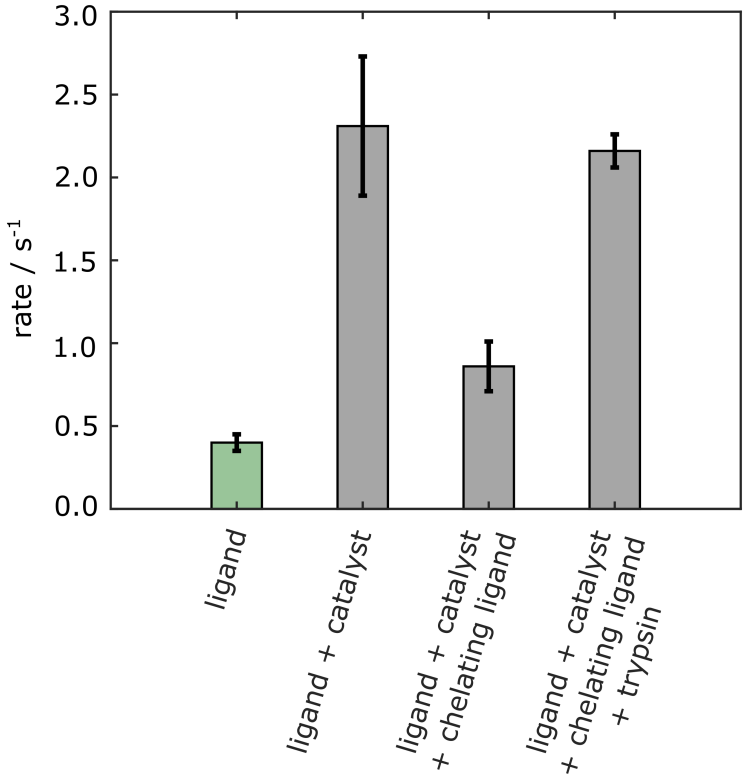

Figure 4.6: R_2 relaxation rates of 4-amidinopyridine. The green bar is from a non-hyperpolarized experiment in the absence of polarization transfer catalyst. The gray bars are from 4-amidinopyridine hyperpolarized by SABRE. Errors are shown as standard deviations from three separate measurements taken from different samples (Table 4.1).

The result of this experiment is in agreement with competitive binding measurements of 4-amidinopyridine to trypsin measured by NMR (Figure 4.7). These measurements indicated a dissociation constant for 4-amidinopyridine that lies in-between the those of the related known ligands for trypsin, benzamidine and 4-(trifluoromethyl)benzene-1-carboximidamide.

Table 4.1: The experimental parameters and the fitted R_2 relaxation rate for each experiment are summarized below in Table 4.1.

[ligand] / mM	[catalyst] / mM	[bipyridine] / mM	[protein] / mM	[ligand]/ [protein/	R_2 / s^{-1}
7.30	1.27	-	-	-	2.40
7.22	1.26	-	-	-	1.86
7.62	1.33	-	-	-	2.68
7.90	1.38	2.81	-	-	1.01
6.80	1.12	3.95	-	-	0.71
7.32	1.28	2.87	-	-	0.86
5.87	0.93	3.02	0.33	17.8	2.28
6.90	1.21	2.53	0.28	24.4	2.10
6.43	1.12	2.73	0.27	23.5	2.11
0.134	0.03	1.14	-	-	0.88
0.125	0.03	1.12	0.0072	17.4	1.89

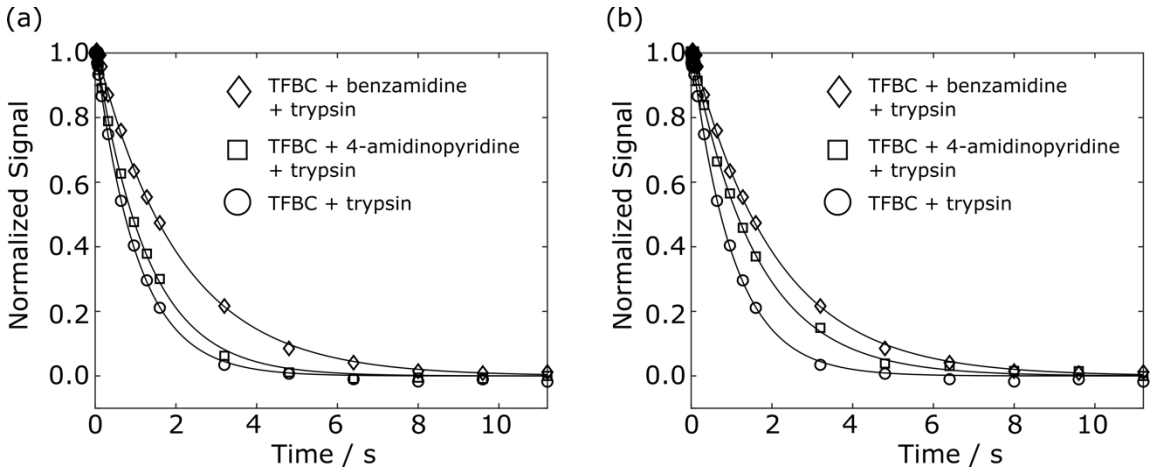

Figure 4.7: Competitive binding experiment with samples prepared in 50 mM sodium phosphate buffer of (a) 1 mM TFBC and 18 µM trypsin (O), 1 mM TFBC, 400 µM 4-amidinopyridine and 18 µM trypsin (□), 1 mM TFBC, 400 µM benzamidine and 18 µM trypsin (◊), and (b) 1 mM TFBC and 18 µM trypsin (O), 1 mM TFBC, 800 µM 4-amidinopyridine and 18 µM trypsin (□), 1 mM TFBC, 400 µM benzamidine and 18 µM trypsin (◊).

The signals of the 2,2'-bipyridine chelating agent would appear in the same spectral region as the signals of interest from the ligand. An efficient transfer of hyperpolarization to 2,2'-bipyridine would not be expected because firstly, this compound is not present in the sample during the SABRE hyperpolarization step in the experiment, and secondly its off-rate is slowed due to its ability to form a bidentate complex with Ir. Nevertheless, to ensure that the rates are determined from the ligand peaks of interest, a control experiment was performed, where the ligand was not included in the reaction mixture. The resulting spectra are shown in Figure 4.8. In this control experiment, no exponential decay is observed for the integrated spectral region, indicating an absence of signal contributions from the chelating ligand. Moreover, when the 2,2'-bipyridine is added to a sample of the activated catalyst and ligand 4-amidinopyridine for a one-pot

experiment performed in the NMR tube, no SABRE hyperpolarized signals were observed (Figure 4.9).

Both the protein and the ligand concentration are lowered for the data of Figure 4.10, to explore concentration limits under current experimental conditions. A smaller volume of ligand solution, 500 µl, with a stock concentration of 1.5 mM, was hyperpolarized. After mixing, the protein concentration reached to the single digit micromolar level, and the ligand was in the range of 100 – 150 µM. Under these conditions, the signal of the hyperpolarized ligand can be obscured by parts of the solvent line (Figures 4.10a and 4.10d, top panels). In the bottom panels of these figures, the solvent signal was reduced by subtracting a reference spectrum that was scaled to the maximum solvent signal intensity. The binding of the ligand is identified by comparing the relaxation rates obtained from the fit in Figures 4.10c and 4.10f.

Nuclear spin hyperpolarization offers significant advantages in the detection of protein-ligand interactions, by allowing a reduction in the ligand concentration. Under conditions of fast exchange between free and bound forms of the ligand, as is the case for 4-amidinopyridine and trypsin, the protein concentration can be reduced to a level several times below the ligand concentration. The reduction in concentration facilitates working with proteins that are unstable or difficult to purify.

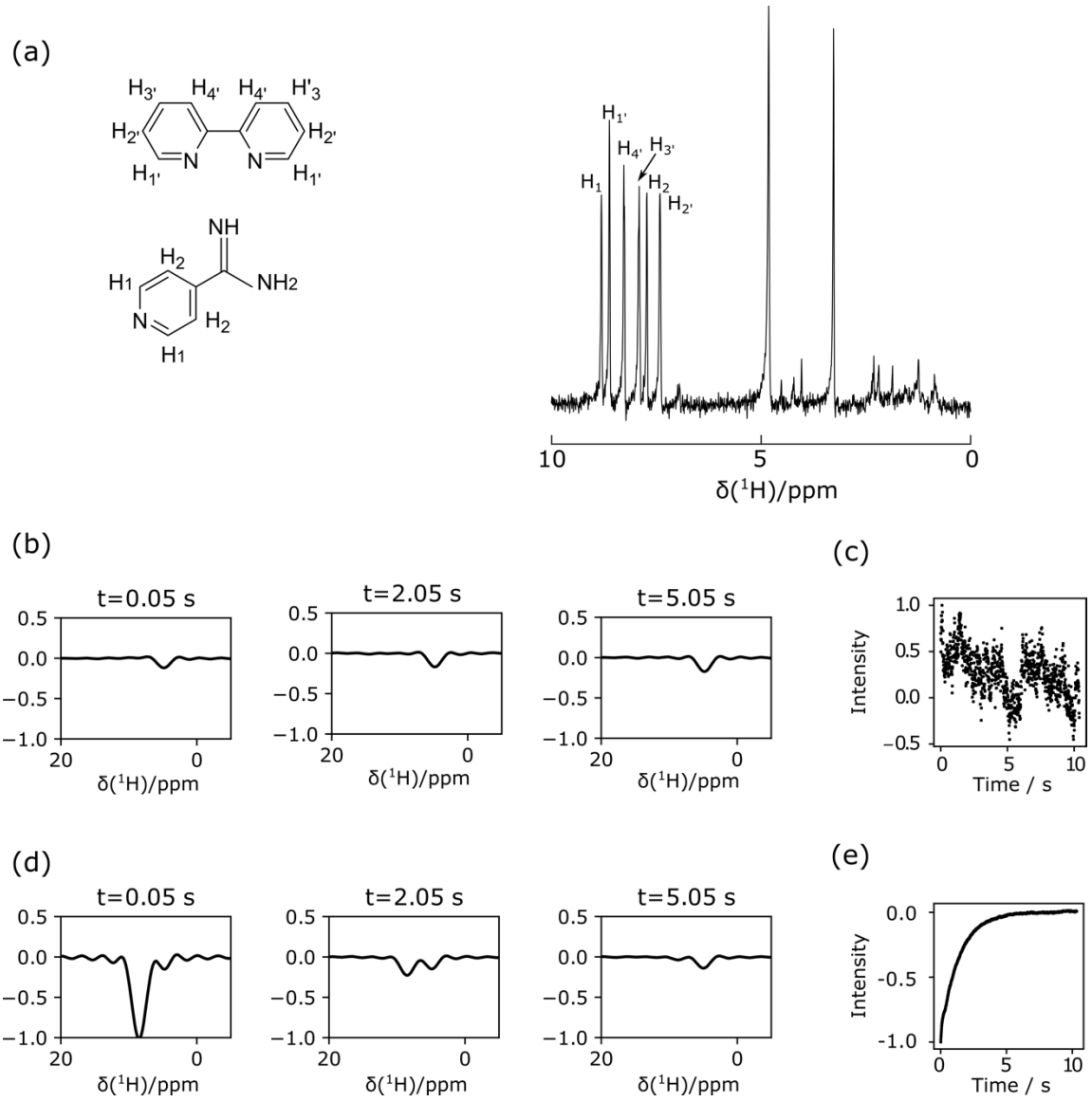

Figure 4.8: (a) Structure of chelating ligand 2,2'-bipyridine (top) and trypsin ligand 4-amidinopyridine (bottom). (b) Non-hyperpolarized spectrum of ligand 4-amidinopyridine and chelating ligand 2,2'-bipyridine with catalyst in d_4-methanol. (b) Signal intensity from single-scan CPMG experiment in the absence of ligand 4-amidinopyridine but presence of 1.2 mM chelating ligand 2,2'-bipyridine (c) Fit from region corresponding to ligands. (d) Signal intensity from single-scan CPMG experiment in the presence of ligand 7.3 mM 4-amidinopyridine and 2.9 mM chelating ligand 2,2'-bipyridine. (e) Fit from region corresponding to ligands.

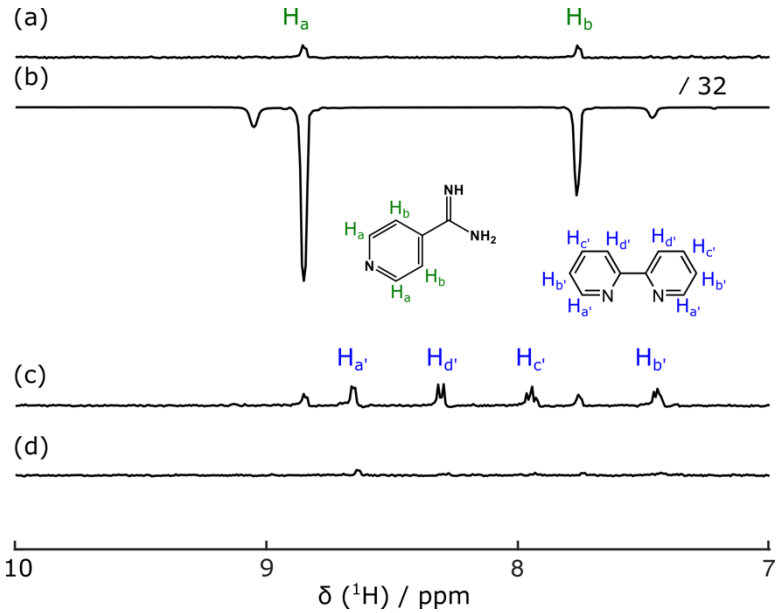

Figure 4.9: (a) Non-hyperpolarized 400 MHz NMR spectra of 10 mM 4-amidinopyridine with Ir(IMeMes) catalyst in methanol-d_4. (b) SABRE hyperpolarized spectra of 4-amidinopyridine acquired at 9.4 T (400 MHz) after 30 s bubbling at 6.5 mT field and manual transfer time of 4 s. (c) Non-hyperpolarized 400 MHz NMR spectra of 10 mM 4-amidinopyridine with 2,2'-bipyridine and activated Ir(Me)(IMes) SABRE catalyst in methanol-d_4. (d) SABRE hyperpolarized spectra of 4-amidinopyridine in the presence of 2,2'-bipyridine acquired at 9.4 T after 30 s bubbling at 6.5 mT field and manual transfer time of 4 s.

Although the fluctuations in the echo signals seen in Figures 4.10b and e are larger than those in Figure 4.4, the experiment at these concentrations is not primarily limited by thermal noise in the spectra. The concentration of the hyperpolarized ligand in the final solution may be further reduced. Because SABRE hyperpolarization is typically most effective for a ligand concentration in the millimolar range,[107] the concentration in the stock solution for hyperpolarization should not be arbitrarily reduced. Rather, the amount of stock solution that is used in the experiment could be lowered. This goal may preferably

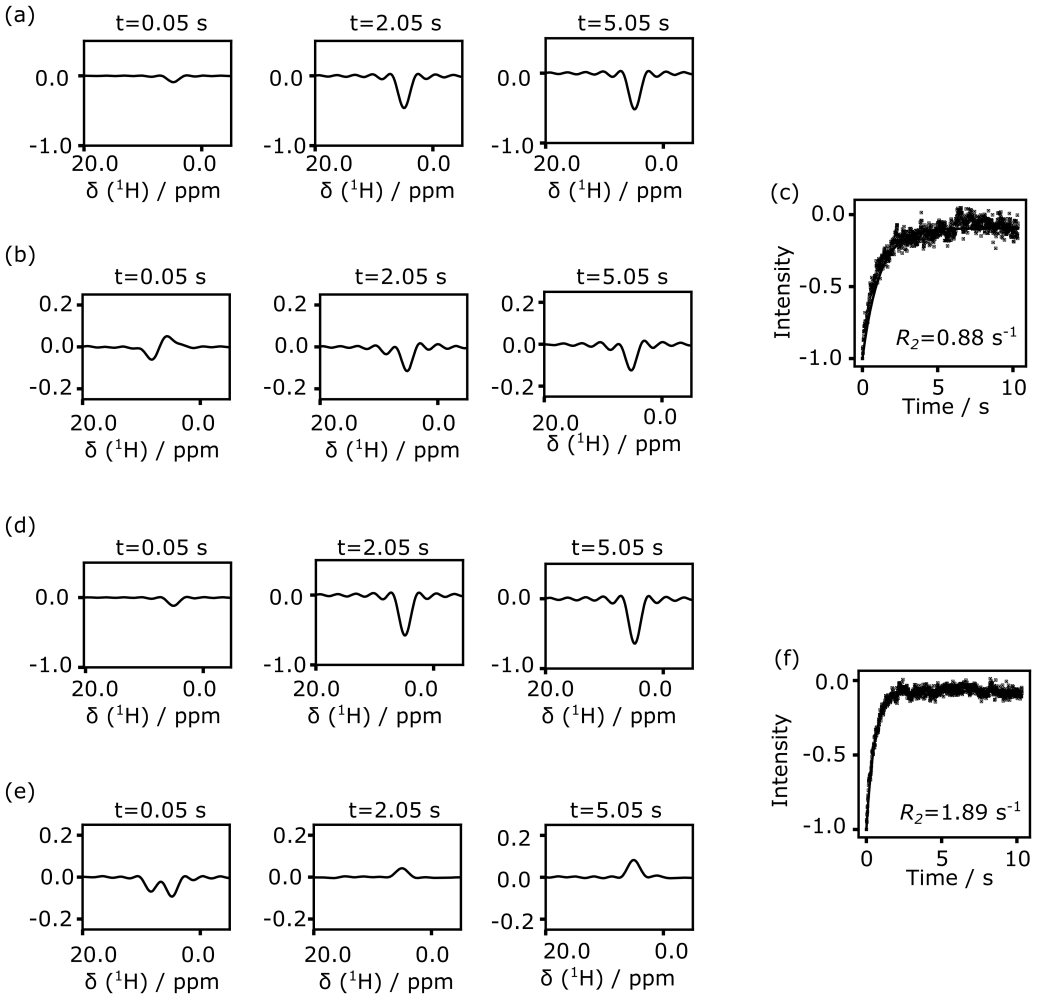

Figure 4.10: a) Spectra from CPMG echoes of 134 μM 4-amidinopyridine in presence of polarization transfer catalyst and chelating ligand. b) Spectra from CPMG echoes of 134 μM 4-amidinopyridine in presence of polarization transfer catalyst and chelating ligand after water signal subtraction. The final methanol fraction in the sample is 8.9%. c) Integrated and fitted signals from (b). d) Spectra of 125 μM 4-amidinopyridine and 7.2 μM trypsin in presence of catalyst and chelating ligand. e) Spectra of 125 μM 4-amidinopyridine and 7.2 μM trypsin in presence of catalyst and chelating ligand after water signal subtraction. The final methanol in the sample is 8.3%. f) Integrated and fitted signals from (e). Where indicated, the reference water spectrum was subtracted after scaling to the maximum solvent signal intensity in each echo. All spectra are plotted at the same scale.

be combined with methods that introduce hyperpolarized gas into a smaller volume of liquid to minimize consumption of the ligand and the polarization transfer catalyst. For example, microfluidic techniques that introduce gases into liquids have previously been described.[130] An experiment reducing the ligand concentration would further benefit from the addition of a technique that facilitates the rapid admixing of a small, microliter-range volume of ligand solution to the protein solution.

Several improvements would further increase achievable signals and lower the minimum ligand concentration. Additional water suppression or use of solvents with higher deuteration level would reduce fluctuations due to solvent signal overlap. The experiments could be performed using hydrogen gas with a higher *para* content. Here, 50% *para*-hydrogen was produced by cooling hydrogen gas to the temperature of 77 K using liquid nitrogen. Increasing the percentage by producing *para*-hydrogen at lower temperature can increase the signal enhancement by another factor of three.[107] An additional improvement of at least a factor of two would be realized by changing the ligand concentration during the polarization step. As is known from the literature,[107] optimal polarization efficiency is achieved in a range of catalyst and ligand concentration, where a sufficient fraction of the ligand is bound to the catalyst. Based on the data in Figure 4.2, a ligand concentration of 10 mM during the polarization step would result in a higher signal enhancement. A lower concentration was used in this work in order to achieve a low ligand concentration after mixing with the protein at a moderate volume-to-volume ratio in the experimental setup as implemented. The mixing ratio could be further

optimized to lower the volume of hyperpolarized ligand solution that is introduced, while increasing the ligand concentration in the hyperpolarization step.

In addition to the other reagents, the achievable signal enhancement depends on the hydrogen gas pressure. The pressure dependence of signal enhancement for this ligand and catalyst is shown in Figure 4.11 over the range of 0.21 to 0.83 MPa. It is evident that the signal enhancement is close to reaching a plateau, indicating that the pressure used in the experiment is sufficient to achieve near saturation in the metal hydride formation and highest enhancements. The same pressure was also used to effectively drive the sample from the polarization vessel to the sample loop.

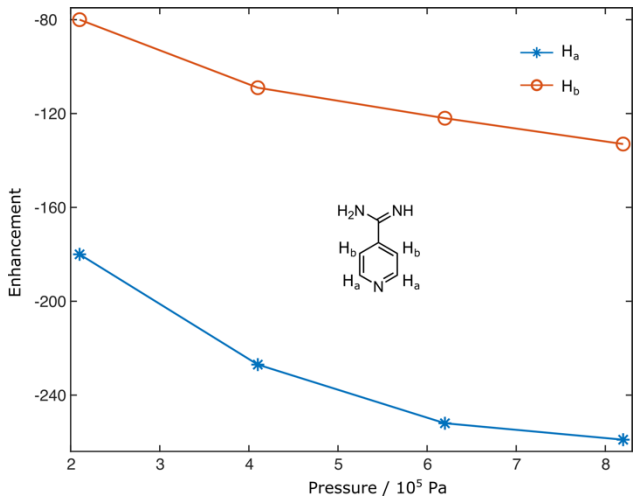

Figure 4.11: *Para*-hydrogen pressure dependence of signal enhancement of 4-amidinopyridine with Ir(IMeMes) SABRE catalyst in methanol-d_4. The SABRE hyperpolarization was carried out at 6.5 mT by bubbling para-enriched hydrogen gas into the sample for 30 s. The NMR spectra were measured at 9.4 T after a manual transfer time of 4 s. The most negative number represents the highest enhancement.

SABRE hyperpolarization using common polarization transfer catalysts is most readily achieved in polar organic solvents, here methanol. Apart from decreasing the protein concentration, a benefit of a large dilution factor upon mixing of the two solutions in this experiment is that the final concentration of the organic solvent component is reduced. The volume ratio of the experiments in Figure 4.10 resulted in a methanol fraction after admixing the protein of < 10%. Proteins are likely to retain their native structure in solutions with a low content of alcohol.[131] Trypsin was previously found to retain the ability to bind a ligand in the presence 30% methanol.[132] Measurements of trypsin catalytic activity confirmed similar initial reaction rate constants in 30% and 10% methanol compared to water, for the first 15 s or reaction time (Figure 4.12). Deactivation of the enzyme occurred after approximately 30 or 60 s, respectively, *i.e.* at a much longer time than the duration of the hyperpolarized NMR experiment. A further reduction of ligand solution volume as described above would entail the additional benefit of reducing the methanol concentration in the final sample.

The use of SABRE for the characterization of protein-ligand interactions can be expanded to other ligands containing appropriate functional groups. These may include the -NH_2[72], -CN[133] groups or the heterocyclic N as demonstrated here. In addition to protons, SABRE hyperpolarization can be achieved for other nuclei, including fluorine. ^{19}F has been hyperpolarized by SABRE both directly and indirectly through the intermediary of a nearby proton.[110,134] The method described here can be adapted for ligands containing this nucleus. Similar to previous D-DNP experiments[23], the observation

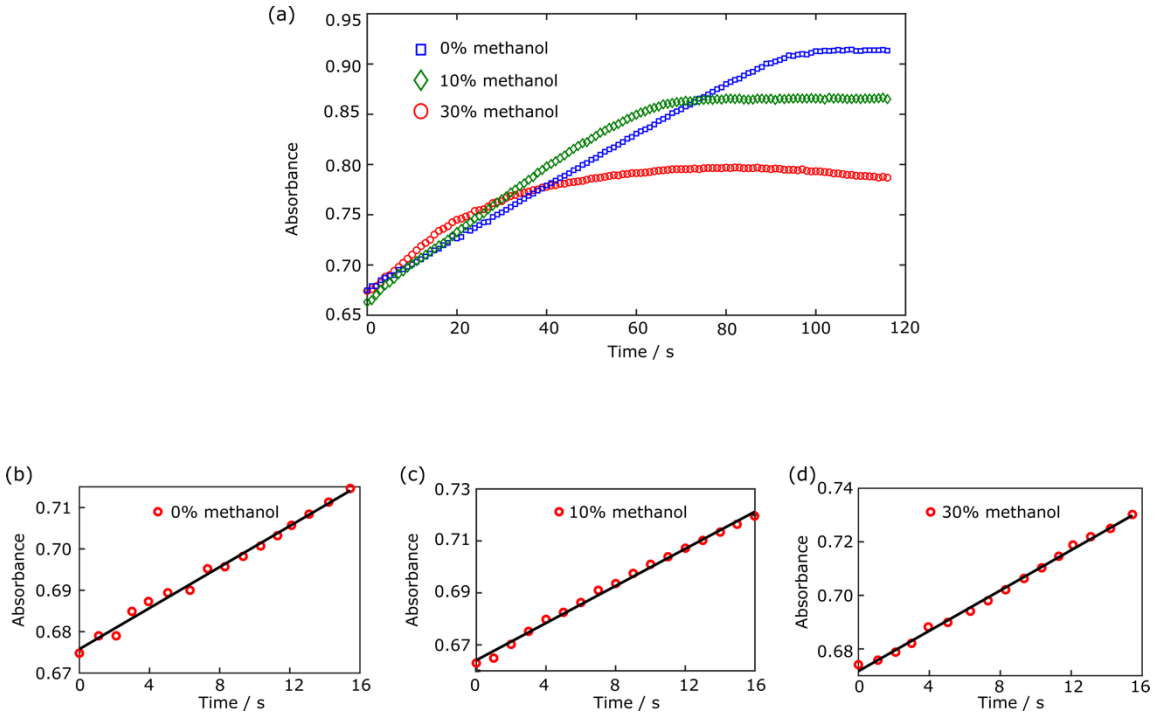

Figure 4.12: (a) Change in Absorbance vs. time for the hydrolysis of BAEE catalyzed by trypsin, when the reaction was in 0% methanol (0.25 mM BAEE with 0.64 µM trypsin in Tris buffer) (□), in 10% methanol (0.25 mM BAEE with 0.64 µM trypsin in 90% Tris buffer and 10% methanol) (◊), and in 30% methanol (0.25 mM BAEE with 0.64 µM trypsin in 70% Tris buffer and 30% methanol) (O). (b) Fit of absorbance vs. time for the first 15 s of the reaction is in 0% methanol. The equation from the fit is y = 0.0024792 s^{-1}·x + 0.67579. (c) Fit of absorbance vs. time for the first 15 s of the reaction in 10% methanol and 90% Tris buffer. The equation from the fit is y = 0.0038 s^{-1}·x + 0.6717. (d) Fit of absorbance vs. time for the first 15 s of the reaction is in 30% methanol and 70% Tris buffer. The equation for the fit is y = 0.0035737 s^{-1}·x + 0.66409.

of fluorine would avoid any interference from the solvent signal. Ligand derived SABRE hyperpolarization may in the future be used for studies of macromolecular structure at the binding site, by employing polarization transfer and using calculations similar to those demonstrated by other hyperpolarization methods.[21] An additional generalization of the experiment includes the use of one molecule with weak affinity and fast exchange rate as a reporter ligand, which becomes displaced upon binding of another ligand.[23,135] This

approach would require the identification of only one SABRE hyperpolarizable ligand for screening of a library of other ligands.

4.3. Conclusion

In summary, the use of *para*-hydrogen derived hyperpolarization using the SABRE method for the determination of protein-ligand binding is demonstrated. The hyperpolarized small molecule contains a binding site for the protein, and at a distant location, for the polarization transfer catalyst. The use of flow-NMR allowed the experiment to be completed in predominantly an aqueous medium. The SABRE hyperpolarization method is cost-effective and can be added-on to standard NMR spectroscopy equipment. Hyperpolarization allows the reduction of protein concentration, enabling the screening of ligand binding in drug discovery and other applications.

4.4. Experimental Section

Hydrogen gas enriched to a level of ~50% para-content was prepared by passing room temperature hydrogen gas over iron (III) oxide spin-flip catalyst (Sigma-Aldrich, St. Louis, MO) in a heat exchanger, which was immersed in liquid nitrogen (Caution: Hydrogen gas is flammable and can form explosive mixtures with air. It should be exhausted through grounded metal piping. Eye protection is required for compressed gases). The ligand sample for hyperpolarization consisted of 20 mM 4-amidinopyridine hydrochloride (Alfa Aesar, Ward Hill, MA) in methanol-d_4 (Cambridge Isotope Libraries, Andover, MA) (Caution: All chemicals require handling using gloves and eye protection.

Methanol and 2,2'-bipyridine are toxic). The sample contained 3.5 mM of the precatalyst [Ir(MeIMes)COD]Cl, which was synthesized according to a previously established protocol.[56] For the experiments at low concentration, this stock solution of ligand was diluted to 1.5 mM and 0.3 mM catalyst. For the SABRE experiments, the para-enriched hydrogen was bubbled through the sample solution at a pressure of $8.3 \cdot 10^5$ Pa and at 294 K. Bubbling was performed for 30 s at a field of 6.5 mT generated by a solenoid coil (diameter 22 cm and length 28 cm). After this polarization transfer step, the sample was pushed to a sample loop using the pressure of the H_2 gas. The hyperpolarized sample was injected into an NMR flow-cell concomitantly with a sample of 50 mM sodium phosphate buffer in D_2O (pH 7.5), or a sample of trypsin (Alfa Aesar) at 1 mM or 18 μM dissolved in the same buffer. Where indicated, 2,2'-bipyridine (Sigma-Aldrich) at 10 mM or 2.5 mM concentration was included with the protein solution. The two solutions mixed in a Y-mixer before entering the magnet. The sample injector that was used for this purpose is described elsewhere.[136] Briefly, both samples were pushed from an injection loop made of poly ether ether ketone (PEEK) tubing of 0.5 mm inner diameter. Two high pressure syringe pumps (Models 500D and 1000D, Teledyne Isco, Lincoln, NE) were filled with water and used to transfer the sample from the injection loop to the Y-mixer and subsequently into the flow-cell. Flow rates were set to 110 ml/min and 150 ml/min, respectively. The injection time was 128 ms, during which the pump was active before sample mixing. The time after mixing but before sample reaching flow cell was 1070 ms, and the stabilization time before triggering the NMR experiment was 500 ms. All measurements were performed with a TXI-probe (Bruker Biospin, Billerica, MA). A

single scan CPMG experiment was performed to find the R_2 relaxation rates of the ^1H spins of the ligand 4-amidinopyridine hydrochloride (Figure 4.13). A water suppression sequence was used prior to collecting the echoes, where EBURP pulses of 20 ms were applied to selectively excite the solvent signal, followed by dephasing using pulsed field gradients ($G_{x,y,z}$ = 70 G/cm; 1 ms). For the CPMG block, a pulsing delay of 1696.2 μs was used, and 64 points were collected per echo. The total experiment time was 10.4 s.

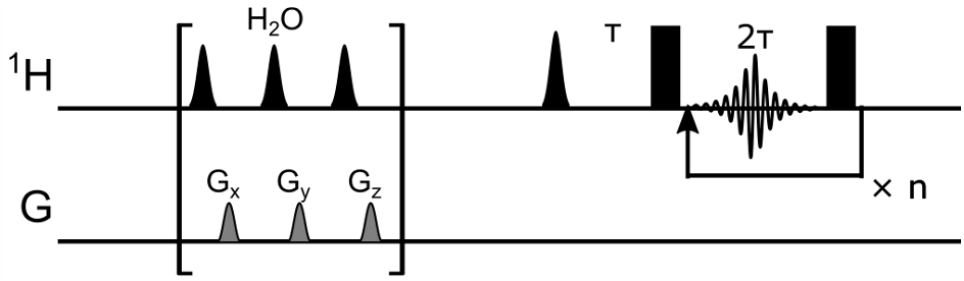

Figure 4.13: Scheme of pulse sequence used for obtaining CPMG echoes. The time for pulsing delay 2τ was 1696.2 μs. A total of 6144 spin echoes were collected for 10.4 s.

5. CHARACTERIZATION OF PROTEIN-LIGAND INTERACTIONS BY COMPETITIVE BINDING WITH A SABRE HYPERPOLARIZED REPORTER

5.1. Introduction

Nuclear magnetic resonance offers significant benefits for the characterization of the binding of ligands to proteins with applications in screening for drug discovery. Specifically, NMR observable parameters such as R_2 relaxation, nuclear Overhauser effect, chemical shift, and others, are sensitive to the binding interaction. Subsets of these parameters can be used to identify binding, characterize binding affinities or determine binding site structures. Nuclear spin hyperpolarization techniques overcome a low sensitivity of acquired signals, which is the most significant drawback of the use of NMR for ligand binding studies. The use of hyperpolarization by dissolution dynamic nuclear polarization (D-DNP)[13] has previously been proposed for this purpose.[20,22,23]

Recently, the application of another hyperpolarization method, the *para*-hydrogen based signal amplification by reversible exchange (SABRE),[50] providing a low-cost alternative for producing ligand hyperpolarization has been demonstrated.[137] SABRE requires that the molecule to be hyperpolarized bind to a polarization transfer catalyst or be hyperpolarized through exchange of protons via another ligand in the SABRE-Relay[70] process. Here, the ligand 4-amidinopyridine which contains a binding site for both the polarization transfer catalyst and the protein is hyperpolarized. This technique is then extended to include a wide variety of ligands that are not necessarily hyperpolarizable through SABRE using the common Ir-based polarization transfer catalysts to gain information about binding to a protein. Using a competitive binding experiment, the

signals from a fast-exchanging ligand can report on the binding of other ligands of interest, as the reporter ligand becomes displaced.[135] Thus, only a single ligand needs to be hyperpolarized. It is anticipated that for most proteins, a weakly binding reporter ligand can be found or modified to contain a binding site for a SABRE polarization transfer catalyst, thus enabling the use of this hyperpolarization method for a ligand screening campaign or other biophysical investigation of the target protein.

5.2. Results and Discussion

The ligand 4-amidinopyridine was hyperpolarized with an asymmetric SABRE catalyst [Ir(IMeMes)(COD)]Cl (IMeMes=1-(2,4,6-trimethylphenyl)-3-methylimidazol-2-ylidene, COD=cyclooctadiene). The proton relaxation rates of this ligand in the presence and absence of protein were determined from single-scan Carr-Purcell-Meiboom-Gill (CPMG) experiments. The ligand was injected into an NMR flow-cell (Figure 5.1a) after the hyperpolarization was established at a low field of 6.5 mT. The chelating ligand 2,2'-bipyridine was included to trap the polarization transfer catalyst during this step. The resulting inactivation of the catalyst alleviates relaxation contributions due to interactions with the reporter ligand during signal acquisition, which would be detrimental to the identification of protein binding.[137] The same NMR measurements of the reporter ligand (Figure 5.1b) with added chelating ligand were performed with or without admixing of protein. Spectra of the reporter ligand obtained from Fourier transform of selected echoes are shown in Figure 5.1c.

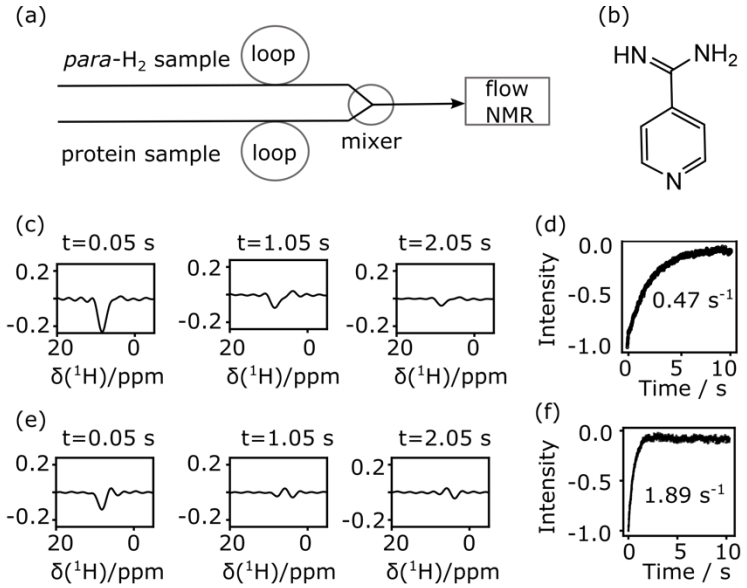

Figure 5.1:(a) Schematic representation of flow-NMR setup for ligand-binding characterization. (b) Structure of the reporter ligand 4-amidinopyridine (c) Spectra of 4-amidinopyridine obtained after Fourier transform of CPMG echoes in the presence of catalyst and 2,2'-bipyridine. (d) Fit obtained from the spectra in panel (b). (c) Fitted relaxation rate for the free ligand 4-amidinopyridine from the spectra in panel (c) is 0.47 s^{-1}. (e) Spectra of 4-amidinopyridine obtained after Fourier transform of CPMG echoes in the presence of catalyst, 2,2'-bipyridine and trypsin (f) Fitted relaxation rate for the ligand in presence of trypsin from the spectra in panel (e) is 1.89 s^{-1}.

The peak at 8.1 ppm contains the signals from both aromatic protons of the ligand 4-amidinopyridine that are merged into one. These signals are not resolved due to the short echo time of 1.7 ms, which results in a spectral resolution of 590 Hz. The peak near 4.7 ppm is from water, which was used to fill the pumps that drive both the hyperpolarized and non-hyperpolarized samples. A signal enhancement of 100-fold for the reporter ligand at the diluted stock concentration of 1.5 mM used for hyperpolarization in the experiments facilitates their observation in the presence of the non-hyperpolarized water.[137] A reference water signal was subtracted to reduce the interference from the solvent signal.

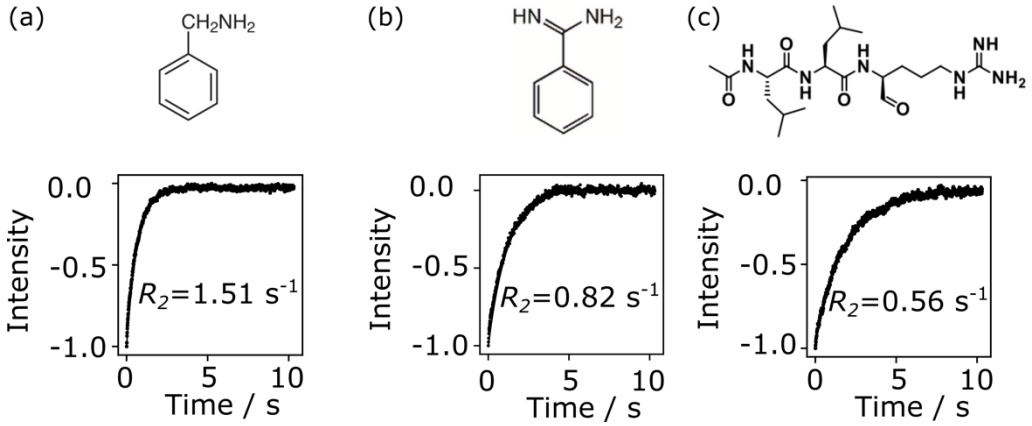

Figure 5.2: Structures of competing ligands and $R_{2,r}^{(c)}$ relaxation rates from CPMG experiments for the reporter ligand 4-amidinopyridine measured in the presence of competing ligands (a) 161 µM 4-amidinopyridine with 166 µM benzylamine, 14.7 µM trypsin and chelating agent 2,2'-bipyridine (b) 146 µM 4-amidinopyridine with 136 µM benzamidine, 13 µM trypsin and chelating agent 2,2'-bipyridine and (c) 140 µM 4-amidinopyridine with 7 µM leupeptin, 8.4 µM trypsin and chelating agent 2,2'-bipyridine. The fit values are 1.51 s^{-1}, 0.82 s^{-1} and 0.56 s^{-1} for (a), (b) and (c), respectively.

As expected for a SABRE experiment, the signals are initially negative, and subsequently relax towards the much smaller positive thermal equilibrium spin polarization (Figure 5.1d). A faster relaxation is observed in the presence of protein, due to averaging of the relaxation rate of the free ligand fraction with the faster rate of the bound fraction (Figure 5.1f). Fitting of a single exponential to the relaxation data resulted in a transverse relaxation rate of the free reporter ligand, $R_{2,r}^{(f)} = 0.47 \pm 0.026$ s^{-1}. In the presence of trypsin, the relaxation rate for the non-competing reporter ligand was $R_{2,r}^{(nc)} = 1.86 \pm 0.13$ s^{-1}.

Subsequently, relaxation rates of the same molecule, 4-amidinopyridine, were measured when a second ligand for the protein, the ligand of interest, was included in the protein solution. Figure 5.2 shows the signal integrals resulting from screening the ligands of interest benzylamine, benzamidine and leupeptin. As these ligands partially displace

the reporter ligand, its observed relaxation rate changes. The relaxation rate of the reporter ligand after displacement falls in-between the rates for free reporter and reporter with protein alone. The weakest ligand of interest, benzylamine, was present at a concentration of 166 μM to achieve partial displacement manifested as an observable change in the relaxation rate (Figure 5.2a). In contrast, the strongly binding leupeptin caused a strong change at the much lower concentration of 7 μM (Figure 5.2c). The corresponding spectra from CPMG echo trains for the three ligands are shown in Figures 5.3–5.5. The partial displacement of the reporter ligand, barring allosteric effects, indicates that the ligand of interest binds to the same binding site of the protein as the reporter ligand.

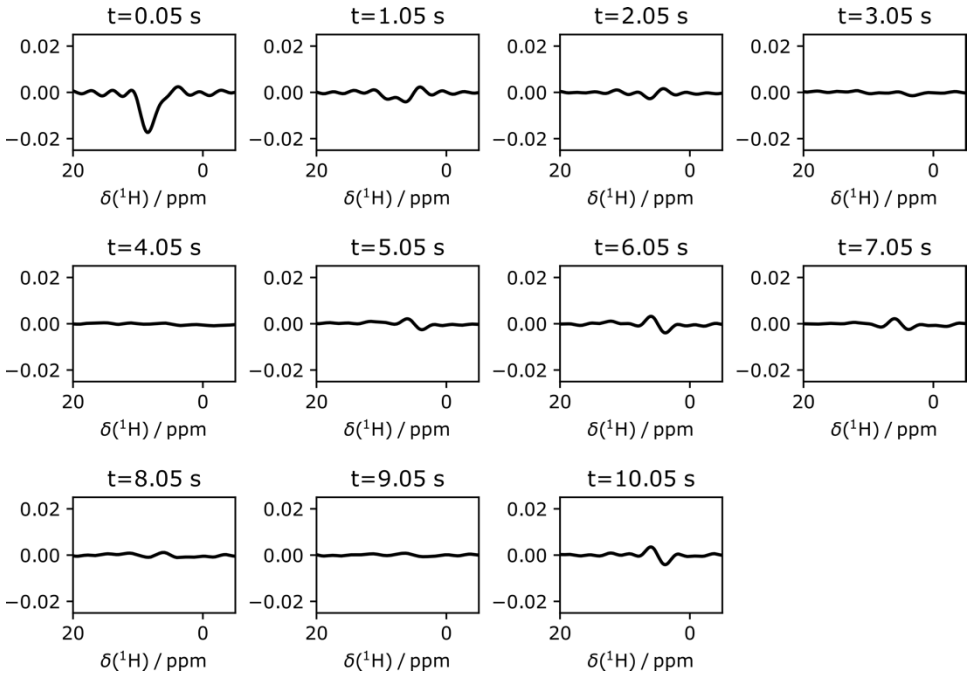

Figure 5.3: Hyperpolarized spectra of 160 μM 4-amidinopyridine in presence of 161 μM benzylamine, 2,2'-bipyridine chelating agent and 14.7 μM trypsin.

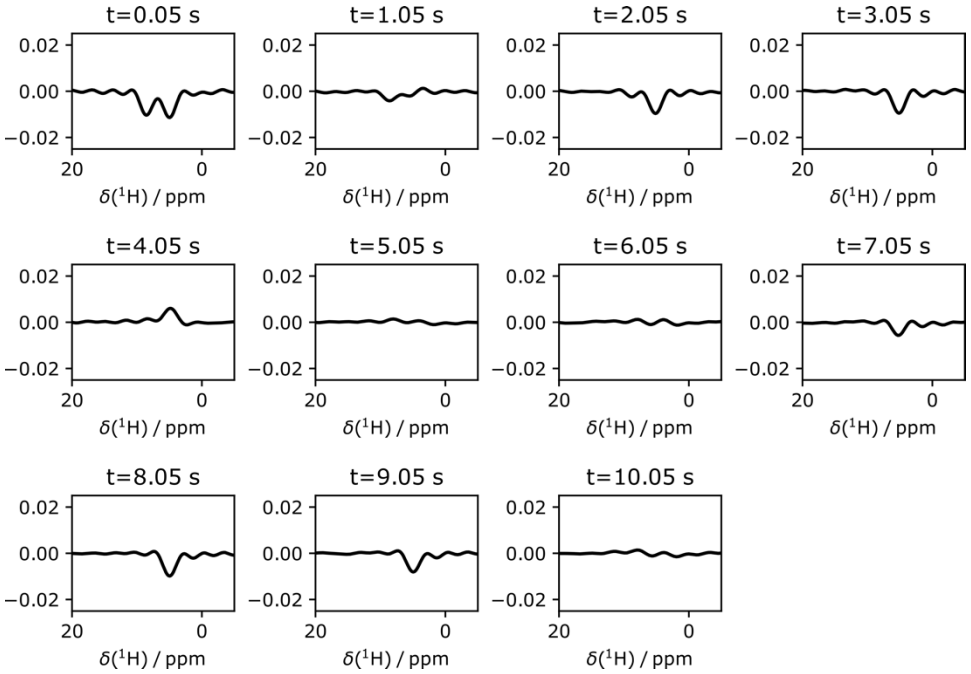

Figure 5.4: Hyperpolarized spectra of 146 µM 4-amidinopyridine in presence of 136 µM benzamidine, 2,2'-bipyridine chelating agent and 11.6 µM trypsin.

Under the solution conditions of the three experiments, the $R_{2,r}^{(c)}$ relaxation rate was fastest with benzylamine at 1.47 ± 0.04 s^{-1}, followed by benzamidine at 0.88 ± 0.06 s^{-1}, and leupeptin at 0.58 ± 0.05 s^{-1}. These indicate that in the first experiment, the smallest fraction of reporter ligand was displaced, with increasing fractions in the second and third experiment. The level of displacement reflected in the relaxation rates depends both on the ligand concentrations and on the dissociation constants of the individual ligands. If the dissociation constant of the reporter ligand $K_{D,r}$, is known, it can be used to determine the dissociation constants of the ligands of interest, $K_{D,c}$.

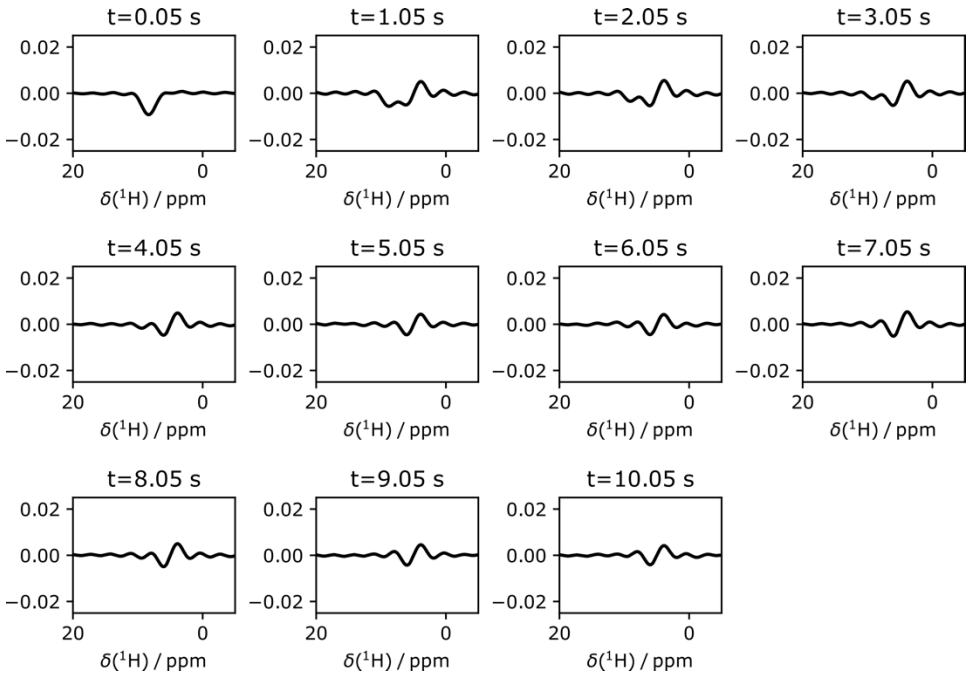

Figure 5.5: Hyperpolarized spectra of 144 µM 4-amidinopyridine in presence of 7.7 µM leupeptin, 2,2'-bipyridine chelating agent and 11.0 µM trypsin.

The dissociation constant of the reporter ligand was independently determined from an NMR titration experiment to be approximately 204 µM (Figure 5.6). A series of non-hyperpolarized CPMG experiments were measured to determine the R_2 rates for samples of fixed protein concentration and varying ligand concentrations. The equations used for the fit were

$$p_{b,r} = \frac{[R]_{tot} + [P]_{tot} + K_{D,r} - \sqrt{([R]_{tot} + [P]_{tot} + K_{D,r} - 4\,[R]_{tot}[P]_{tot}}}{2[R]_{tot}} \quad (5.1)$$

and

$$R_{2,obs} = R_{2,f}.p_{f,r} + R_{2,b}.p_{b,r} \quad (5.2)$$

In the equations, $p_{b,r}$ is the fraction of bound reporter ligand and $p_{f,r}$ is the free ligand determined from 1–$p_{b,r}$. The $[R]_{tot}$ and $[P]_{tot}$ are the total reporter ligand and trypsin concentrations, respectively.

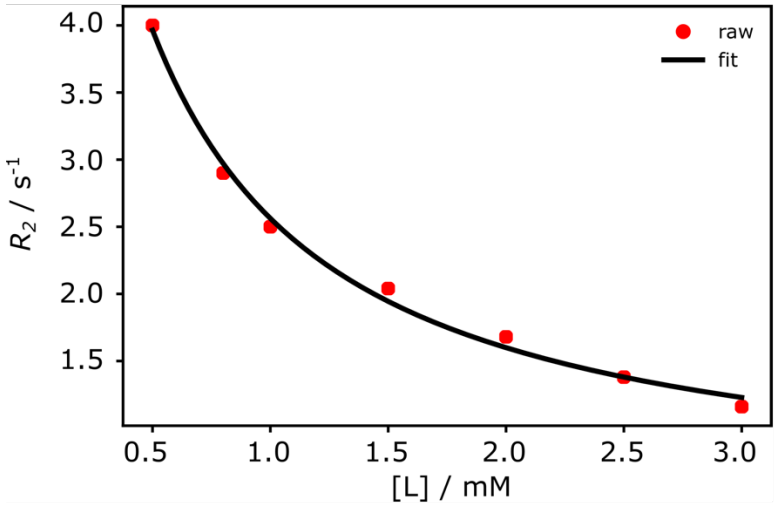

Figure 5.6: Plot of R_2 vs ligand concentration. The R_2 rates were determined from a non-hyperpolarized CPMG experiment. The ligand concentration was varied from 0.5 to 3 mM and the trypsin concentration was 100 μM. The K_D from the fit was 204 μM.

The determination of the $K_{D,r}$ for the reporter ligand allowed to calculate the $K_{D,c}$ of the competing ligands. This was done following an established method from ref [23]. The errors in the determined $K_{D,c}$ values propagate from the error in the measured R_2 rates. The $K_{D,c}$ and associated errors were estimated based on the average and standard deviations of the R_2 values from three separate measurements (Table 5.1). The $K_{D,c}$ values determined are 230 ± 70 µM for benzylamine, 33 ± 8 µM for benzamidine and 0.37 ± 0.16 µM for leupeptin. Therefore, the order of binding affinity strengths for inhibitors of trypsin can be determined from SABRE using the competitive binding experiment, which corroborates the trend reported earlier, with the benzylamine being the weakest binder and

the leupeptin the strongest amongst the three.[23] Error in the determination of the $K_{D,r}$ value for the reporter ligand will lead to an additional error in the determination of the $K_{D,c}$ value for the competing ligands, but not in the ordering of $K_{D,c}$ for the series of competing ligands. The value of the $K_{D,r}$ used for the above calculations is from an NMR titration experiment. In the future, additional experiments may establish a range for this value.

Previously, fluorinated reporter ligands have been hyperpolarized and used as a reporter ligand to screen a range of ligands with different binding affinities using D-DNP.[23] Signal enhancement values of over 1000-fold were achieved for the ^{19}F and concentrations down to 1 μM could be detected for the reporter ligand. Detection of ^{19}F had the advantage that the interference from the large solvent signal could be avoided. It also allows for the collection of NMR data with short echo time. Here, for stock concentrations of 1.5 mM for the reporter ligand, signal enhancement values of ~100-fold can be achieved with 50% *para*-hydrogen, and concentrations in the range of 100 μM can be detected. As discussed in ref. [137] and Chapter 3, modifications in the experimental setup will allow to lower the concentration of the reporter ligand. This in-turn will allow to lower the concentrations of the competing ligands. For ligands that have affinities that lie between benzylamine and benzamidine, it should be possible to lower the concentration by an amount similar to the reporter ligand as the ratios used are 1:1 for the two ligands here. The limiting concentration for a ligand in general however would depend on the relative values of the dissociation constants of the reporter and competing ligands used.

Table 5.1: The experimental parameters and the fitted $R_{2,r}^{(c)}$ relaxation rate for each experiment are summarized below in Table 5.1.

[ligand] / mM	[catalyst] / mM	[protein] / mM	[competing ligand] / mM	$R_{2,r}^{(c)}$ / s^{-1}
benzamidine				
0.146	0.028	0.0116	0.136	0.82
0.159	0.032	0.0149	0.149	0.88
0.169	0.025	0.0112	0.140	0.94
benzylamine				
0.161	0.024	0.017	0.166	1.51
0.190	0.028	0.014	0.146	1.43
0.160	0.032	0.0148	0.185	1.47
leupeptin				
0.180	0.027	0.0107	0.0107	0.63
0.144	0.022	0.011	0.0077	0.56
0.160	0.024	0.011	0.0092	0.54

^{19}F SABRE polarization would provide an alternate choice for performing the ligand screening experiments using the competitive binding. In such cases, as discussed above, the large signal from the solvent can be avoided. Moreover, only one fluorinated reporter ligand would need to be identified for the protein. Ligands that are non-fluorinated can then be screened using this reporter ligand. To hyperpolarize ^{19}F using SABRE, the

experimental conditions may need to be optimized, as the reported signal enhancement values for this nucleus are lower[110,134] compared to ^{1}H.

Compared to the widely reported trypsin ligand benzamidine, the chosen reporter ligand contains an additional N-atom in the ring. Benzamidine cannot be hyperpolarized by SABRE. The change in the structure of the ligand leads to a change in the dissociation constant. The higher K_D value allows it to be used as a reporter ligand in the competitive binding experiment, as in this experiment the reporter ligand is in fast exchange with the protein. In general, although drug candidate molecules may not themselves be SABRE hyperpolarizable, the described method requires only a single weakly binding reporter ligand for a screening campaign. Such a reporter ligand may be found by modifying a known ligand to the target protein. A reduction in affinity by the introduction of an N-binding site for the polarization transfer catalyst may not necessarily be a disadvantage for the experiment. It may place the exchange rate of an originally more strongly binding ligand in the fast exchange regime necessary for the NMR experiment. Additionally, computational methods may be utilized to identify a weakly binding ligand *in silico.* Relevant methods include combining docking methods with molecular dynamics simulations and determination of free energies for the protein-ligand binding process.[138] The K_D of modified ligands in the μM to mM range can be independently determined from methods such as isothermal titration calorimetry or ligand observed NMR experiments.[4]

With the measurement of competitive binding, the K_D of a wide range of ligands can be determined. SABRE polarization enhances the signals of ^{1}H, which are detectable

with high sensitivity. Compared to non-hyperpolarized NMR, the increased signal further facilitates the distinction from the water peak. The ability for continuously producing SABRE hyperpolarization for a reporter ligand mixture, in combination with additional improvements of the injection device to include autosampling, would enable true high-throughput screening using this method. The time required per sample would be reduced close to the NMR scan time on the order of tens of seconds or less.

5.3. Conclusion

In summary, the use of a reporter ligand hyperpolarized by the SABRE method to screen for the binding of other ligands of interest to a target protein is demonstrated. This method significantly expands the utility of SABRE hyperpolarization for the characterization of ligand binding. Only a single SABRE hyperpolarizable ligand, which needs to include a binding site for the polarization transfer catalyst, and which binds weakly the protein, is required. A range of ligands with different binding affinities from tight to weak can then be screened using SABRE. The combination of the protein and SABRE hyperpolarizable reporter ligand can serve as a basis for high-throughput screening of protein-ligand interactions.

5.4. Materials and Methods

Para-hydrogen was produced by passing room temperature hydrogen over iron (III) oxide spin-flip catalyst (Sigma-Aldrich, St. Louis, MO) in a heat exchanger at liquid nitrogen temperature of 77 K. The *para* content was 50% as determined from the ratios of

the signal intensities of *ortho*-hydrogen using Equation 1.11. The sample for hyperpolarization consisted of 0.3 mM of the asymmetric precatalyst [Ir(IMeMes)(COD)]Cl and 2.0 mM ligand 4-amidinopyridine hydrochloride (Alfa Aesar, Ward Hill, MA) in methanol-d_4 (Cambridge Isotope Libraries, Andover, MA). For the SABRE experiment, the *para*-hydrogen was bubbled through the sample at a pressure of $8.3 \cdot 10^5$ Pa and at 294 K. The magnetic field for hyperpolarization was 6.5 mT. After the hyperpolarization was established, the sample was pushed to a sample loop using the pressure of the hydrogen gas. Following this step, the sample was pushed to a flow-cell that was pre-installed in the 9.4 T magnet. The injector device used for this purpose is described elsewhere[136] and in Chapter 3. At the same time, a sample consisting of 50 mM sodium phosphate buffer (pH=7.6) and 2,2'-bipyridine or a sample of buffer, 2,2'-bipyridine, trypsin and competing ligand (benzylamine, benzamidine or leupeptin) was included. The two samples mixed in a Y-mixer before entering the magnet. For the NMR experiments, a single scan Carr-Purcell-Meiboom-Gill (CPMG) experiment was performed to determine the R_2 relaxation rates of the ^{1}H spins of the 4-amidinopyridine ligand. Before acquiring the echoes, a water suppression sequence was used consisting of EBURP pulses of 20 ms duration to excite the water signals and dephasing by pulsed field gradients. A pulsing delay of 1696.2 μs was used in the CPMG block, and 64 points were collected per echo. A total experiment time of 10.4 s was used to acquire the data.

6. SUMMARY AND CONCLUSIONS

Hyperpolarization techniques have been combined with Nuclear Magnetic Resonance (NMR) spectroscopy for the characterization of interactions between proteins and small molecules. NMR can give information about binding affinities and conformational changes due to interactions between biological macromolecules and small molecules under solution conditions. However, due to the low detection sensitivity of NMR, higher sample concentrations and long experimental times because of signal-averaging, are required. Hyperpolarization solves the problem of low sensitivity of NMR by increasing the signal gain which avoids the need for long experimental times and higher sample concentrations. The large signal gain allows to characterize intermolecular interactions often under conditions not accessible by conventional NMR.

NMR has been previously used to characterize interactions between lipid molecules and the unfolded membrane protein X (OmpX) dissolved in denaturants 8 M urea or guanidine hydrochloride. Absence of denaturants leads to the precipitation of an unfolded membrane protein. Using the dissolution dynamic nuclear polarization (D-DNP), interactions between the lipid dodecyl phosphocholine (DPC) and a membrane protein were determined in the absence of a denaturant. When DPC was hyperpolarized below its critical micelle concentration (CMC), a ~1000-fold signal enhancement over the equilibrium signal intensity was obtained. The transfer of the large signal gain to OmpX through the nuclear Overhauser effect (NOE) led to a ~6-fold increase of the protein signal. The dissolution process in this experiment leads to a large dilution of the denaturant urea. Cross-relaxation rates were determined between the different functional groups in

the lipid and protein in the absence of denaturant. The rapid timescale of the DNP experiment allows to access this sample condition as it prevents protein precipitation. Dilution of the denaturant can also lead to protein folding. Therefore, this method can be used to monitor protein-folding and structural changes in membrane proteins when the folding timescale is similar to the DNP experimental time.

The *para*-Hydrogen Induced Polarization (PHIP) is a hyperpolarization technique that has relatively simple instrumentation needs and is cost-effective. The non-hydrogenative variant of PHIP is the Signal Amplification by Reversible Exchange (SABRE), which does not alter the chemical structure of the substrate to be polarized. Therefore, bubbling *para*-hydrogen into the reaction mixture allows the polarization to be renewed in solution. Due to these advantages, methods were developed for the applications of SABRE in biological systems. The challenges of applying SABRE for characterizing interactions involving biomolecules were the insolubility of the SABRE precatalyst in water and lower solubility of hydrogen in water compared to in organic solvents. Here, an application of SABRE was developed to hyperpolarize biological molecules that have hindered binding to the polarization transfer catalyst. The *ortho*-substituted pyridine and pyrimidine moieties are common in biological motifs but gave low signal enhancement values with SABRE. The low signal enhancement is due to the steric hindrance, which prevents the formation of the active polarization transfer complex. A coligand molecule was added to the reaction mixture to activate the catalyst and form the polarization transfer complex. This modification allowed to obtain signal enhancement values >200 with 50% *para*-hydrogen for the -NH_2 substituted molecules. The signal

enhancement for the -CH_3 substituted molecules however remained low, yielding values of 25. This difference in signal enhancement was attributed to the difference in the binding affinities of the molecules as the steric hindrance and the spin-lattice relaxation times (T_1) do not account for the large differences in the enhancement values. Changing the ligands in the catalyst and use of different coligands to achieve optimal exchange rate for the substrate may allow to increase the signal enhancement values of the -CH_3 substituted molecules. The addition of coligands allowed to broaden the pool of ligand molecules that can be hyperpolarized by SABRE. Elucidating factors that affect the SABRE polarization will thus enable the tuning of catalyst structures for different substrates.

Subsequently, the SABRE was developed to characterize protein-ligand binding interactions. A molecule that can bind both to the SABRE catalyst and a protein is required. A two-step approach involving flow-NMR was designed as including the protein in the same reaction mixture with the catalyst, quenches the SABRE signal. The flow-NMR approach allowed to hyperpolarize the ligand in methanol that is conducive to the catalyst and following the hyperpolarization step, acquiring the data in a predominantly aqueous solution that is suitable for the protein. The transverse relaxation rate (R_2) was measured using a single scan Carr-Purcell-Meiboom-Gill (CPMG) experiment in the absence and presence of protein to prove the binding. This method was further extended to find the dissociation constants (K_D) of ligands binding to trypsin that vary over several orders of magnitude using a competitive binding experiment. This experiment required only a single reporter ligand that can be hyperpolarized by SABRE and is in fast exchange with the protein. Previously, a fluorinated molecule had been used as reporter ligand.

Using ^{19}F NMR with DNP, the K_D of various ligands was determined. SABRE however requires less time for polarization build-up. The throughput of a ligand screening method can be higher compared to other hyperpolarization techniques. On the other hand, SABRE requires a ligand that can coordinate to the polarization transfer catalyst. Using the competitive binding experiment, the K_D can be determined for ligands that do not have adequate binding to the catalyst thereby expanding the range of ligands that can be screened. In general, it is proposed to design a reporter ligand that has a SABRE hyperpolarizable moiety and is in fast exchange with the protein, to screen a range of ligands using this method.

In the future, the concentrations of ligands and proteins can be further lowered. As the signal enhancement is concentration dependent, samples can be hyperpolarized where the SABRE signal enhancement is maximum. The signal enhancement can be further increased by increasing the *para*-hydrogen percentage. Therefore, optimal sample conditions and implementing modifications to the existing injection device to facilitate the mixing of small volume of ligand with protein solutions will lead to lower sample concentrations. Combining these factors, the ligand concentration should be decreased considerably, to the ~10 μM range and the protein concentration in the submicromolar range. These concentrations are close to physiological conditions. The throughput of NMR based drug screening processes may be improved using this method, as the time for screening will be close to the NMR scan time, on the order of tens of seconds or less. Additional developments combining autosampling techniques with the injection device would facilitate this application.

In summary, hyperpolarization techniques were developed for characterizing intermolecular interactions by NMR. For the PHIP-based SABRE specifically, applications to biomolecules including the identification of protein-ligand interactions have been demonstrated. Methods developed here are a cost-effective way of characterizing protein-ligand interactions and may be further developed for applications in high throughput drug discovery.

REFERENCES

(1) Purslow, J. A.; Khatiwada, B.; Bayro, M. J.; Venditti, V. NMR Methods for Structural Characterization of Protein-Protein Complexes. *Front. Mol. Biosci.* **2020**, *7*, 9.

(2) Lipchock, J. M.; Loria, J. P. Monitoring Molecular Interactions by NMR. In *Protein Structure, Stability, and Interactions*; Shriver, J. W., Ed.; Methods in Molecular Biology; Humana Press: Totowa, NJ, 2009; Vol. 490, pp 115–134.

(3) Lu, H.; Zhou, Q.; He, J.; Jiang, Z.; Peng, C.; Tong, R.; Shi, J. Recent Advances in the Development of Protein–Protein Interactions Modulators: Mechanisms and Clinical Trials. *Signal Transduct. Target. Ther.* **2020**, *5* (1), 1–23.

(4) Becker, W.; Bhattiprolu, K. C.; Gubensäk, N.; Zangger, K. Investigating Protein–Ligand Interactions by Solution Nuclear Magnetic Resonance Spectroscopy. *ChemPhysChem* **2018**, *19* (8), 895–906.

(5) Meiboom, S.; Gill, D. Modified Spin-Echo Method for Measuring Nuclear Relaxation Times. *Rev. Sci. Instrum.* **1958**, *29* (8), 688–691.

(6) Williamson, M. P. Using Chemical Shift Perturbation to Characterise Ligand Binding. *Prog. Nucl. Magn. Reson. Spectrosc.* **2013**, *73*, 1–16.

(7) Anglister, J.; Srivastava, G.; Naider, F. Detection of Intermolecular NOE Interactions in Large Protein Complexes. *Prog. Nucl. Magn. Reson. Spectrosc.* **2016**, *97*, 40–56.

(8) Skinner, A. L.; Laurence, J. S. High-Field Solution NMR Spectroscopy as a Tool for Assessing Protein Interactions with Small Molecule Ligands. *J. Pharm. Sci.* **2008**, *97* (11), 4670–4695.

(9) Dalvit, C.; Fogliatto, G.; Stewart, A.; Veronesi, M.; Stockman, B. WaterLOGSY as a Method for Primary NMR Screening: Practical Aspects and Range of Applicability. *J. Biomol. NMR* **2001**, *21* (4), 349–359.

(10) Orts, J.; Griesinger, C.; Carlomagno, T. The INPHARMA Technique for Pharmacophore Mapping: A Theoretical Guide to the Method. *J. Magn. Reson.* **2009**, *200* (1), 64–73.

(11) Anthis, N. J.; Clore, G. M. Visualizing Transient Dark States by NMR Spectroscopy. *Q. Rev. Biophys.* **2015**, *48* (1), 35–116.

(12) Bernini, A.; Venditti, V.; Spiga, O.; Niccolai, N. Probing Protein Surface Accessibility with Solvent and Paramagnetic Molecules. *Prog. Nucl. Magn. Reson. Spectrosc.* **2009**, *54* (3), 278–289.

(13) Ardenkjaer-Larsen, J. H.; Fridlund, B.; Gram, A.; Hansson, G.; Hansson, L.; Lerche, M. H.; Servin, R.; Thaning, M.; Golman, K. Increase in Signal-to-Noise Ratio of > 10,000 Times in Liquid-State NMR. *Proc. Natl. Acad. Sci.* **2003**, *100* (18), 10158–10163.

(14) Stewart, N. J.; Matsumoto, S. Biomedical Applications of the Dynamic Nuclear Polarization and Parahydrogen Induced Polarization Techniques for Hyperpolarized 13C MR Imaging. *Magn. Reson. Med. Sci.* **2019**, *20* (1), 1–17.

(15) Kim, J.; Liu, M.; Hilty, C. Modeling of Polarization Transfer Kinetics in Protein Hydration Using Hyperpolarized Water. *J. Phys. Chem. B* **2017**, *121* (27), 6492–6498.

(16) Harris, T.; Szekely, O.; Frydman, L. On the Potential of Hyperpolarized Water in Biomolecular NMR Studies. *J. Phys. Chem. B* **2014**, *118* (12), 3281–3290.

(17) Kim, J.; Mandal, R.; Hilty, C. Observation of Fast Two-Dimensional NMR Spectra during Protein Folding Using Polarization Transfer from Hyperpolarized Water. *J. Phys. Chem. Lett.* **2019**, *10* (18), 5463–5467.

(18) Kim, J.; Mandal, R.; Hilty, C. 2D NMR Spectroscopy of Refolding RNase Sa Using Polarization Transfer from Hyperpolarized Water. *J. Magn. Reson.* **2021**, *326*, 106942.

(19) Novakovic, M.; Olsen, G. L.; Pintér, G.; Hymon, D.; Fürtig, B.; Schwalbe, H.; Frydman, L. A 300-Fold Enhancement of Imino Nucleic Acid Resonances by Hyperpolarized Water Provides a New Window for Probing RNA Refolding by 1D and 2D NMR. *Proc. Natl. Acad. Sci.* **2020**, *117* (5), 2449–2455.

(20) Wang, Y.; Ragavan, M.; Hilty, C. Site Specific Polarization Transfer from a Hyperpolarized Ligand of Dihydrofolate Reductase. *J. Biomol. NMR* **2016**, *65* (1), 41–48.

(21) Wang, Y.; Kim, J.; Hilty, C. Determination of Protein–Ligand Binding Modes Using Fast Multi-Dimensional NMR with Hyperpolarization. *Chem. Sci.* **2020**, *11* (23), 5935–5943.

(22) Lee, Y.; Zeng, H.; Ruedisser, S.; Gossert, A. D.; Hilty, C. Nuclear Magnetic Resonance of Hyperpolarized Fluorine for Characterization of Protein–Ligand Interactions. *J. Am. Chem. Soc.* **2012**, *134* (42), 17448–17451.

(23) Kim, Y.; Hilty, C. Affinity Screening Using Competitive Binding with Fluorine-19 Hyperpolarized Ligands. *Angew. Chem. Int. Ed.* **2015**, *54* (16), 4941–4944.

(24) Min, H.; Sekar, G.; Hilty, C. Polarization Transfer from Ligands Hyperpolarized by Dissolution Dynamic Nuclear Polarization for Screening in Drug Discovery. *ChemMedChem* **2015**, *10* (9), 1559–1563.

(25) Ward, H. Roy.; Lawler, R. G. Nuclear Magnetic Resonance Emission and Enhanced Absorption in Rapid Organometallic Reactions. *J. Am. Chem. Soc.* **1967**, *89* (21), 5518–5519.

(26) Kaptein, R.; Dijkstra, K.; Nicolay, K. Laser Photo-CIDNP as a Surface Probe for Proteins in Solution. *Nature* **1978**, *274* (5668), 293–294.

(27) Hore, J.; Broadhurst, R. W. Photo-CIDNP of Biopolymers. *Prog. Nucl. Magn. Reson. Spectrosc.* **1993**, *25* (4), 345–402.

(28) Mok, K. Photo-CIDNP NMR Methods for Studying Protein Folding. *Methods* **2004**, *34* (1), 75–87.

(29) Mok, K. H.; Nagashima, T.; Day, I. J.; Jones, J. A.; Jones, C. J. V.; Dobson, C. M.; Hore, P. J. Rapid Sample-Mixing Technique for Transient NMR and Photo-CIDNP Spectroscopy: Applications to Real-Time Protein Folding. *J. Am. Chem. Soc.* **2003**, *125* (41), 12484–12492.

(30) Schleich, T.; Scheek, R. M.; Stob, S.; Alma, N. C. M.; Hilbers, C. W.; Kaptein, R. Photo-Cidnp Study of Adenylyl-Containing Deoxy-Dinucleotides. Pair Substitution Effects Due to Intramolecular Cation Radical Deprotonation. *Photochem. Photobiol.* **1982**, *35* (4), 575–577.

(31) Armstrong, B. D.; Han, S. Overhauser Dynamic Nuclear Polarization To Study Local Water Dynamics. *J. Am. Chem. Soc.* **2009**, *131* (13), 4641–4647.

(32) McCarney, E. R.; Armstrong, B. D.; Kausik, R.; Han, S. Dynamic Nuclear Polarization Enhanced Nuclear Magnetic Resonance and Electron Spin Resonance Studies of Hydration and Local Water Dynamics in Micelle and Vesicle Assemblies. *Langmuir* **2008**, *24* (18), 10062–10072.

(33) Armstrong, B. D.; Choi, J.; López, C.; Wesener, D. A.; Hubbell, W.; Cavagnero, S.; Han, S. Site-Specific Hydration Dynamics in the Nonpolar Core of a Molten Globule by Dynamic Nuclear Polarization of Water. *J. Am. Chem. Soc.* **2011**, *133* (15), 5987–5995.

(34) Segawa, T. F.; Doppelbauer, M.; Garbuio, L.; Doll, A.; Polyhach, Y. O.; Jeschke, G. Water Accessibility in a Membrane-Inserting Peptide Comparing Overhauser DNP and Pulse EPR Methods. *J. Chem. Phys.* **2016**, *144* (19), 194201.

(35) Walker, T. G.; Happer, W. Spin-Exchange Optical Pumping of Noble-Gas Nuclei. *Rev. Mod. Phys.* **1997**, *69* (2), 629–642.

(36) Jayapaul, J.; Schröder, L. Molecular Sensing with Host Systems for Hyperpolarized 129Xe. *Molecules* **2020**, *25* (20), 4627.

(37) Navon, G.; Song, Y.-Q.; Rõõm, T.; Appelt, S.; Taylor, R. E.; Pines, A. Enhancement of Solution NMR and MRI with Laser-Polarized Xenon. *Science* **1996**, *271* (5257), 1848–1851.

(38) Bowers, C. R.; Storhaug, V.; Webster, C. E.; Bharatam, J.; Cottone, A.; Gianna, R.; Betsey, K.; Gaffney, B. J. Exploring Surfaces and Cavities in Lipoxygenase and Other Proteins by Hyperpolarized Xenon-129 NMR. *J. Am. Chem. Soc.* **1999**, *121* (40), 9370–9377.

(39) Rubin, S. M.; Spence, M. M.; Dimitrov, I. E.; Ruiz, E. J.; Pines, A.; Wemmer, D. E. Detection of a Conformational Change in Maltose Binding Protein by 129Xe NMR Spectroscopy. *J. Am. Chem. Soc.* **2001**, *123* (35), 8616–8617.

(40) Feng, B.; Coffey, A. M.; Colon, R. D.; Chekmenev, E. Y.; Waddell, K. W. A Pulsed Injection Parahydrogen Generator and Techniques for Quantifying Enrichment. *J. Magn. Reson.* **2012**, *214*, 258–262.

(41) Bowers, C. R.; Weitekamp, D. P. Transformation of Symmetrization Order to Nuclear-Spin Magnetization by Chemical Reaction and Nuclear Magnetic Resonance. *Phys. Rev. Lett.* **1986**, *57* (21), 2645–2648.

(42) Bowers, C. R.; Weitekamp, D. P. Parahydrogen and Synthesis Allow Dramatically Enhanced Nuclear Alignment. *J. Am. Chem. Soc.* **1987**, *109* (18), 5541–5542.

(43) Colebrooke, S. A.; Duckett, S. B.; Lohman, J. A. B. Characterisation and Kinetic Behaviour of H2Rh(PPh3)2(μ-Cl)2Rh(PPh3)(Alkene) and Related Binuclear Complexes Detected during Hydrogenation Studies Involving Parahydrogen Induced Polarisation. *Chem. Commun.* **2000**, No. 8, 685–686.

(44) A. Messerle, B.; J. Sleigh, C.; G. Partridge, M.; B. Duckett, S. Structure and Dynamics in Metal Phosphine Complexes Using Advanced NMR Studies with Para-Hydrogen Induced Polarisation. *J. Chem. Soc. Dalton Trans.* **1999**, No. 9, 1429.

(45) Bhattacharya, P.; Chekmenev, E. Y.; Perman, W. H.; Harris, K. C.; Lin, A. P.; Norton, V. A.; Tan, C. T.; Ross, B. D.; Weitekamp, D. P. Towards Hyperpolarized 13C-Succinate Imaging of Brain Cancer. *J. Magn. Reson. San Diego Calif 1997* **2007**, *186* (1), 150–155.

(46) Shchepin, R. V.; Coffey, A. M.; Waddell, K. W.; Chekmenev, E. Y. PASADENA Hyperpolarized 13C Phospholactate. *J. Am. Chem. Soc.* **2012**, *134* (9), 3957–3960.

(47) Golman, K.; Axelsson, O.; Jóhannesson, H.; Månsson, S.; Olofsson, C.; Petersson, J. S. Parahydrogen-Induced Polarization in Imaging: Subsecond 13C Angiography. *Magn. Reson. Med.* **2001**, *46* (1), 1–5.

(48) Roth, M.; Koch, A.; Kindervater, P.; Bargon, J.; Spiess, H. W.; Münnemann, K. 13C Hyperpolarization of a Barbituric Acid Derivative via Parahydrogen Induced Polarization. *J. Magn. Reson.* **2010**, *204* (1), 50–55.

(49) Reineri, F.; Boi, T.; Aime, S. ParaHydrogen Induced Polarization of 13C Carboxylate Resonance in Acetate and Pyruvate. *Nat. Commun.* **2015**, *6* (1), 5858.

(50) Adams, R. W.; Aguilar, J. A.; Atkinson, K. D.; Cowley, M. J.; Elliott, P. I. P.; Duckett, S. B.; Green, G. G. R.; Khazal, I. G.; Lopez-Serrano, J.; Williamson, D. C. Reversible Interactions with Para-Hydrogen Enhance NMR Sensitivity by Polarization Transfer. *Science* **2009**, *323* (5922), 1708–1711.

(51) Pravdivtsev, A. N.; Yurkovskaya, A. V.; Vieth, H.-M.; Ivanov, K. L.; Kaptein, R. Level Anti-Crossings Are a Key Factor for Understanding Para-Hydrogen-Induced Hyperpolarization in SABRE Experiments. *ChemPhysChem* **2013**, *14* (14), 3327–3331.

(52) Theis, T.; Truong, M. L.; Coffey, A. M.; Shchepin, R. V.; Waddell, K. W.; Shi, F.; Goodson, B. M.; Warren, W. S.; Chekmenev, E. Y. Microtesla SABRE Enables 10% Nitrogen-15 Nuclear Spin Polarization. *J. Am. Chem. Soc.* **2015**, *137* (4), 1404–1407.

(53) Pravdivtsev, A. N.; Yurkovskaya, A. V.; Vieth, H.-M.; Ivanov, K. L. RF-SABRE: A Way to Continuous Spin Hyperpolarization at High Magnetic Fields. *J. Phys. Chem. B* **2015**, *119* (43), 13619–13629.

(54) Barskiy, D. A.; Kovtunov, K. V.; Koptyug, I. V.; He, P.; Groome, K. A.; Best, Q. A.; Shi, F.; Goodson, B. M.; Shchepin, R. V.; Coffey, A. M.; Waddell, K. W.; Chekmenev, E. Y. The Feasibility of Formation and Kinetics of NMR Signal Amplification by Reversible Exchange (SABRE) at High Magnetic Field (9.4 T). *J. Am. Chem. Soc.* **2014**, *136* (9), 3322–3325.

(55) Cowley, M. J.; Adams, R. W.; Atkinson, K. D.; Cockett, M. C. R.; Duckett, S. B.; Green, G. G. R.; Lohman, J. A. B.; Kerssebaum, R.; Kilgour, D.; Mewis, R. E. Iridium N-Heterocyclic Carbene Complexes as Efficient Catalysts for Magnetization Transfer from Para-Hydrogen. *J. Am. Chem. Soc.* **2011**, *133* (16), 6134–6137.

(56) Wong, C. M.; Fekete, M.; Nelson-Forde, R.; Gatus, M. R. D.; Rayner, P. J.; Whitwood, A. C.; Duckett, S. B.; Messerle, B. A. Harnessing Asymmetric N-Heterocyclic Carbene Ligands to Optimise SABRE Hyperpolarisation. *Catal. Sci. Technol.* **2018**, *8* (19), 4925–4933.

(57) Colell, J. F. P.; Logan, A. W. J.; Zhou, Z.; Lindale, J. R.; Laasner, R.; Shchepin, R. V.; Chekmenev, E. Y.; Blum, V.; Warren, W. S.; Malcolmson, S. J.; Theis, T. Rational Ligand Choice Extends the SABRE Substrate Scope. *Chem. Commun.* **2020**, *56* (65), 9336–9339.

(58) Pham, P.; Hilty, C. Tunable Iridium Catalyst Designs with Bidentate N-Heterocyclic Carbene Ligands for SABRE Hyperpolarization of Sterically Hindered Substrates. *Chem. Commun.* **2020**, *56* (98), 15466–15469.

(59) Rayner, P. J.; Gillions, J. P.; Hannibal, V. D.; John, R. O.; Duckett, S. B. Hyperpolarisation of Weakly Binding N-Heterocycles Using Signal Amplification by Reversible Exchange. *Chem. Sci.* **2021**, *12* (16), 5910–5917.

(60) Muhammad, S. R.; Greer, R. B.; Ramirez, S. B.; Goodson, B. M.; Fout, A. R. Cobalt-Catalyzed Hyperpolarization of Structurally Intact Olefins. *ACS Catal.* **2021**, *11* (4), 2011–2020.

(61) Mewis, R. E.; Fekete, M.; Green, G. G. R.; Whitwood, A. C.; Duckett, S. B. Deactivation of Signal Amplification by Reversible Exchange Catalysis, Progress towards in Vivo Application. *Chem. Commun.* **2015**, *51* (48), 9857–9859.

(62) E. Mewis, R.; Fekete, M.; R. Green, G. G.; C. Whitwood, A.; B. Duckett, S. Deactivation of Signal Amplification by Reversible Exchange Catalysis, Progress towards in Vivo Application. *Chem. Commun.* **2015**, *51* (48), 9857–9859.

(63) Barskiy, D. A.; Ke, L. A.; Li, X.; Stevenson, V.; Widarman, N.; Zhang, H.; Truxal, A.; Pines, A. Rapid Catalyst Capture Enables Metal-Free Para-Hydrogen-Based Hyperpolarized Contrast Agents. *J. Phys. Chem. Lett.* **2018**, *9* (11), 2721–2724.

(64) Iali, W.; Olaru, A. M.; Green, G. G. R.; Duckett, S. B. Achieving High Levels of NMR-Hyperpolarization in Aqueous Media With Minimal Catalyst Contamination Using SABRE. *Chem. – Eur. J.* **2017**, *23* (44), 10491–10495.

(65) Rayner, P. J.; Burns, M. J.; Olaru, A. M.; Norcott, P.; Fekete, M.; Green, G. G. R.; Highton, L. A. R.; Mewis, R. E.; Duckett, S. B. Delivering Strong 1H Nuclear Hyperpolarization Levels and Long Magnetic Lifetimes through Signal Amplification by Reversible Exchange. *Proc. Natl. Acad. Sci.* **2017**, *114* (16), E3188–E3194.

(66) Purwanto; Deshpande, R. M.; Chaudhari, R. V.; Delmas, H. Solubility of Hydrogen, Carbon Monoxide, and 1-Octene in Various Solvents and Solvent Mixtures. *J. Chem. Eng. Data* **1996**, *41* (6), 1414–1417.

(67) Rayner, P. J.; Richardson, P. M.; Duckett, S. B. The Detection and Reactivity of Silanols and Silanes Using Hyperpolarized 29Si Nuclear Magnetic Resonance. *Angew. Chem.* **2020**, *132* (7), 2732–2736.

(68) Tickner, Ben. J.; Rayner, P. J.; Duckett, S. B. Using SABRE Hyperpolarized ^{13}C NMR Spectroscopy to Interrogate Organic Transformations of Pyruvate. *Anal. Chem.* **2020**, *92* (13), 9095–9103.

(69) Chae, H.; Min, S.; Jeong, H. J.; Namgoong, S. K.; Oh, S.; Kim, K.; Jeong, K. Organic Reaction Monitoring of a Glycine Derivative Using Signal Amplification by Reversible Exchange-Hyperpolarized Benchtop Nuclear Magnetic Resonance Spectroscopy. *Anal. Chem.* **2020**, *92* (16), 10902–10907.

(70) Roy, S. S.; Appleby, K. M.; Fear, E. J.; Duckett, S. B. SABRE-Relay: A Versatile Route to Hyperpolarization. *J. Phys. Chem. Lett.* **2018**, *9* (5), 1112–1117.

(71) Iali, W.; Rayner, P. J.; Duckett, S. B. Using Parahydrogen to Hyperpolarize Amines, Amides, Carboxylic Acids, Alcohols, Phosphates, and Carbonates. *Sci. Adv.* **2018,** *4*(1), eaao6250.

(72) Iali, W.; Rayner, P. J.; Alshehri, A.; Holmes, A. Jonathan.; Ruddlesden, A. J.; Duckett, S. B. Direct and Indirect Hyperpolarisation of Amines Using *Para* Hydrogen. *Chem. Sci.* **2018**, *9* (15), 3677–3684.

(73) Rayner, P. J.; Tickner, B. J.; Iali, W.; Fekete, M.; Robinson, A. D.; Duckett, S. B. Relayed Hyperpolarization from Para-Hydrogen Improves the NMR Detectability of Alcohols. *Chem. Sci.* **2019**, *10* (33), 7709–7717.

(74) Truong, M. L.; Shi, F.; He, P.; Yuan, B.; Plunkett, K. N.; Coffey, A. M.; Shchepin, R. V.; Barskiy, D. A.; Kovtunov, K. V.; Koptyug, I. V.; Waddell, K. W.; Goodson, B. M.; Chekmenev, E. Y. Irreversible Catalyst Activation Enables

Hyperpolarization and Water Solubility for NMR Signal Amplification by Reversible Exchange. *J. Phys. Chem. B* **2014**, *118* (48), 13882–13889.

(75) Zeng, H.; Xu, J.; McMahon, M. T.; Lohman, J. A. B.; van Zijl, P. C. M. Achieving 1% NMR Polarization in Water in Less than 1min Using SABRE. *J. Magn. Reson.* **2014**, *246*, 119–121.

(76) Phillips, R.; Ursell, T.; Wiggins, P.; Sens, P. Emerging Roles for Lipids in Shaping Membrane-Protein Function. *Nature* **2009**, *459* (7245), 379–385.

(77) Kucharska, I.; Tamm, L. K. Solution NMR Provides New Insight into Lipid–Protein Interaction. *Biochemistry* **2017**, *56* (33), 4291–4292.

(78) Gupta, K.; Li, J.; Liko, I.; Gault, J.; Bechara, C.; Wu, D.; Hopper, J. T. S.; Giles, K.; Benesch, J. L. P.; Robinson, C. V. Identifying Key Membrane Protein Lipid Interactions Using Mass Spectrometry. *Nat. Protoc.* **2018**, *13* (5), 1106–1120.

(79) Vogt, J.; Schulz, G. E. The Structure of the Outer Membrane Protein OmpX from Escherichia Coli Reveals Possible Mechanisms of Virulence. *Structure* **1999**, *7* (10), 1301–1309.

(80) Fernández, C.; Hilty, C.; Wider, G.; Güntert, P.; Wüthrich, K. NMR Structure of the Integral Membrane Protein OmpX. *J. Mol. Biol.* **2004**, *336* (5), 1211–1221.

(81) Mahalakshmi, R.; Marassi, F. M. Orientation of the Escherichia Coli Outer Membrane Protein OmpX in Phospholipid Bilayer Membranes Determined by Solid-State NMR. *Biochemistry* **2008**, *47* (25), 6531–6538.

(82) Fernández, C.; Hilty, C.; Wider, G.; Wüthrich, K. Lipid–Protein Interactions in DHPC Micelles Containing the Integral Membrane Protein OmpX Investigated by NMR Spectroscopy. *Proc. Natl. Acad. Sci.* **2002**, *99* (21), 13533–13537.

(83) Lee, D.; Walter, K. F. A.; Brückner, A.-K.; Hilty, C.; Becker, S.; Griesinger, C. Bilayer in Small Bicelles Revealed by Lipid−Protein Interactions Using NMR Spectroscopy. *J. Am. Chem. Soc.* **2008**, *130* (42), 13822–13823.

(84) Hilty, C.; Wider, G.; Fernández, C.; Wüthrich, K. Membrane Protein–Lipid Interactions in Mixed Micelles Studied by NMR Spectroscopy with the Use of Paramagnetic Reagents. *ChemBioChem* **2004**, *5* (4), 467–473.

(85) Hiller, S.; Wider, G.; Imbach, L. L.; Wüthrich, K. Interactions with Hydrophobic Clusters in the Urea-Unfolded Membrane Protein OmpX. *Angew. Chem. Int. Ed.* **2008**, *47* (5), 977–981.

(86) Tafer, H.; Hiller, S.; Hilty, C.; Fernández, C.; Wüthrich, K. Nonrandom Structure in the Urea-Unfolded *Escherichia Coli* Outer Membrane Protein X (OmpX) †. *Biochemistry* **2004**, *43* (4), 860–869.

(87) Bowen, S.; Hilty, C. Time-Resolved Dynamic Nuclear Polarization Enhanced NMR Spectroscopy. *Angew. Chem.* **2008**, *120* (28), 5313–5315.

(88) Chen, H.-Y.; Ragavan, M.; Hilty, C. Protein Folding Studied by Dissolution Dynamic Nuclear Polarization. *Angew. Chem. Int. Ed.* **2013**, *52* (35), 9192–9195.

(89) Lee, Y.; Zeng, H.; Mazur, A.; Wegstroth, M.; Carlomagno, T.; Reese, M.; Lee, D.; Becker, S.; Griesinger, C.; Hilty, C. Hyperpolarized Binding Pocket Nuclear

Overhauser Effect for Determination of Competitive Ligand Binding. *Angew. Chem. Int. Ed.* **2012**, *51* (21), 5179–5182.

(90) Manzo, G.; Carboni, M.; Rinaldi, A. C.; Casu, M.; Scorciapino, M. A. Characterization of Sodium Dodecylsulphate and Dodecylphosphocholine Mixed Micelles through NMR and Dynamic Light Scattering. *Magn. Reson. Chem.* **2013**, *51* (3), 176–183.

(91) Israelachvili, J.N. *Intermolecular and Surface Forces*, Elsevier, **2011**; pp 545.

(92) Raschle, T.; Rios Flores, P.; Opitz, C.; Müller, D. J.; Hiller, S. Monitoring Backbone Hydrogen-Bond Formation in Beta-Barrel Membrane Protein Folding. *Angew. Chem. Int. Ed.* **2016**, *55* (20), 5952–5955.

(93) Kawahara, K.; Tanford, C. Viscosity and Density of Aqueous Solutions of Urea and Guanidine Hydrochloride. *J. Biol. Chem.* **1966**, *241* (13), 3228–3232.

(94) Bruning, W.; Holtzer, A. The Effect of Urea on Hydrophobic Bonds: The Critical Micelle Concentration of n-Dodecyltrimethylammonium bromide in Aqueous Solutions of Urea. *J. Am. Chem. Soc.* **1961**, *83* (23), 4865–4866.

(95) Broecker, J.; Keller, S. Impact of Urea on Detergent Micelle Properties. *Langmuir* **2013**, *29* (27), 8502–8510.

(96) Schanda, P.; Brutscher, B. Very Fast Two-Dimensional NMR Spectroscopy for Real-Time Investigation of Dynamic Events in Proteins on the Time Scale of Seconds. *J. Am. Chem. Soc.* **2005**, *127* (22), 8014–8015.

(97) Chaturvedi, D.; Mahalakshmi, R. Methionine Mutations of Outer Membrane Protein X Influence Structural Stability and Beta-Barrel Unfolding. *PLOS ONE* **2013**, *8* (11), e79351.

(98) Bowen, S.; Hilty, C. Rapid Sample Injection for Hyperpolarized NMR Spectroscopy. *Phys. Chem. Chem. Phys.* **2010**, *12* (22), 5766–5770.

(99) Zeng, H.; Lee, Y.; Hilty, C. Quantitative Rate Determination by Dynamic Nuclear Polarization Enhanced NMR of a Diels−Alder Reaction. *Anal. Chem.* **2010**, *82* (21), 8897–8902.

(100) Solomon, I. Relaxation Processes in a System of Two Spins. *Phys. Rev.* **1955**, *99* (2), 559–565.

(101) Geen, H.; Freeman, R. Band-Selective Radiofrequency Pulses. *J. Magn. Reson. 1969* **1991**, *93* (1), 93–141.

(102) Rayner, P. J.; Norcott, P.; Appleby, K. M.; Iali, W.; John, R. O.; Hart, S. J.; Whitwood, A. C.; Duckett, S. B. Fine-Tuning the Efficiency of Para-Hydrogen-Induced Hyperpolarization by Rational N-Heterocyclic Carbene Design. *Nat. Commun.* **2018**, *9* (1), 4251.

(103) Lloyd, L. S.; Adams, R. W.; Bernstein, M.; Coombes, S.; Duckett, S. B.; Green, G. G. R.; Lewis, Richard. J.; Mewis, R. E.; Sleigh, C. J. Utilization of SABRE-Derived Hyperpolarization To Detect Low-Concentration Analytes via 1D and 2D NMR Methods. *J. Am. Chem. Soc.* **2012**, *134* (31), 12904–12907.

(104) Shen, K.; Logan, A. W. J.; Colell, J. F. P.; Bae, J.; Ortiz, G. X.; Theis, T.; Warren, W. S.; Malcolmson, S. J.; Wang, Q. Diazirines as Potential Molecular Imaging

Tags: Probing the Requirements for Efficient and Long-Lived SABRE-Induced Hyperpolarization. *Angew. Chem. Int. Ed.* **2017**, *56* (40), 12112–12116.

(105) Fekete, M.; Rayner, P. J.; Green, G. G. R.; Duckett, S. B. Harnessing Polarisation Transfer to Indazole and Imidazole through Signal Amplification by Reversible Exchange to Improve Their NMR Detectability. *Magn. Reson. Chem.* **2017**, *55* (10), 944–957.

(106) Iali, W.; Roy, S. S.; Tickner, B. J.; Ahwal, F.; Kennerley, A. J.; Duckett, S. B. Hyperpolarising Pyruvate through Signal Amplification by Reversible Exchange (SABRE). *Angew. Chem. Int. Ed.* **2019**, *58* (30), 10271–10275.

(107) Eshuis, N.; Hermkens, N.; van Weerdenburg, B. J. A.; Feiters, M. C.; Rutjes, F. P. J. T.; Wijmenga, S. S.; Tessari, M. Toward Nanomolar Detection by NMR Through SABRE Hyperpolarization. *J. Am. Chem. Soc.* **2014**, *136* (7), 2695–2698.

(108) Fekete, M.; Ahwal, F.; Duckett, S. B. Remarkable Levels of 15N Polarization Delivered through SABRE into Unlabeled Pyridine, Pyrazine, or Metronidazole Enable Single Scan NMR Quantification at the MM Level. *J. Phys. Chem. B* **2020**, *124* (22), 4573–4580.

(109) Tickner, B.; John, R. O.; Roy, S. S.; Hart, S.; Whitwood, A. C.; Duckett, S. B. Using Coligands to Gain Mechanistic Insight into Iridium Complexes Hyperpolarized with Para-Hydrogen. *Chem. Sci.* **2019**, *10*, 5235–5245.

(110) Olaru, A. M.; Robertson, T. B. R.; Lewis, J. S.; Antony, A.; Iali, W.; Mewis, R. E.; Duckett, S. B. Extending the Scope of 19F Hyperpolarization through Signal

Amplification by Reversible Exchange in MRI and NMR Spectroscopy. *ChemistryOpen* **2017**, *7* (1), 97–105.

(111) Shchepin, R. V.; Truong, M. L.; Theis, T.; Coffey, A. M.; Shi, F.; Waddell, K. W.; Warren, W. S.; Goodson, B. M.; Chekmenev, E. Y. Hyperpolarization of "Neat" Liquids by NMR Signal Amplification by Reversible Exchange. *J. Phys. Chem. Lett.* **2015**, *6* (10), 1961–1967.

(112) Siega, P.; Randaccio, L.; Marzilli, P. A.; Marzilli, L. G. Metal Coordination by Sterically Hindered Heterocyclic Ligands, Including 2-Vinylpyridine, Assessed by Investigation of Cobaloximes. *Inorg. Chem.* **2006**, *45* (8), 3359–3368.

(113) Wang, Y.; Hilty, C. Amplification of Nuclear Overhauser Effect Signals by Hyperpolarization for Screening of Ligand Binding to Immobilized Target Proteins. *Anal. Chem.* **2020**, *92* (20), 13718–13723.

(114) Lee, Y.; Zeng, H.; Mazur, A.; Wegstroth, M.; Carlomagno, T.; Reese, M.; Lee, D.; Becker, S.; Griesinger, C.; Hilty, C. Hyperpolarized Binding Pocket Nuclear Overhauser Effect for Determination of Competitive Ligand Binding. *Angew. Chem. Int. Ed.* **2012**, *51* (21), 5179–5182.

(115) Wang, Y.; Hilty, C. Determination of Ligand Binding Epitope Structures Using Polarization Transfer from Hyperpolarized Ligands. *J. Med. Chem.* **2019**, *62* (5), 2419–2427.

(116) Ragavan, M.; Chen, H.-Y.; Sekar, G.; Hilty, C. Solution NMR of Polypeptides Hyperpolarized by Dynamic Nuclear Polarization. *Anal. Chem.* **2011**, *83* (15), 6054–6059.

(117) Novakovic, M.; Olsen, G. L.; Pintér, G.; Hymon, D.; Fürtig, B.; Schwalbe, H.; Frydman, L. A 300-Fold Enhancement of Imino Nucleic Acid Resonances by Hyperpolarized Water Provides a New Window for Probing RNA Refolding by 1D and 2D NMR. *Proc. Natl. Acad. Sci.* **2020**, *117* (5), 2449–2455.

(118) Szekely, O.; Olsen, G. L.; Novakovic, M.; Rosenzweig, R.; Frydman, L. Assessing Site-Specific Enhancements Imparted by Hyperpolarized Water in Folded and Unfolded Proteins by 2D HMQC NMR. *J. Am. Chem. Soc.* **2020**, *142* (20), 9267–9284.

(119) Zeng, H.; Xu, J.; Gillen, J.; McMahon, M. T.; Artemov, D.; Tyburn, J.-M.; Lohman, J. A. B.; Mewis, R. E.; Atkinson, K. D.; Green, G. G. R.; Duckett, S. B.; van Zijl, P. C. M. Optimization of SABRE for Polarization of the Tuberculosis Drugs Pyrazinamide and Isoniazid. *J. Magn. Reson.* **2013**, *237*, 73–78.

(120) Jeong, H. J.; Min, S.; Chae, H.; Kim, S.; Lee, G.; Namgoong, S. K.; Jeong, K. Signal Amplification by Reversible Exchange for COVID-19 Antiviral Drug Candidates. *Sci. Rep.* **2020**, *10* (1), 14290.

(121) Salnikov, O. G.; Chukanov, N. V.; Svyatova, A.; Trofimov, I. A.; Kabir, M. S. H.; Gelovani, J. G.; Kovtunov, K. V.; Koptyug, I. V.; Chekmenev, E. Y. 15N NMR Hyperpolarization of Radiosensitizing Antibiotic Nimorazole by Reversible Parahydrogen Exchange in Microtesla Magnetic Fields. *Angew. Chem. Int. Ed.* **2021**, *60* (5), 2406–2413.

(122) Skovpin, I. V.; Svyatova, A.; Chukanov, N.; Chekmenev, E. Y.; Kovtunov, K. V.; Koptyug, I. V. 15N Hyperpolarization of Dalfampridine at Natural Abundance for Magnetic Resonance Imaging. *Chem. – Eur. J.* **2019**, *25* (55), 12694–12697.

(123) Colell, J. F. P.; Emondts, M.; Logan, A. W. J.; Shen, K.; Bae, J.; Shchepin, R. V.; Ortiz, G. X.; Spannring, P.; Wang, Q.; Malcolmson, S. J.; Chekmenev, E. Y.; Feiters, M. C.; Rutjes, F. P. J. T.; Blümich, B.; Theis, T.; Warren, W. S. Direct Hyperpolarization of Nitrogen-15 in Aqueous Media with Parahydrogen in Reversible Exchange. *J. Am. Chem. Soc.* **2017**, *139* (23), 7761–7767.

(124) Shi, F.; He, P.; Best, Q. A.; Groome, K.; Truong, M. L.; Coffey, A. M.; Zimay, G.; Shchepin, R. V.; Waddell, K. W.; Chekmenev, E. Y.; Goodson, B. M. Aqueous NMR Signal Enhancement by Reversible Exchange in a Single Step Using Water-Soluble Catalysts. *J. Phys. Chem. C* **2016**, *120* (22), 12149–12156.

(125) Manoharan, A.; Rayner, P. J.; Iali, W.; Burns, M. J.; Perry, V. H.; Duckett, S. B. Achieving Biocompatible SABRE: An in Vitro Cytotoxicity Study. *ChemMedChem* **2018**, *13* (4), 352–359.

(126) Kovtunov, K. V.; Kidd, B. E.; Salnikov, O. G.; Bales, L. B.; Gemeinhardt, M. E.; Gesiorski, J.; Shchepin, R. V.; Chekmenev, E. Y.; Goodson, B. M.; Koptyug, I. V. Imaging of Biomolecular NMR Signals Amplified by Reversible Exchange with Parahydrogen Inside an MRI Scanner. *J. Phys. Chem. C* **2017**, *121* (46), 25994–25999.

(127) Renatus, M.; Bode, W.; Huber, R.; Stürzebecher, J.; Stubbs, M. T. Structural and Functional Analyses of Benzamidine-Based Inhibitors in Complex with Trypsin:

Implications for the Inhibition of Factor Xa, TPA, and Urokinase. *J. Med. Chem.* **1998**, *41* (27), 5445–5456.

(128) Stanbury, E. V.; Richardson, P. M.; Duckett, S. B. Understanding Substrate Substituent Effects to Improve Catalytic Efficiency in the SABRE Hyperpolarisation Process. *Catal. Sci. Technol.* **2019**, *9* (15), 3914–3922.

(129) Kim, Y.; Liu, M.; Hilty, C. Parallelized Ligand Screening Using Dissolution Dynamic Nuclear Polarization. *Anal. Chem.* **2016**, *88* (22), 11178–11183.

(130) Rebordão, G.; Palma, S. I. C. J.; Roque, A. C. A. Microfluidics in Gas Sensing and Artificial Olfaction. *Sensors* **2020**, *20* (20), 5742.

(131) Yamazaki, K.; Iwura, T.; Ishikawa, R.; Ozaki, Y. Methanol-Induced Tertiary and Secondary Structure Changes of Granulocyte-Colony Stimulating Factor. *J. Biochem. (Tokyo)* **2006**, *140* (1), 49–56.

(132) M. Gopal, S.; Klumpers, F.; Herrmann, C.; V. Schäfer, L. Solvent Effects on Ligand Binding to a Serine Protease. *Phys. Chem. Chem. Phys.* **2017**, *19* (17), 10753–10766.

(133) Mewis, R. E.; Green, R. A.; Cockett, M. C. R.; Cowley, M. J.; Duckett, S. B.; Green, G. G. R.; John, R. O.; Rayner, P. J.; Williamson, D. C. Strategies for the Hyperpolarization of Acetonitrile and Related Ligands by SABRE. *J. Phys. Chem. B* **2015**, *119* (4), 1416–1424.

(134) Chukanov, N. V.; Salnikov, O. G.; Shchepin, R. V.; Svyatova, A.; Kovtunov, K. V.; Koptyug, I. V.; Chekmenev, E. Y. 19F Hyperpolarization of 15N-3-19F-

Pyridine via Signal Amplification by Reversible Exchange. *J. Phys. Chem. C* **2018**, *122* (40), 23002–23010.

(135) Dalvit, C.; Flocco, M.; Knapp, S.; Mostardini, M.; Perego, R.; Stockman, B. J.; Veronesi, M.; Varasi, M. High-Throughput NMR-Based Screening with Competition Binding Experiments. *J. Am. Chem. Soc.* **2002**, *124* (26), 7702–7709.

(136) Chen, H.-Y.; Hilty, C. Implementation and Characterization of Flow Injection in Dissolution Dynamic Nuclear Polarization NMR Spectroscopy. *ChemPhysChem* **2015**, *16* (12), 2646–2652.

(137) Mandal, R.; Pham, P.; Hilty, C. Characterization of Protein–Ligand Interactions by SABRE. *Chem. Sci.* **2021**, *12*, 12950–12958.

(138) Wang, J.; Guo, Z.; Fu, Y.; Wu, Z.; Huang, C.; Zheng, C.; Shar, P. A.; Wang, Z.; Xiao, W.; Wang, Y. Weak-Binding Molecules Are Not Drugs? —Toward a Systematic Strategy for Finding Effective Weak-Binding Drugs. *Brief. Bioinform* **2017**, *18* (2), 321–332.